

Louisiana State University

LSU Scholarly Repository

LSU Master's Theses

Graduate School

September 2021

A Modular Open-Technology Device to Measure and Adjust Concentration of Sperm Samples for Cryopreservation

Nikolas C. Zuchowicz

Louisiana State University and Agricultural and Mechanical College

Follow this and additional works at: https://repository.lsu.edu/gradschool_theses



Part of the [Aquaculture and Fisheries Commons](#), and the [Electrical and Electronics Commons](#)

Recommended Citation

Zuchowicz, Nikolas C., "A Modular Open-Technology Device to Measure and Adjust Concentration of Sperm Samples for Cryopreservation" (2021). *LSU Master's Theses*. 5435.

https://repository.lsu.edu/gradschool_theses/5435

This Thesis is brought to you for free and open access by the Graduate School at LSU Scholarly Repository. It has been accepted for inclusion in LSU Master's Theses by an authorized graduate school editor of LSU Scholarly Repository. For more information, please contact gradetd@lsu.edu.

**A MODULAR OPEN-TECHNOLOGY DEVICE
TO MEASURE AND ADJUST CONCENTRATION
OF SPERM SAMPLES FOR CRYOPRESERVATION**

A Thesis

Submitted to the Graduate Faculty of the
Louisiana State University and
Agricultural and Mechanical College
in partial fulfillment of the
requirements for the degree of
Master of Science

in

The School of Renewable Natural Resources

by
Nikolas Casimir Zuchowicz
B.A., Carleton University, 2017
December 2021

Acknowledgements

I thank Dr. Terry Tiersch, who took me on as a project, and the other members of my committee for shaping my work: namely Dr. Todd Monroe, Dr. Michael Hellberg, and Dr. Yue Liu. The staff and students of the Aquatic Germplasm and Genetic Resources Center – Bill, Amy, Sarah, Mike, Dr. Teresa, and many others – taught me a great deal and eased my path.

My love to my parents Barbara and Dominik, whose policy of benign neglect (their words) seems to have worked out all right. Likewise to my exceptional friends: Ann, Emily, Adam, Rachael, and Kelsey, among others, who got me through a degree in a pandemic with a touch of dark humor.

My special gratitude to the Paul M. Angell Family Foundation, which funded my master's studies, the National Institutes of Health – Office of Research Infrastructure Programs, which funded the facilities, equipment, and supplies that supported this project, and Dr. Mary Hagedorn, who made it all happen.

Table of Contents

| | |
|--|----|
| Acknowledgements | ii |
| List of Tables | v |
| List of Figures | vi |
| Abstract | ix |
| Foreword | x |
| Chapter 1. Introduction | 1 |
| Cryopreservation | 2 |
| Fabrication Methods..... | 3 |
| Parametric Design | 5 |
| Open Technology | 5 |
| Chapter 2. A Custom Peristaltic Pump and Optical Evaluation Module to Estimate Aquatic Sperm Concentration | 9 |
| Introduction | 9 |
| Methods | 10 |
| Results | 16 |
| Discussion | 22 |
| Conclusions | 23 |
| Chapter 3. A Concentration Measurement and Adjustment System to Prepare Aquatic Germplasm for Cryopreservation | 24 |
| Introduction | 24 |
| Methods | 25 |
| Results | 32 |
| Discussion | 40 |
| Conclusions | 42 |
| Chapter 4. Identifying Opportunities for Microfabrication with Low-Cost Resin Printing | 44 |
| Introduction | 44 |
| Methods | 46 |
| Results | 46 |
| Discussion | 48 |
| Conclusions | 49 |
| Chapter 5. Summary and Conclusions..... | 50 |
| Ch. 2. A custom peristaltic pump and optical evaluation module to estimate aquatic sperm concentration | 50 |
| Ch. 3. A concentration measurement and adjustment system to prepare aquatic germplasm for cryopreservation | 50 |
| Ch. 4. Identifying opportunities for microfluidics with low-cost resin printing | 50 |
| Design for Open Fabrication | 50 |

| | |
|--|----|
| Variations on the AGGRC Prototyping Process | 53 |
| Conclusions | 55 |
| Appendix A. Guide to Fabrication and Assembly of the Concentration Measurement and Adjustment System | 56 |
| Overview | 56 |
| 3-D printing of the .stl files | 56 |
| Laser cutting the body panels..... | 59 |
| Assembling the electronics..... | 60 |
| Assembling the frame..... | 62 |
| Appendix B. CMAS Bill of Materials | 65 |
| Appendix C. CMAS Circuit Diagrams | 71 |
| Appendix D. CMAS Arduino Code..... | 75 |
| Appendix E. Using the Parametric CMAS Form Factor | 87 |
| Appendix F. Preparation of Hanks' Balanced Salt Solution (HBSS), 300 mOsmol/kg | 91 |
| References..... | 92 |
| Vita..... | 98 |

List of Tables

| | |
|---|----|
| 2.1. Properties of four water–glycerol solutions used in testing the peristaltic pump | 11 |
| A.1. 3-D printed components..... | 56 |
| A.2. Body panels to cut..... | 59 |
| B.1. Fabrication technologies and tools..... | 65 |
| B.2. Hardware and raw fabrication materials | 66 |
| B.3. Electronic components | 68 |
| B.4. Total costs to build the CMAS..... | 70 |
| E.1. Supplies and tools to fabricate the CMAS form factor | 86 |
| E.2. Parameters that may be modified in Fusion 360 to generate a custom-dimensioned CMAS form factor | 87 |
| G.1. Ingredients to produce Hanks’ balanced salt solution | 90 |

List of Figures

| | |
|--|----|
| 2.1. Existing open peristaltic pump designs were 3-D printed and evaluated | 10 |
| 2.2. Illustrations of the optical enclosure | 12 |
| 2.3. The LED was driven by a digital–analog converter and the photodiode signal was amplified by an operational amplifier | 13 |
| 2.4. The pump and optical sub-modules were secured to a frame to allow their evaluation as a combined module..... | 14 |
| 2.5. The custom peristaltic pump sub-module was prototyped in three iterations | 16 |
| 2.6. Peristaltic pump flow rates of water (solid line), 10% glycerol (long dashes), and 20% glycerol (short dashes) were linearly dependent on signal pulse rate up to 100 Hz (i.e., 100 pulses/s) | 17 |
| 2.7. The optical evaluation sub-module passed through three prototyping iterations | 18 |
| 2.8. Spectral distributions of emissions from the QT-Brightek tri-color (red/green/blue) LED | 19 |
| 2.9. Optical measurements on the POEM of serial dilutions of channel catfish sperm allowed fitting of a regression line..... | 20 |
| 2.10. Calculated sperm concentration in a blind trial correlated closely with known concentration..... | 21 |
| 3.1. 3-D printed components for the CMAS on the build plate of an Ultimaker 3 Extended | 26 |
| 3.2. A sheet of acrylic with laser-cut features on the bed of the laser cutter | 27 |
| 3.3. Exploded views of the second and third versions of the CMAS case as seen in Fusion 360 CAD software | 28 |
| 3.4. Iterative prototyping of the electronic components of the CMAS..... | 29 |
| 3.5. The finite-state machine logic flow that controlled the CMAS..... | 31 |
| 3.6. Design concept for the CMAS..... | 33 |

| | |
|--|----|
| 3.7. The first prototype of the CMAS | 34 |
| 3.8. Demonstration of fluidic pumping and mixing in the first prototype of the CMAS, before addition of optical sensors..... | 34 |
| 3.9. The second prototype of the CMAS | 35 |
| 3.10. The third prototype of the CMAS | 36 |
| 3.11. Spectral absorbance of a sample of the algae <i>Tetraselmis chuii</i> (3.6×10^6 cells/mL) measured on a Nanodrop 1000 spectrophotometer | 37 |
| 3.12. The optical signals from algal samples evaluated on the CMAS of concentration $> 3 \times 10^5$ cells/mL were fitted by linear regression | 38 |
| 3.13. The optical absorbance of the same algal samples as in Figure 3.11, evaluated on a Nanodrop 1000 spectrophotometer ($\lambda = 625$ nm)..... | 39 |
| 3.14. Results of automatic dilutions by the CMAS of algal samples | 40 |
| 4.1. MSLA resin 3-D printing produced geometries comparable to traditional microfluidic fabrication with photolithography..... | 47 |
| 4.2. Specific post-processing steps greatly improved the results of MSLA printing | 48 |
| 5.1. A DIN rail mounting system based on 3-D printing and heat-set threaded inserts | 51 |
| 5.2. The CMAS form factor..... | 52 |
| 5.3. Labeling wires with color-coded shrink tubing | 53 |
| 5.4. A possible elaboration of the operation prototyping phase of device development | 55 |
| A.1. An assortment of CMAS parts printed on the Ultimaker 3 Extended 3-D printer..... | 58 |
| A.2. The two main breadboards of the CMAS | 60 |
| A.3. A DAC IC in a SOT-23 package soldered to an adapter board | 61 |
| A.4. An example of wiring in the CMAS | 62 |
| A.5. Assembling the frame | 62 |

| | |
|---|----|
| A.6. Assembly of the top and front panels..... | 63 |
| A.7. The assembled CMAS | 64 |
| C.1. Circuit diagram of the power supply..... | 71 |
| C.2. Pinout of the Arduino Nano microcontroller platform..... | 71 |
| C.3. Pinouts and circuit diagrams of the MicroSD card module, 2004 LCD module, and rotary encoder..... | 72 |
| C.4. Circuit diagram of an optics module..... | 73 |
| C.5. Circuit diagram of a NEMA 17 stepper motor and its controller module..... | 74 |
| E.1. An exploded view of the elements of the CMAS form factor within the CAD software Fusion 360 | 86 |
| E.2. Illustrations of the customizable parameters in the CMAS form factor..... | 88 |
| E.3. Three variations of the CMAS form factor that are possible with custom parameters | 89 |

Abstract

Repositories for aquatic germplasm can safeguard the genetic diversity of species of interest to aquaculture, research, and conservation. The development of such repositories is impeded by a lack of standardization both within laboratories and across the research community. Protocols for cryopreservation are often developed *ad hoc* and without close attention to variables, such as sperm concentration, that strongly affect the success and consistency of cryopreservation. The wide dissemination and use of specialized tools and devices can improve processing reliability, provide data logging, produce custom hardware to address unique problems, and save costs, time, and labor. The goal of the present work was to develop a low-cost and open-technology approach to standardize the concentration of sperm samples prior to cryopreservation. The specific objectives were to: 1) fabricate and test a peristaltic pump and optical evaluation module (POEM); 2) fabricate and test a prototype of the modular, open-technology concentration measurement and adjustment system (CMAS), which incorporated the POEM; 3) identify opportunities to extend the CMAS to microliter volumes through low-cost resin 3-D printing, and 4) identify strategies from this work that can be applied to future open fabrication efforts. The POEM and CMAS were prototyped and tested with biological samples. A relationship between optical signal and cell concentration of channel catfish (*Ictalurus punctatus*) sperm samples was established by linear regression. In a blind trial, cell concentrations were estimated with the POEM and correlated closely to their known concentrations (linear regression $R^2 = 0.9945$) in a range of 1×10^8 to 4×10^9 cells/mL. The CMAS was able to estimate and adjust the concentration of a sample of the marine microalgae *Tetraselmis chuii* as a preparatory step for cryopreservation. To explore the possible use of the CMAS with microliter sample volumes in future work, evaluation of low-cost resin 3-D printing showed that this technology can approach conventional microfabrication techniques in feature quality and resolution. The development of the CMAS as open technology can provide opportunities for community-level standardization in cryopreservation of aquatic germplasm, invite new users, makers, and developers into the open-technology community, and increase the reach and capabilities of aquatic germplasm repositories.

Foreword

The development of repositories for aquatic germplasm is beset by problems of scale, profitability, standardization, and production capacity. Without resolution of these problems, repositories cannot meet their aim: to preserve genetic resources for future use in aquaculture, biomedical research, conservation, and restoration.

The Aquatic Germplasm and Genetic Resources Center (AGGRC) at the Louisiana State University Agricultural Center, where this work was conceived and executed, aims to support the development of aquatic germplasm repositories through interdisciplinary collaboration in research, technology development, commercial-scale processing, and outreach. It is in this context that the development of open technologies has emerged as an approach to standardize the cryopreservation of genetic resources from aquatic species at a community level.

With the distribution of open-technology devices, designs, and documentation, the AGGRC can promote adherence to standard handling of samples, improve the consistency and value of stored genetic resources, and support the growth of repositories for aquatic germplasm. Open technology encourages makers, researchers, and engineers in aquatic research and adjacent fields to broaden their skills into new disciplines, develop designs that meet specialized needs, and develop interdisciplinary collaborations to combine diverse ideas and skills in pursuit of common aims.

Through a grant from the National Institutes of Health – Office of Research Infrastructure Programs (NIH–ORIP), the AGGRC works as a resource for a network of five national stock centers for biomedical organisms and a central repository of the United States Department of Agriculture (USDA) in Fort Collins, Colorado. The five stock centers are the National Resource for *Aplysia* (NRA, aplysia.rsmas.miami.edu), the *Xiphophorus* Genetic Stock Center (XGSC, xiphophorus.txstate.edu), the Zebrafish International Resource Center (ZIRC, zebrafish.org), the National *Xenopus* Resource (NXR, mbl.edu/xenopus), and the *Ambystoma* Genetic Stock Center (AGSC, ambystoma.uky.edu/genetic-stock-center). The central repository is the National Animal Germplasm Program (NAGP) of the USDA Agricultural Research Service (USDA–ARS, agrin.ars.usda.gov/main_webpage_dev/ars). In this context, the AGGRC aims to establish comprehensive repository systems for *Aplysia* (sea hares), *Xiphophorus* species and *Danio rerio* (small-bodied biomedical fishes), *Xenopus* (clawed frogs), and *Ambystoma* (salamanders), and to serve as a centralized hub to develop documentation, protocols, and pathways for cryopreservation across all five biomedical model systems.

As one avenue to help achieve these aims, the AGGRC is developing dozens of open-technology devices to improve the standardization and reproducibility of cryopreservation processes for aquatic germplasm. Diverse fabrication methods can be used to produce open devices, such as three-dimensional (3-D) printing, laser cutting, and custom electronic breadboard design.

For the AGGRC, the present work is a first venture into a prototyping process that incorporates electronics, laser cutting, and 3-D printing as fabrication approaches in a single device from the beginning of the development timeline. Researchers at the AGGRC have in recent years proposed an iterative prototyping process in which a design goes through several phases¹: 1. *component prototyping*, in which individual components are fabricated, tested independently, and iteratively improved; 2. *operation prototyping*, in which the assembled device is assessed by developers for function, tested with non-biological samples, and improved; 3. *performance prototyping*, in which the device is tested by developers with biological samples

and improved; 4. *early test product (closed)*, in which the device is sent out to a limited set of user–collaborators and evaluators for assessment, and 5. *late test product (open)*, in which the device is distributed to a wider user audience for assessment. The movement through these phases need not be only in one direction: for example, if major problems are identified in the *early test product* phase, development can return to an earlier phase to revise the design entirely, before advancing again to *early test product*.

The work described herein comprises component and operation prototyping of a device (steps 1 and 2 in the process described above). It establishes through biological testing the feasibility of open technology to automate part of the workflow for the cryopreservation of aquatic germplasm. This proof-of-concept can be carried forward in future work to later prototyping phases, in which internal developers and external users test the flexibility, reliability, and usability of this technology in a breadth of laboratory, hatchery, and repository contexts.

This thesis is organized in five chapters. **Chapter 1** introduces essential concepts in repositories, cryopreservation, fabrication, and open technology that are relevant to the subsequent chapters. **Chapter 2** describes the development of a custom peristaltic pump and optical evaluation module (POEM) that evaluates the optical density of aquatic sperm samples and thereby allows the estimation of cell concentration. **Chapter 3** integrates the POEM into the concentration measurement and adjustment system (CMAS), an open-technology device designed to mix sperm samples with extender and cryoprotectant solutions to target sample concentrations prior to cryopreservation. **Chapter 4** explores the possibility of extending the CMAS into microliter sample volumes with recently developed consumer-level, resin-based 3-D printing technology. **Chapter 5** briefly reviews the results of chapters 2–4, presents three fabrication techniques that may be found useful to future efforts in rapid prototyping and open fabrication, and presents conclusions and future directions.

Parts of this work addressing open technology, with the prototyping of the CMAS as a brief case study, were presented at the 2021 virtual meeting of the Louisiana Chapter of the American Fisheries Society under the title “Applying open technology concepts to aquatic research” (oral presentation, Zuchowicz, N. and Tiersch, T. R.). Chapters 1 and 5 are not intended for publication separately from this thesis. Chapters 2 and 3 are intended for publication as peer-reviewed manuscripts.

Chapter 4, with differences and additions relative to the version presented herein, is in preparation as a manuscript for submission (authors: Zuchowicz, N., Semmes, I., Belgodere, J., Liu, Y., Monroe, W. T., and Tiersch, T. R.). This chapter arises from an interdisciplinary effort between researchers at the AGGRC and the laboratory of Dr. W. Todd Monroe in the Department of Biological Engineering (BE) at Louisiana State University. Work in Chapter 4 that was carried out by collaborators from BE is identified as such in the corresponding figure captions.

This thesis follows the formatting guide of the Louisiana State University Graduate School. References are in the commonly used format of the scientific journal *Nature*. Italics are used to indicate binomial names of species and to introduce new terms.

With the development of the CMAS, the AGGRC is reaching into new territory integrating parametric design, multiple fabrication technologies, programming, and electronics. The CMAS will have served its most important purpose, even if it sits dustily on a shelf, if it inspires others at the AGGRC and beyond to tackle complex, multi-technology design projects and carry them through to completion. This thesis thus aims, in part, to lay down a development pattern and a set of design ideas for others to follow.

Chapter 1. Introduction

The successful cryopreservation of sperm requires carefully controlled sample preparation, cooling, storage, and warming before use in fertilization². A cryopreservation protocol should specify the sample container, sperm concentration, cryoprotectant concentration, equilibration time, and cooling curve³. Deviation from any element of the protocol is likely to produce injury to the sperm due to cryoprotectant toxicity or intracellular ice formation during cooling or warming^{4,5}.

For mammalian species, germplasm repositories around the world rely on repeatable, well characterized protocols and technologies to support their operations⁶. Commercial and research repositories must have confidence in their frozen collections. On thawing, a sperm sample must fertilize a known number of eggs or achieve a threshold motility^{7,8}; a sample of vitrified eggs or embryos must reliably produce a viable, growing organism⁹; and a sample of stem cells must be sufficiently intact to be grown out in culture and applied in cellular therapeutics¹⁰.

Unfortunately, in aquatic species many of these important parameters of cryopreservation are not controlled in practice, often owing to limits of budget, time, personnel, or training. This impedes the development of repositories for aquatic germplasm, which in scale and application remain far behind their counterparts for mammalian species¹¹.

With fish and shellfish, the adjustment of sperm concentration before freezing is commonly neglected, even if the concentration itself is measured³. Low sperm concentration may not permit a high enough sperm-to-egg ratio for reliable post-thaw fertilization¹², while high sperm concentration can exceed the protective abilities of the cryoprotectant, leading to agglutination of the thawed sample¹³. Moreover, the optimal sperm concentration for cryopreservation is not a fixed figure. There is some suggestion that species-by-species variation in this optimum may exist¹⁴. For example, in livestock species the Food and Agriculture Organization of the United Nations recommends sperm concentrations at freezing that vary across an order of magnitude, from 1×10^8 cells/mL for buffalo semen to 1.5×10^9 cells/mL for pigs². More importantly, the ‘dose’ of sperm required to fertilize a given number of eggs can vary according to the intended application¹⁵. Samples that are cryopreserved without controlling for concentration are likely to be of variable or poor quality, and thus may waste time, money, genetic resources, and repository space². Adjustment of sperm concentration before freezing is therefore an essential feature of a well-crafted protocol.

The goal of this thesis work was to develop a low-cost and open-technology approach to standardize the concentration of sperm samples prior to cryopreservation. The specific objectives were to: 1) fabricate and test a peristaltic pump and optical evaluation module (POEM) to measure sperm concentration (**Chapter 2** of this thesis); 2) fabricate and test a prototype of the modular, open-technology concentration measurement and adjustment system (CMAS), incorporating the POEM and extending its use to actively adjust sperm concentration (**Chapter 3**); 3) identify future opportunities to extend the use of the CMAS to microliter volumes through low-cost resin 3-D printing (**Chapter 4**), and 4) find applications for this thesis work in the open-technology and aquatic germplasm communities (**Chapter 5**). Each of these top-level objectives served as the goal for one of the research chapters, and each chapter had its own specific objectives to implement that chapter’s goal. This introductory chapter describes key concepts and fabrication approaches that are used in the research chapters: namely cryopreservation, fabrication methods, parametric computer-aided design, and open technology.

Cryopreservation

Cryopreservation is the preservation at cryogenic temperatures ($-80\text{ }^{\circ}\text{C}$ and below) of biological materials that can be stored, warmed, and used in medicine, research, agriculture, and other applications. It was first shown in 1949 that glycerol had a strong cryoprotective effect on fowl spermatozoa¹⁶, allowing the recovery of robust motility following freezing and thawing, but it was also shown that the benefits of glycerol for spermatozoa during freezing varied greatly from species to species. Further work has achieved cryopreservation in red blood cells¹⁷, human oocytes¹⁸, and many other cell types.

Several compounds have joined glycerol as common cryoprotective agents (CPAs), such as dimethyl sulfoxide, propylene glycol, methanol, and trehalose. These confer several benefits in cryopreservation. They depress the melting point of a solution, delaying the onset of ice formation during cooling; they mitigate the high concentration of salts within a cell as it desiccates during cooling, and they stabilize the membranes of cells to prevent rupture². Some may pass easily through the cell membrane, as with dimethyl sulfoxide: these are called *permeating* CPAs. Others cannot pass into the cell, as with trehalose: these are called *non-permeating* CPAs. To avoid the toxicity of a high concentration of any one CPA, solutions can be prepared that include both permeating and non-permeating compounds.

Two broad approaches are applied in cooling protocols for cryopreservation. Each aims to preserve cells in a glassy (vitrified) state, in which little ice crystalline structure is present. The lack of such structure can improve the survival of preserved cells¹⁹. *Equilibrium cooling* (also called slow freezing), which is the dominant approach in the cryopreservation of sperm, relies on the formation of water ice in the surrounding medium to extract liquid water from cells and to increase the effective concentration of CPAs in the unfrozen fraction of the sample until the cells therein reach a glassy state. *Non-equilibrium cooling* (also called vitrification) relies on cooling rates that can exceed $-10,000\text{ }^{\circ}\text{C}/\text{min}$ ²⁰ and a much higher concentration of CPAs (often $\geq 40\%$ by volume²¹) to produce dehydration. It aims to convert the entire sample, both medium and cells, to a glassy state².

In equilibrium cooling, the optimal cooling rate to cryopreserve biological samples is a balance between two harmful effects²². On one hand, a sample that is cooled too slowly will be damaged by excessive dehydration (the *solution effect*) and concomitant reduction in pH. On the other hand, a cell that is cooled too quickly will not desiccate sufficiently to avoid the formation of ice crystals within the cell.

Many factors beyond the choice of CPA and cooling rate will also influence the success of cryopreservation. To give a few examples, the reproductive condition of the adult, collection methods, handling, method of cryoprotectant addition, manner of transportation of frozen samples, and thawing method all may affect the final quality of the cryopreserved sample³.

Evaluation of concentration

Sperm concentration (usually expressed as a number of cells per milliliter, i.e., cells/mL) is usually measured by one of three means: spectrophotometry, as is the practice at the Zebrafish International Resource Center²³; computer-assisted sperm analysis, as is common in agriculture², research^{24,25}, and assisted breeding²⁶ applications; or counting by eye with counting chambers, such as hemocytometers or Makler[®] chambers, viewed on a phase or dark-field microscope, as is practiced at the AGGRC²⁷ and elsewhere.

The cryopreservation workflow

A typical cryopreservation workflow is a combination of manual and automated steps. To collect a sperm sample, one may use relatively non-invasive stripping of the male, as in zebrafish²⁸, or sacrifice the male and dissect the testes, as in catfishes²⁹. Once a sample has been collected, it must be measured and diluted to an appropriate concentration for cryopreservation. Dilution can consist of two steps: in the first, the sample is diluted with an *extender medium* such as Hanks' balanced salt solution (HBSS) to an intermediate target concentration. Sperm of some aquatic species will become active in hypotonic or hypertonic medium, depleting their energy. To prevent this, the extender medium is prepared as isosmotic salt solution that can keep sperm immotile¹¹. In the second step, a solution containing one or more CPAs at double the final target CPA concentration is mixed 1:1 with the intermediate diluted sample to achieve the final cell concentration and final CPA concentration²⁷. This sample may be transferred to containers for freezing.

Various containers are used for cryopreserved samples. A common standard is the 0.25-mL or 0.5-mL French straw, a simple plastic tube that may be filled by suction or injection, and crimped or plugged at each end. This container has the appeal of low cost, readily available standardized storage, and a high surface-to-volume ratio, which enables rapid temperature equilibration with the surroundings, as is generally required during cooling². However, French straws can be difficult and time-consuming to fill and label without expensive automated equipment³.

Cooling devices for filled containers are commercially available in a wide variety. These range from controlled-rate freezers costing tens of thousands of dollars, which draw from a pressurized dewar of liquid nitrogen, to simple floating racks that can support dozens of French straws at a roughly consistent distance above the surface of a bath of liquid nitrogen, cooling the straws in the cold vapor above the liquid². Although these latter racks are inexpensive, they offer less control over the cooling rate, especially if they are cobbled together from foam and spare parts, as is often the case.

As the cryopreservation process combines manual and automatic steps, it has bottlenecks in throughput. These appear at all stages: collection, sample preparation, concentration estimation and adjustment, and freezing³. As the number of distinct samples to be processed increases, more bottlenecks appear, and downstream processes are blocked. The present work concerns itself with relieving bottlenecks that appear in the measurement of cell concentration and in the subsequent dilution of the sample with extender medium and cryoprotectants.

Fabrication Methods

3-D printing: Fused deposition modeling

Fused deposition modeling (FDM), also known as fused filament fabrication (FFF), is a fabrication method that consists of extruding thermoplastic through a heated nozzle onto a build platform. The product is built layer-by-layer by a microcontroller that precisely moves the nozzle as it extrudes a continuous bead of molten plastic. Such printing systems were first conceived in the late 1980s³⁰, but in the past two decades they have entered the mass consumer market and have become a common fixture of classrooms and laboratories. A variety of materials can be printed with FDM printers³¹. Polylactic acid (PLA) is a common beginner's material, but with more sophisticated printers capable of operating at higher temperatures and with more abrasive

materials, advanced users can range into nylons, filaments incorporating carbon fiber or fiberglass, and flexible thermoplastics for pliable parts.

To 3-D print a digital model exported from computer-aided design (CAD) software, the user must first *slice* the model using specialized software that is usually referred to as a *licer*³¹. This software converts the digital model, one layer at a time, into a set of instructions that guide the nozzle of the printer along a series of *toolpaths* to progressively build an object on the build platform. These instructions are referred to as *g-code*, and they must be customized to suit the printer at hand. It is for this reason that digital models for 3-D printing are usually provided in a format such as .stl (stereolithography format) that represents the geometry of the model directly, rather than as finished g-code toolpaths.

3-D printing: Mask-based stereolithography

Resin-based 3-D printing by the focused application of ultraviolet light, known as stereolithography (SLA), was invented in the early 1980s³². The two dominant designs until recent years have been laser-based and digital-light-projection-based stereolithography³³ (often referred to as laser SLA and DLP SLA). Both approaches have been applied to manufacture relatively expensive machines, well suited to the industrial and commercial prototyping markets, but relatively inaccessible to the hobby user.

An increasingly popular approach projects an array of ultraviolet light-emitting diodes (LEDs) through a liquid crystal display (LCD). The LCD functions as a mask that controls the transmission of UV light to the vat of photo-curable resin, hence it is known as mask-based SLA (MSLA or LCD SLA). This technology has the special advantages of low cost, modest learning curve, and mass market appeal. Such printers may cost as little as US\$200, as is true of entry-level offerings from the companies Phrozen (phrozen3d.com), Monoprice (monoprice.com/category/3d-printing-&-hobbies), and Anycubic (anycubic.com). Although resin printing requires more care, cleanup, and post-processing than the FDM approach, it can produce geometries at a far finer scale³⁴. Current FDM printers reach their feature resolution limit around 0.1 mm in the Z-axis (i.e., the up-down axis), but MSLA printers can reach a resolution of 0.01 mm in the same Z-axis.

Laser cutting and engraving

A laser cutter system consists of control software and a powerful commercial laser mounted to a 2.5-axis gantry system. It can be used to cut precise patterns out of certain sheet materials up to a few millimeters thick, or to engrave decorative or functional patterns into the surface of materials. Designs may be exported in .svg, .dxf, or .pdf formats from computer-aided design software and imported into the laser control software.

Raw materials for laser cutting must in most cases be flat, relatively thin sheet stock. A thickness of a few millimeters is ideal, but thicker stock can be cut with several passes of the laser. Commonly available CO₂ laser cutter-engravers can safely be used only with a subset of flat stock materials. Acrylic (polymethylmethacrylate, PMMA) is ideally suited to this work, while polycarbonate and vinyl will not cut cleanly under a CO₂ laser and will emit noxious fumes.

As with FDM and MSLA 3-D printers, laser cutter-engravers have recently become widely accessible to the consumer-level market. However, as with any fabrication technology, laser cutter-engravers have their limitations. A cutting pass leaves a kerf that must be accounted for:

that is, it removes material as it cuts two pieces apart, so designs must account for this loss. Moreover, lasers do not cut perfectly vertical faces: this is especially the case with lower-powered CO₂ lasers. For this reason, a circular hole cut by a laser, e.g., for a machine screw to pass through, will have an entry (upper) diameter different from the exit (lower) diameter. All these factors must be considered in the design and prototyping process.

Parametric Design

Parametric computer-aided design (CAD) allows for flexible and reconfigurable design work. A good CAD package includes parameter-driven sketching and a design history that can be revised to update downstream features ‘later’ in the timeline. Several advanced software packages are popular in industry, such as Creo (PTC, ptc.com/en/products/creo), SolidWorks (Dassault Systèmes, solidworks.com), CATIA (Dassault Systèmes, 3ds.com/products-services/catia), and Inventor (Autodesk, autodesk.com). However, these packages tend to have expensive and restrictive licensing, and the barrier to entry can be high from a training and knowledge perspective. There are also open-source alternatives such as FreeCAD (freecadweb.org), which offers many of the same capabilities, but it is not yet in version 1.0 and is considered under development.

Fusion 360 (Autodesk, autodesk.com) is a relatively recent entrant into the CAD community, but it is rapidly gaining market share in hobby, commercial startup, and educational use. It is the design tool of choice in the present work owing to its straightforward educational license terms and relative ease of use. Autodesk offers no-cost licenses to hobby and academic users, expanding the utility and reach of the native Fusion 360 files that accompany this thesis.

Open Technology

One approach to increasing the scale of sample processing for aquatic germplasm repositories is to take advantage of aggregate throughput. In this approach, samples are processed in smaller batches by many users and are collected and stored at central repositories³⁵. This strategy requires that the community of makers have access to standardized tools and devices. An open-technology approach (that is, one including open hardware and open software), in which design files, instructions, code, and other supporting information are freely provided, can enable dissemination of devices into the community.

The structure of this community can be thought of as threefold: it comprises developers, makers, and users. Developers create designs, code, and documentation; makers reproduce and improve this work; and users apply the work to real-world problems. There are no definite dividing lines between these communities, but certainly members of each can fall along a spectrum of skills and experience. The open-technology project presented here is accessible to developers and skilled makers, but presents a level of complexity, especially in the electronics, that may not be suited to beginners in fabrication and open technology.

The open-technology movement has its roots in software. The term *open source* originated in the software context in the mid-1980s, and is now generally understood to include software whose source code is freely available for inspection, use, modification, and redistribution³⁶. With the recent growth of *open-source hardware*, questions of effective distribution have become more complex³⁷. To make software open source means to provide source code, clear documentation, and a permissive license. To distribute hardware in an equivalent way, the developer must prepare (for example) design files, a bill of materials, a list of suppliers, a guide

to fabrication and assembly, circuit diagrams, and cut patterns. Moreover, there is a monetary cost to building open hardware that is essentially absent in the distribution of software. These problems impede the efficient spread of open hardware, but a developer can compensate by designing for *open fabrication* technologies such as 3-D printing and laser cutting, i.e., technologies that are easily learned, adopted, and applied to new problems by the maker community.

In this thesis, the term *open* is used instead of *open source*. *Open* suggests that enough information is provided to reconstruct the project independently; *open source* implies a level of openness that includes two-way interaction between the developer and the users, wherein the users contribute their ideas and improvements to the project. The CMAS has not yet achieved this level of openness.

Commercial and open-technology peristaltic pumps

In pumping of sterile fluids or those containing biological samples, it is desirable to keep the sample from direct contact with the pumping mechanism. To achieve this, peristaltic pumps use rollers to push fluid through tubing in a manner similar to the action of peristalsis in the human digestive tract. The tubing is pinched between a wall and a moving roller; continuous rotary movement of a gang of rollers pushes a series of pockets of fluid through the tubing. The design usually allows for the tubing to be sterilized or replaced. This approach also allows for finer control of flow rates than is possible with centrifugal pumps, which are common in bulk fluid pumping applications (e.g., tens to thousands of L/h). Due to these advantages, peristaltic pumps see wide use in medical³⁸ and biological research³⁹.

For the application contemplated in this thesis, a peristaltic pump should have easily replaceable tubing, should be inexpensive, and should work well with tubing of internal diameter ~1 mm to reduce dead volume in the device (i.e., fluid volume that is contained in the device and is not accessible for other uses). It is possible to buy a wide range of commercial peristaltic pumps meant for diverse applications, flow rates, and tubing sizes, but often no single pump meets all these needs. The tubing inside an inexpensive pump may be replaced, but not always easily: the pump in most cases must be partly disassembled to remove the tubing. Some commercial pumps allow the easy change-out of tubing, but they are in general designed for tubing of at least 4-mm internal diameter, which leaves too much dead volume inside the pump for the present, low-volume application. Pumps for small volumes are available but they can be expensive: for example, the Takasago Fluidic Systems BCP/RCP Series Ultra-Small Peristaltic Pump was listed by the manufacturer at US\$856 as of 2021, and the fluidic element was available only as a proprietary consumable that integrated the small-bore tubing (internal diameter 0.5 mm) into a plastic frame.

Open-technology peristaltic pump designs are available online. The design-sharing website Thingiverse (thingiverse.com), for example, offers several options with a simple search for ‘peristaltic pump.’ Some of these options are examined in Chapter 2, but all are designed for tubing diameters larger than those contemplated here. In the scientific literature, several designs are again available. Some work at the appropriate fluidic scale, but they rely on specialized fabrication technologies such as soft lithography⁴⁰, which make them unsuitable to open fabrication by a more general audience. Some use fabrication technologies suited to open hardware: the FAST pump⁴¹ is a largely 3-D printed multi-channel system, but it does not allow for a different fluid flow rate in each fluidic channel. Others, including some intended for

microfluidic applications⁴², have flow rates too low for application in the CMAS. However, these open designs make for valuable starting points in the present design.

Open-technology concentration detection

Photometry, measurement of the optical transmittance (or equivalently, absorbance) of a sample, is a common technique in the biological and related sciences. Several open-technology photometers and spectrophotometers have been developed. A 3-D printed chamber to measure cell culture progress⁴³ provides a useful starting point for the electronics and detection systems described in Chapter 2, but it is designed for incubation of a sample in a large chamber rather than the evaluation of fluids in continuous flow through narrow tubing. A USB-connected photometer⁴⁴ has been built around perfluoroalkoxy tubing; it was principally intended for flow chemistry, but a similar approach is suitable for the present application.

The Arduino microcontroller platform

A device that incorporates electromechanical, sensing, and user interface components often incorporates a microcontroller, essentially a small computer, to coordinate the operation of its components. Arduino (arduino.cc) is an inexpensive, open-source electronic development platform that mounts a microcontroller on a printed circuit board (PCB) for use by developers of diverse skill levels. The PCB includes several electronic components, such as a USB interface and a resonator to supply a clock signal, that reduce the number of components the user must include around the microcontroller to make it practically useful. Arduino boards are produced in several variants: larger boards such as the Uno and Mega have more breakout pins and are suited to more elaborate applications, while smaller boards such as the Nano and Micro are more compact, and in some applications such as remote sensing can draw far less power. Arduino and closely related microcontroller platforms are common in open-technology projects such as an open data logger (thecavepearlproject.org)⁴⁵, an open echo-stethoscope (echopen.org), and even an open polymerase chain reaction thermocycler (openpcr.org). This proven power and flexibility of the Arduino as an open development platform is well suited to drive the multi-technology CMAS described in this work.

The Arduino Nano, which was chosen for the present work, offers inter-integrated circuit (I²C) and serial peripheral interface (SPI) communication protocols, allowing the developer to interface cleanly with such common peripherals as liquid crystal display (LCD) screens, microSD storage cards, and various integrated circuits (ICs) such as digital-analog converter chips. It offers 23 input/output pins to allow reading buttons and sensors, sending signals to motors, and other similar functions. It is supported by an array of open-source software libraries, written both by Arduino employees and by users, that simplify common tasks such as controlling motor speed and analyzing simple data.

The Inter-Integrated Circuit (I²C) communication protocol allows short-range communication between ICs over only two wires: data and clock, plus a ground reference, which is typically excluded from the wire count. When several I²C devices are present on a single bus, each 'slave' device must have a unique numerical address by which the 'master' device, such as an Arduino, may address it. Some slave devices have fixed addresses, but many can be configured so that several instances of the same device may be addressed individually. In the context of the CMAS, I²C is used to control a real-time clock, an LCD screen, and five separate

digital-analog converter (DAC) ICs on one two-wire bus. This saves scarce input–output pins for other uses.

Serial Peripheral Interface (SPI) is an alternative to I²C that requires two more wires, but that allows higher data transfer speeds. It is used in the CMAS to write optional log data to a microSD card. Conveniently, microSD cards support SPI natively, so an Arduino can communicate almost directly with it. Only a simple voltage level shifter intervenes (the Arduino works at 5 V, while the microSD card needs 3.3 V).

The finite-state machine

The device described in this chapter combines mechanical, electronic, sensing, and user-interface components. In such a device the programming must be structured, reliable, and logical. The finite-state machine (FSM) is a computational model that constrains the microprocessor to exactly one of a finite number of well-defined states at any moment. For example, the CMAS might be in its top-level menu, or in a system information screen, or in a pump adjustment menu. However, it can only be in one of these states at a given time, and only certain functions may be used in each. The transitions between these states are similarly well defined. To program an Arduino or similar microcontroller with attention to FSM principles is to design modular, easily debugged firmware.

Chapter 2. A Custom Peristaltic Pump and Optical Evaluation Module to Estimate Aquatic Sperm Concentration

Introduction

Cryopreservation workflows have been in continual development since the inception of the field of modern cryopreservation over 70 years ago¹⁶. These workflows support agricultural, conservation, and human health objectives. Protocols and hardware for collection, freezing, and storage are well developed in medicine and in the operation of germplasm repositories for mammalian species². The development of repositories lags far behind in the field of aquatic germplasm³, which includes many species of economic importance and conservation interest.

Important bottlenecks exist in the workflow for processing aquatic germplasm, which limit throughput and inhibit efficient quality control. For example, collection of germplasm from many animals may be slowed by manual steps involving dissection or careful pipetting⁴⁶. The evaluation, dilution, packaging, and cryopreservation of samples from many individual animals can be labor-intensive and time-consuming^{11,46}. Such bottlenecks may be mitigated or resolved through the development of open technology to meet the specialized needs of aquatic cryopreservation.

It is essential that the concentration of sperm be measured and adjusted before cryopreservation³. Without such adjustment, frozen samples may be degraded or of unpredictable quality. This can be due to insufficient cryoprotectant for excessively high cell concentration, resulting in agglutination of the sample¹³. On the other hand, low cell concentration might not result in reliable fertilization⁴⁶. In the absence of diligent quality control, such problems may not be apparent until the samples are thawed decades into the future. A failure of standardization could become a failure to save a species⁴⁷ or to recover a genetic line of interest².

Although some laboratory groups use expensive semi-automated methods such as computer-assisted sperm analysis or spectrophotometry to evaluate sperm concentration²³, others rely on manual counts under a microscope as their principal evaluation method²⁷. Unfortunately, most groups simply neglect to perform concentration measurement and adjustment. A suitable device could replace the manual activities with automatic processes: first, it could replace cell counts by eye with automated optical detection of concentration, improving standardization among technicians and laboratories; second, it could replace manual pipetting with automated pumping, saving effort and reducing errors. Such a device could also provide needed capability to groups that would otherwise ignore sperm concentration.

Therefore, the goal of the work in this chapter was to fabricate and test a peristaltic pump and optical evaluation module (POEM) for estimation of sperm concentration. The specific objectives were to: 1) design and fabricate a low-volume peristaltic pump; 2) evaluate the capabilities of the peristaltic pump; 3) design and fabricate an optical enclosure to measure the cell concentration in fluids passing through tubing, and 4) evaluate the function of the assembled POEM with sperm of the channel catfish *Ictalurus punctatus*. The POEM was shown to reliably pump viscous solutions (up to 20% glycerol) at controlled rates up to 1.1 mL/min, and to be able to estimate the concentration of channel catfish sperm at concentrations between 1×10^8 and 4×10^9 cells/mL.

Methods

Objective 1. Design and fabricate a low-volume peristaltic pump

To begin design work on a custom low-volume peristaltic pump, existing designs were fabricated and evaluated. Three open peristaltic pump designs from Thingiverse were prepared in Cura slicing software 4.9.0 (Ultimaker, Utrecht, Netherlands) and 3-D printed with polylactic acid thermoplastic (PLA) (eSun, Shenzhen, China, esun3d.net) on an Ultimaker 3 Extended (Ultimaker) 3-D printer (Figure 2.1; URLs are provided in the figure caption). Desirable features demonstrated in the existing designs included freely rotating rollers, clamping features to hold the tubing in place, and flexibility in the type of motor used with the pump. Some designs were compatible with any motor meeting the NEMA 17 (1.7" \times 1.7" faceplate) standard, which encompasses a set of motors of varying manufacturer, design, and torque. Several features did not meet the needs of the present work. For example, existing pumps had tubing wrap entirely around the rotor inside the pump, entering and leaving on the same outer face of the pump. A straight-through design would decrease the path length of the tubing and allow for an in-line arrangement of pumping and optical evaluation elements. The tubing that these pumps were designed for was larger (3 mm inner diameter or greater) than the tubing used in the present work.

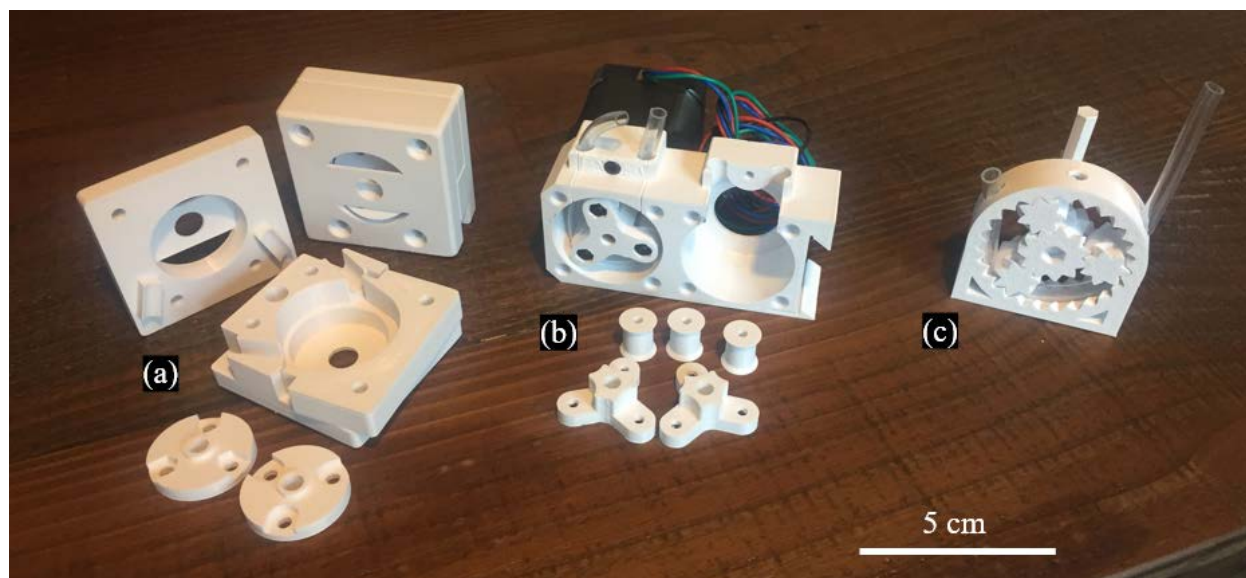


Figure 2.1. Existing open peristaltic pump designs were 3-D printed and evaluated. Features adapted from these pumps into the POEM design included the use of a NEMA 17 stepper motor, two-piece design of the rotor-roller groups, and clamping features to prevent movement of the tubing within the pump. Design files were downloaded from:

- (a) [thingiverse.com/thing:1134817](https://www.thingiverse.com/thing:1134817) (user silisand, license CC BY-NC 4.0);
- (b) [thingiverse.com/thing:1638619](https://www.thingiverse.com/thing:1638619) (user jimmysleep, license CC BY-NC 4.0), and
- (c) [thingiverse.com/thing:1696019](https://www.thingiverse.com/thing:1696019) (user hiuwo, license CC BY-SA 3.0).

Based on these design observations, a custom peristaltic pump sub-module was designed in Fusion 360 parametric computer-aided design software (Autodesk, San Rafael, California, USA; [autodesk.com](https://www.autodesk.com)). Three prototypes of the pump were designed, each improving upon the previous

version. As with the existing open designs discussed above, each prototype was fabricated in PLA (eSun) thermoplastic on an Ultimaker 3 Extended 3-D printer. The methods to assemble the final version of the pump and a list of the materials used are provided in Appendices A and B.

Objective 2. Evaluate the capabilities of the peristaltic pump

The flow rate capabilities of the new peristaltic pump were assessed. The NEMA 17 stepper motors used in the design relied on a continuous train of electrical pulses to increment their position (and so rotation), pushing fluid through the pump. The correlation between this pulse rate and the fluidic flow rate through the pump was evaluated with four deionized-water–glycerol solutions at 22 °C: 100% water, 10% glycerol (Sigma Life Science, St. Louis, MO, USA) in 90% water by volume, 20% glycerol in 80% water by volume, and 100% glycerol. With each solution, eight different pulse rates were assessed (10, 30, 50, 75, 100, 125, 150, and 200 Hz), and each pulse rate was assessed three times. A 30-cm length of tubing was inserted into the pump and primed with solution by running the pump manually. The pump was operated at the given pulse rate for 60 s and the pumped solution was directly collected in a tared plastic weigh boat. The mass of the pumped solution was measured on an AE 166 DeltaRange balance (Mettler-Toledo, Columbus, Ohio, USA; mt.com). The pumped volume was calculated from the measured masses and the specific gravities given in Table 2.1. The resulting flow rates (mL/min) were plotted.

Table 2.1. Properties of four water–glycerol solutions used in testing the peristaltic pump. Viscosities were obtained by linear interpolation of values in the literature⁴⁸ (available at 20 and 30 °C) to obtain estimates at 22 °C. Specific gravity of glycerol was obtained from the label of the glycerol container; other specific gravities were interpolated.

| Solution | Viscosity (cP) | Specific gravity (g/mL) |
|-------------------------|----------------|-------------------------|
| 100% water | 0.9641 | 1.000 |
| 10% glycerol, 90% water | 1.254 | 1.025 |
| 20% glycerol, 80% water | 1.678 | 1.050 |
| 100% glycerol | 1252 | 1.250 |

Objective 3. Design and fabricate an optical enclosure to measure cell concentration

To evaluate the optical transmittance of fluidic samples, it was necessary to design an enclosure that would exclude ambient light and incorporate a light-producing and a light-measuring element. An existing design⁴³ for measuring the optical density of fluidic samples in a closed chamber was studied and adapted for use in measuring fluidic samples flowing through narrow tubing. A custom optics housing was developed as a 3-D printed enclosure (Figure 2.2).

A three-color light-emitting diode (LED) (QT-Brightek 5-mm tri-color round lamp, part number QBL8RGB60D0-2897, qt-brightek.com) was chosen as the light source for the optical evaluation sub-module. This LED had four electrical connections: a common anode and a separate cathode for each of the three colors. The LED was therefore able to produce red (according to the manufacturer datasheet, peak $\lambda = 624$ nm), green ($\lambda = 525$ nm), or blue ($\lambda = 470$ nm) light with changes only to the electronics, rather than by changing of the LED. Only red light was used in this work; the other two colors were left as options for future work.

The LED spectral distributions were measured and each distribution of *full width at half maximum* (a common measure of the width of the distribution) was determined. The emissions of

the three LED colors were captured on a USB2000 UV-vis spectrometer (Ocean Insight, Orlando, FL, USA) using OceanView 2.0.8 software (Ocean Insight) and plotted.

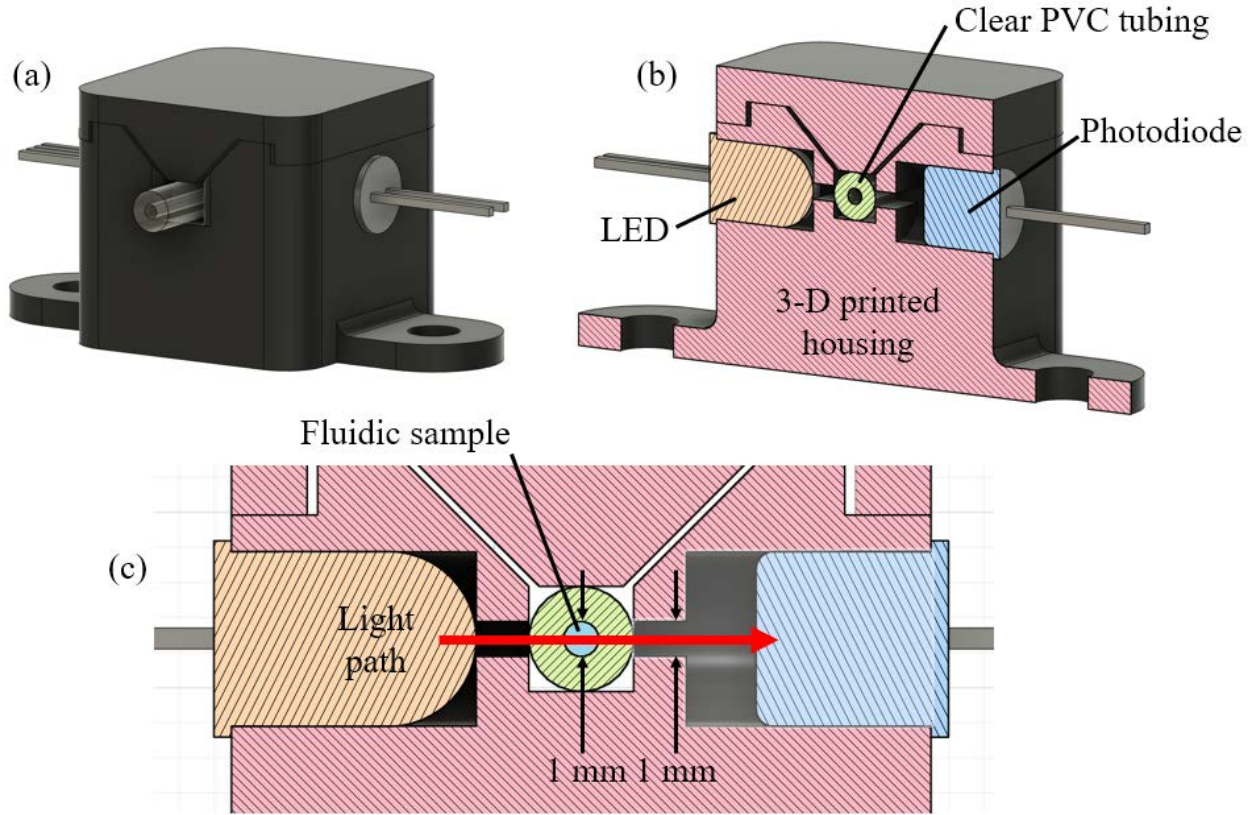


Figure 2.2. Illustrations of the optical enclosure. (a) The optics housing was designed to measure light passing through a sample in clear PVC tubing. The LED, photodiode, and tubing were enclosed in a 3-D printed housing to exclude ambient light. (b) A cutaway illustration to show internal features. (c) Light (red arrow) passed from a light-emitting diode (LED), through the walls of the tubing and through the sample, to a photodiode. Note that the tubing internal diameter and the slit through which light was admitted were each 1 mm.

A silicon PIN (p-type–intrinsic–n-type) photodiode was chosen as the optical sensing element⁴³ (Osram Opto Semiconductors, part number SFH 203, osram-os.com). This component was connected in reverse bias, i.e., with the cathode connected to the positive voltage, in series with a fixed resistor to form a voltage divider. The voltage, relative to signal ground, at the node between the photodiode and the resistor varied according to the incident light on the photodiode. This voltage could therefore be measured by logic circuitry to infer the brightness of the incident light. The sensitivity of the photodiode to the LED emission wavelengths was checked in the photodiode datasheet from the manufacturer: this indicated a relative spectral sensitivity corresponding to the LED wavelengths of approximately 70% (red light, $\lambda = 624$ nm), 50% (green, $\lambda = 525$ nm), and 35% (blue, $\lambda = 470$ nm). The photodiode had peak spectral sensitivity, i.e., 100%, at $\lambda = 850$ nm.

To control the brightness of the LED, a digital–analog converter integrated circuit (Microchip Technology, part MCP4725A0) was connected to the anode of the LED

corresponding to the red LED element. The signal from the photodiode was sent through an operational amplifier (Microchip Technology, part MCP6002) integrated circuit set up for a gain of $A = 20\times$. The circuit diagram for both is shown in Figure 2.3.

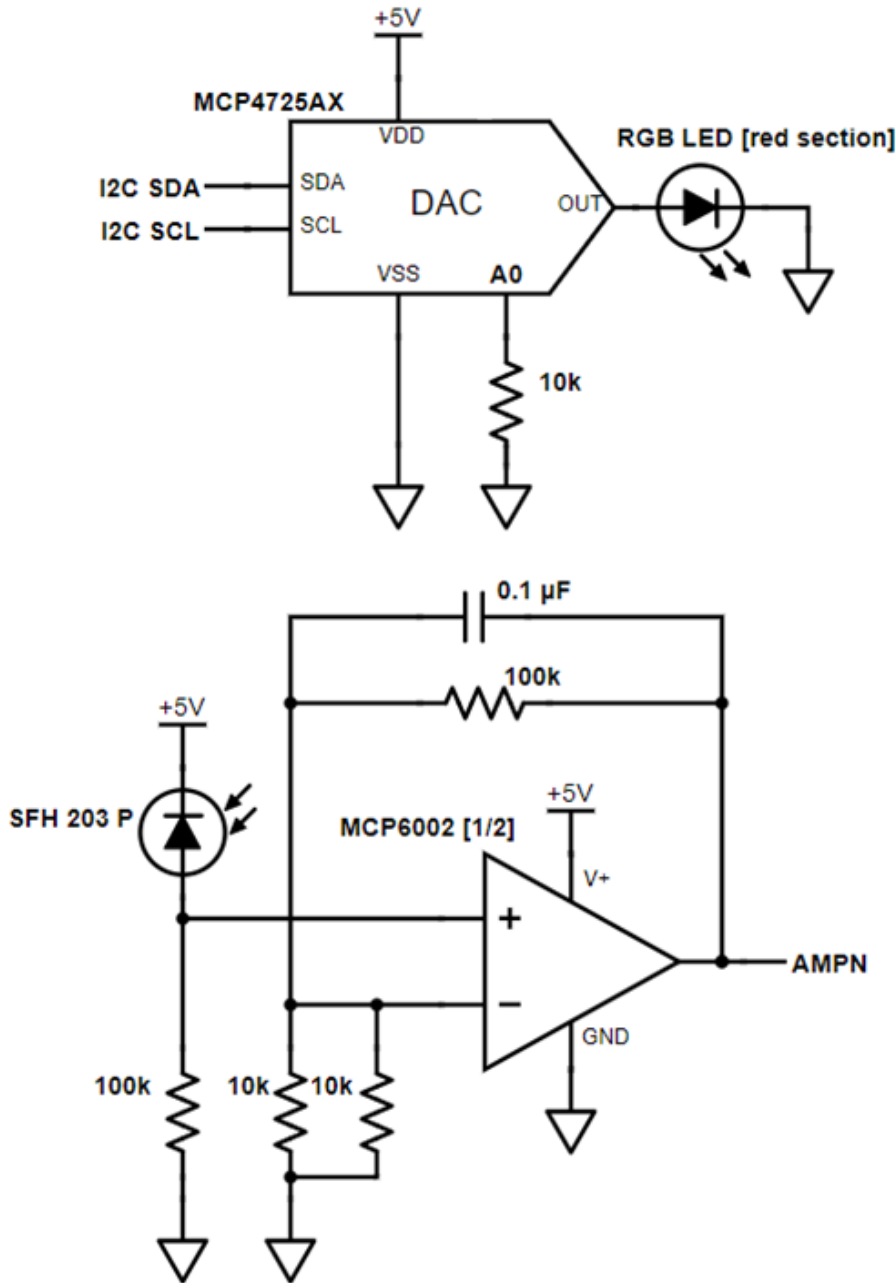


Figure 2.3. The LED was driven by a digital–analog converter and the photodiode signal was amplified by an operational amplifier. See Appendix C for complete circuit diagrams.

Objective 4. Evaluate the function of the assembled POEM with sperm of the channel catfish

To evaluate the sensitivity and performance of the POEM with sperm samples from channel catfish, the peristaltic pump sub-module and the optical evaluation sub-module were attached to a single frame (Figure 2.4). This allowed the pump to actively draw fluidic samples into the optical sub-module for evaluation.

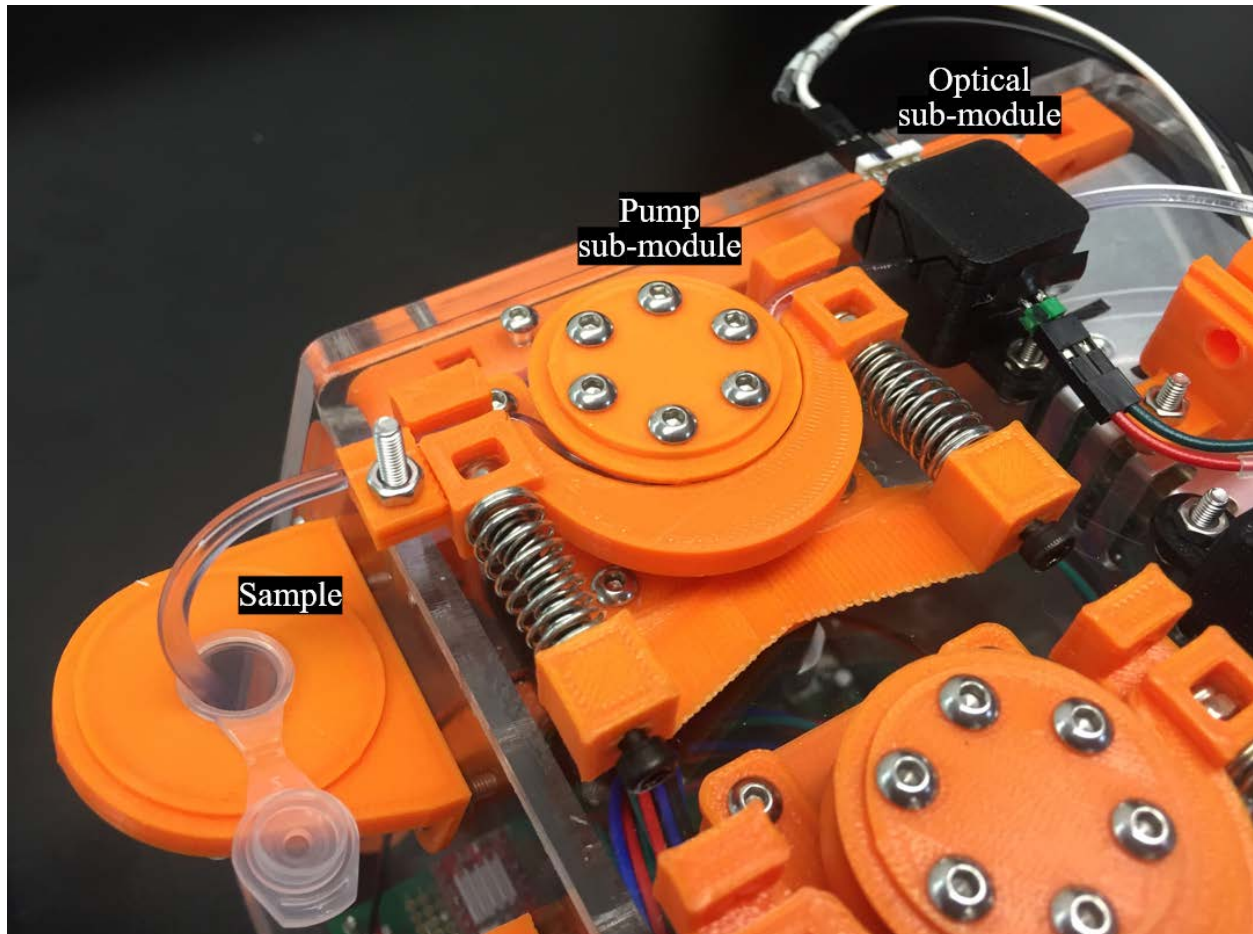


Figure 2.4. The pump and optical sub-modules were secured to a frame to allow their evaluation as a combined module.

To allow dilution of catfish sperm samples in isotonic solution, Hanks' balanced salt solution was prepared according to the instructions in Appendix F. The osmolality of the HBSS was measured and adjusted to 301 mOsm/kg by use of an Osmette III freezing point osmometer (Precision Systems, Natick, Massachusetts, USA).

Male channel catfish were supplied on June 2 and 3, 2021 by the United States Department of Agriculture station at Stoneville, Mississippi and processed on the same day that they were received. All animals were handled in accordance with protocols approved by the LSU AgCenter Institutional Animal Care and Use Committee. The catfish were killed by a blow to the neurocranium. The testes from each catfish were dissected, cleaned by removing excess tissue and blood clots, and weighed. The testes from each animal were placed in a small plastic bag with 1 mL of HBSS per 1 g of testis mass. The testes were folded into a small square of window

screen wire mesh and crushed inside the plastic bag until coherent tissue was no longer visible, thereby releasing sperm into the HBSS. The mesh was removed with the bulk of the crushed tissue inside it. The sperm solution was filtered through a 100- μ m filter into a 50-mL Falcon tube. The sample from each male was kept in a separate tube, each marked with a tracking number. A small aliquot for evaluation was removed and diluted in a ratio of 100:1 (HBSS:sperm solution). The diluted aliquot was pipetted into a Makler[®] counting chamber (Sefi-Medical Instruments, Haifa, Israel; sefimedical.com) and the concentration of sperm of the undiluted sample was estimated by visual counting of the diluted samples and calculation. (For the channel catfish assessed, $n = 54$, mean body mass 2.35 ± 0.79 kg (mass ± 1 standard deviation), mean body length 50 ± 5 cm, mean initial sperm concentration $3.1 \pm 1.4 \times 10^9$ cells/mL, mean mass of dissected testes 8.95 ± 4.34 g).

To evaluate the response of the photometer to different concentrations of sperm, a series of dilutions of sperm samples was prepared from a single catfish (fish tracking number CCFH21M027, 'Belle Prairie' origin, body mass 1.77 kg, body length 46 cm, mass of dissected testes 9.62 g). This fish was chosen because it provided a high concentration of sperm, a large volume of sample (> 30 mL) in excess of that required for cryopreservation and other experiments, and low contamination with blood (as determined visually) compared to other samples. Calculating from the diluted aliquot, the undiluted concentration of this sample was estimated to be 4.0×10^9 cells/mL. Ten 0.5-mL samples were prepared in all, each of a different cell concentration. The first was an aliquot of the undiluted sample; the second sample and onward were prepared by 1:1 serial dilution of undiluted sample with HBSS. The ten serially diluted samples were therefore estimated to have concentrations of 4.0×10^9 , 2.0×10^9 , 1.0×10^9 , 5.0×10^8 , 2.5×10^8 , 1.3×10^8 , 6.3×10^7 , 3.1×10^7 , 1.6×10^7 , and 7.8×10^6 cells/mL.

Clean, empty polyvinyl chloride (PVC) tubing (McMaster-Carr item 3774N1, durometer 55A, inner diameter 1 mm, outer diameter 3 mm) was inserted into the optical evaluation sub-module. The brightness of the LED was calibrated by manually adjusting the voltage produced by the DAC. The aim was to produce a baseline output voltage from the operational amplifier (i.e., the output voltage with empty tubing) of 1.50 V. This value was chosen from testing (data not shown) indicating that using this voltage as a starting point, a deionized water sample produced an output voltage of approximately 4.1 V, while a sample of undiluted blue food dye (Spice Supreme food color, Gel Spice Co., Bayonne, New Jersey, USA), which permits very little transmission of red light, produced an output voltage of approximately 0.5 V. It was anticipated that all practical fluidic samples would fall between the optical density of deionized water and that of undiluted blue food dye. With these settings, no practical sample would saturate the bottom or top of the output range (i.e., approach 5 V or 0 V). Such saturation would make it impossible to distinguish between samples of different concentration within the saturated range. The ten diluted sperm samples were pumped through the POEM (one 'pull' from each sample tube from highest to lowest concentration, and this series was repeated four times) and the resulting signals were recorded. Between samples, HBSS was used to flush the tubing. The recorded signals were plotted against the calculated cell concentrations, and a best-fit linear regression was determined in Excel (Microsoft Excel for Microsoft 365 MSO 16.0 64-bit).

To verify the predictive power of the equation obtained by linear regression, a new set of ten dilutions of sperm from the same male catfish was prepared, with two replicates of each. These samples were labelled and randomized by a collaborator. The correspondence between sample number and 'known' concentration was recorded but hidden from the author (i.e., a single-blinded evaluation). The samples were evaluated with the POEM and the concentration of each

sample was estimated by use of the equation determined above. The estimated concentrations were plotted against the ‘known’ concentrations.

Results

Objective 1. Design and fabricate a low-volume peristaltic pump

The first version of the pump, 3-D printed in white PLA (Figure 2.5a), incorporated six roller bearings in the rotor. Compared to conventional three-roller pumps, this approach increased the number of points of contact between the rotor and the tubing. This in turn allowed the tubing to pass directly from one side of the pump to the other, eliminating the requirement to have the tubing wrap around the rotor completely, entering and exiting the pump on the same side, as was the case in some existing designs. The pump was designed to fit a NEMA 17 stepper motor, chosen for its high torque and precisely controllable rotation (as contrasted with a direct current motor, which normally has no precise rotational feedback or control). The stepper motor was driven by a generic A4988 driver board, which greatly simplified the interface between the motor and the microcontroller used to drive it.

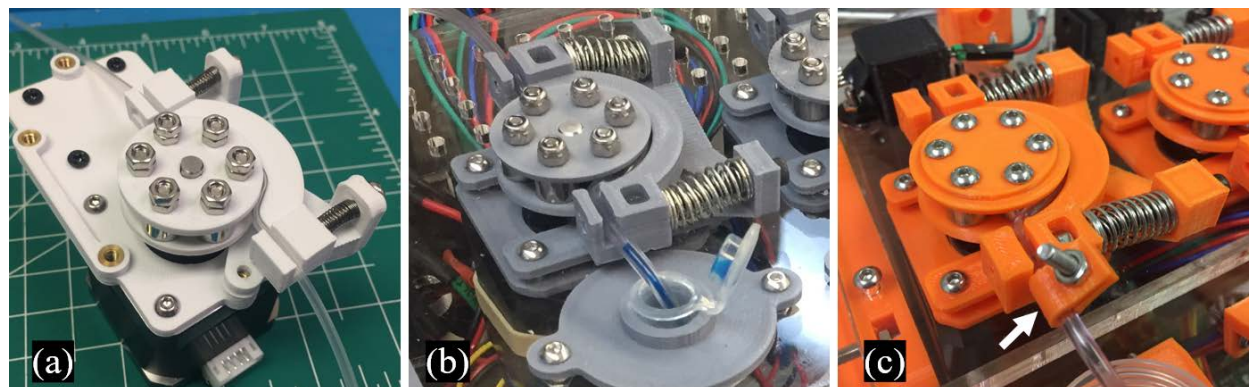


Figure 2.5. The custom peristaltic pump sub-module was prototyped in three iterations. All versions were designed to be driven by a NEMA 17 stepper motor. (a) The first version was designed on a 3-D printed mount meant for attachment to metal DIN rails, common in networking and power cabinets. (b) The second version featured stronger springs and was designed to mount onto a clear acrylic panel. (c) The third version featured a strengthened frame and a redesigned rotor assembly. A tubing clamp, indicated by a white arrow, prevented tubing from being drawn into the pump.

The second version of the pump, 3-D printed in gray PLA (Figure 2.5b), incorporated strengthened compression springs to improve compression of the tubing to increase the reliability of the pumping action. The third version, 3-D printed in orange PLA (Figure 2.5c), added a small clamp to hold the tubing in place to prevent it from being drawn into the pump during operation, more robust frame elements to prevent bending of the frame under spring forces, and an improved rotor design that prevented the rotor from slipping down the shaft of the stepper motor.

Objective 2. Evaluate the capabilities of the peristaltic pump

Pumping water, 10% glycerol, and 20% glycerol, the pump flow rate increased linearly with the signal pulse rate up to 100 Hz, after which the correlation deviated sharply from the linear

relationship (Figure 2.6). At a pulse rate of 200 Hz, a chattering sound in the motor was heard, suggesting that the motor was not responding reliably to the fast pulse train. With 100% glycerol, no linear relationship between pump flow rate and signal pulse rate was observed. The pump flow rate increased up to a pulse rate of 100 Hz, but it increased more slowly as the pulse rate approached 100 Hz. At a pulse rate of 100 Hz, the peristaltic pump was able to pump deionized water at a flow rate of 1.13 mL/min. This rate was slightly increased with 10% glycerol (1.23 mL/min) and 20% glycerol (1.16 mL/min), and greatly reduced with 100% glycerol (0.64 mL/min).

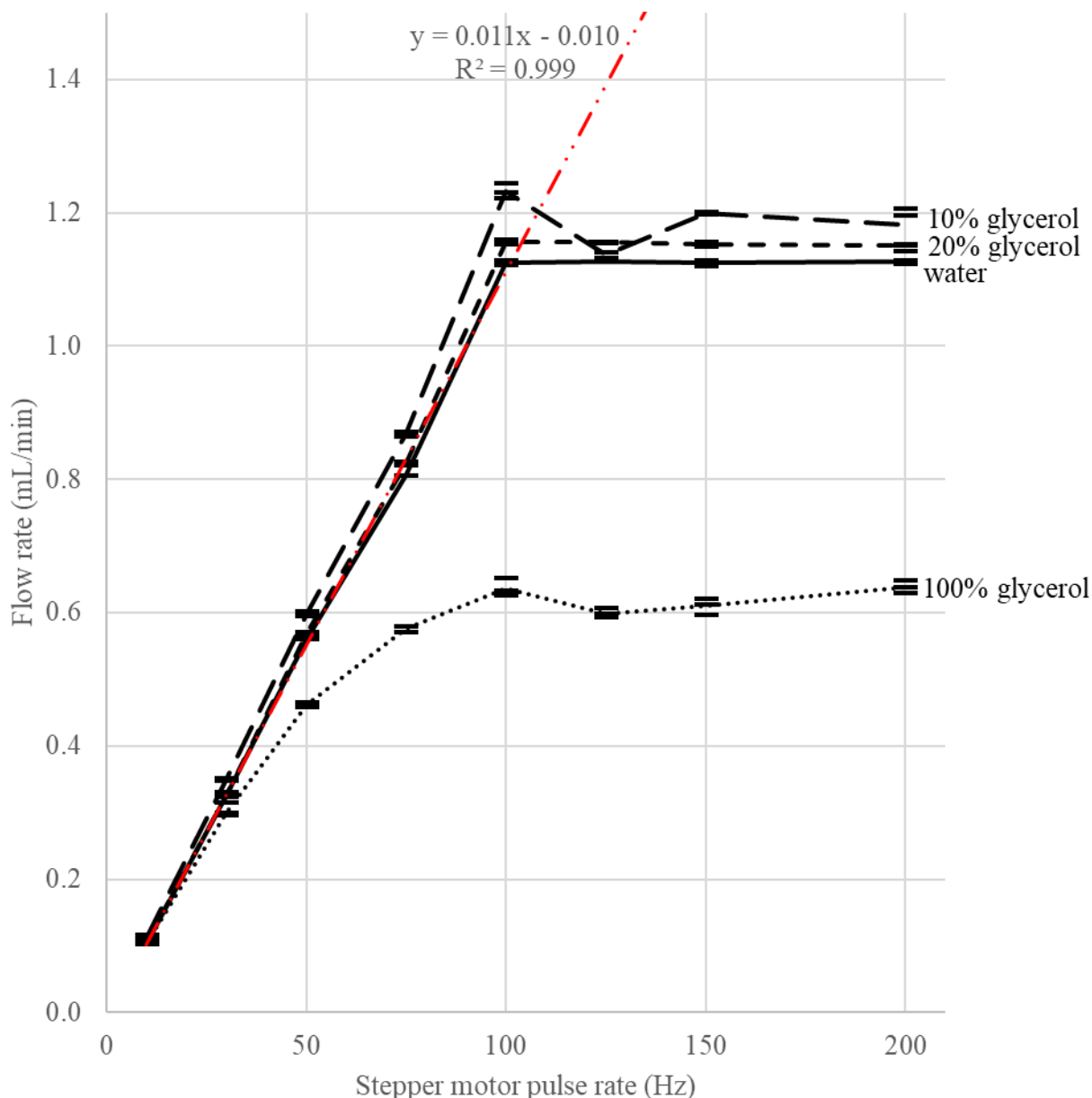


Figure 2.6. Peristaltic pump flow rates of water (solid line), 10% glycerol (long dashes), and 20% glycerol (short dashes) were linearly dependent on signal pulse rate up to 100 Hz (i.e., 100 pulses/s). Water: $y = 0.011x - 0.010$, $R^2 = 0.999$; 10% glycerol: $y = 0.012x - 0.017$, $R^2 = 0.998$; 20% glycerol: $y = 0.012x - 0.016$, $R^2 = 0.998$. All linear regressions were calculated with only

the data points from 10 to 100 Hz. Flow rate plateaued for all solutions above 100 Hz. The flow rate of 100% glycerol (dotted line) was visibly nonlinear with increasing pulse rate up to 100 Hz ($y = 0.006x + 0.104$, $R^2 = 0.937$). Individual data points, three points per solution per pulse rate, are represented by short horizontal dashes. Long black solid and broken lines join the mean values for each solution at each pulse rate. The red broken line is the linear regression of the data points for water from 10 to 100 Hz, with the equation of the line and goodness-of-fit indicated on the plot.

Objective 3. Design and fabricate an optical enclosure to measure cell concentration

As with the peristaltic pump sub-module, the optical evaluation sub-module passed through three prototyping iterations. The first prototype (Figure 2.7a) was fabricated in white plastic and was of a simple design that permitted light to travel through the full thickness of the tubing on its path from the LED to the photodiode. The second prototype (Figure 2.7b) was designed to exclude more light. In particular, the openings on either side of the tubing, through which light passed from the LED and into the photodiode, were narrowed to 1 mm, the same width as the internal diameter of the tubing. This restricted the light used for measurement to pass mainly through the flow path of the sample. The third prototype (Figure 2.7c; same design as shown in Figure 2.2) was designed with mounting holes, allowing it to be bolted to a frame. It was printed in black PLA thermoplastic to exclude as much light as possible. It also incorporated a snap-fit lid to allow easy replacement of tubing.

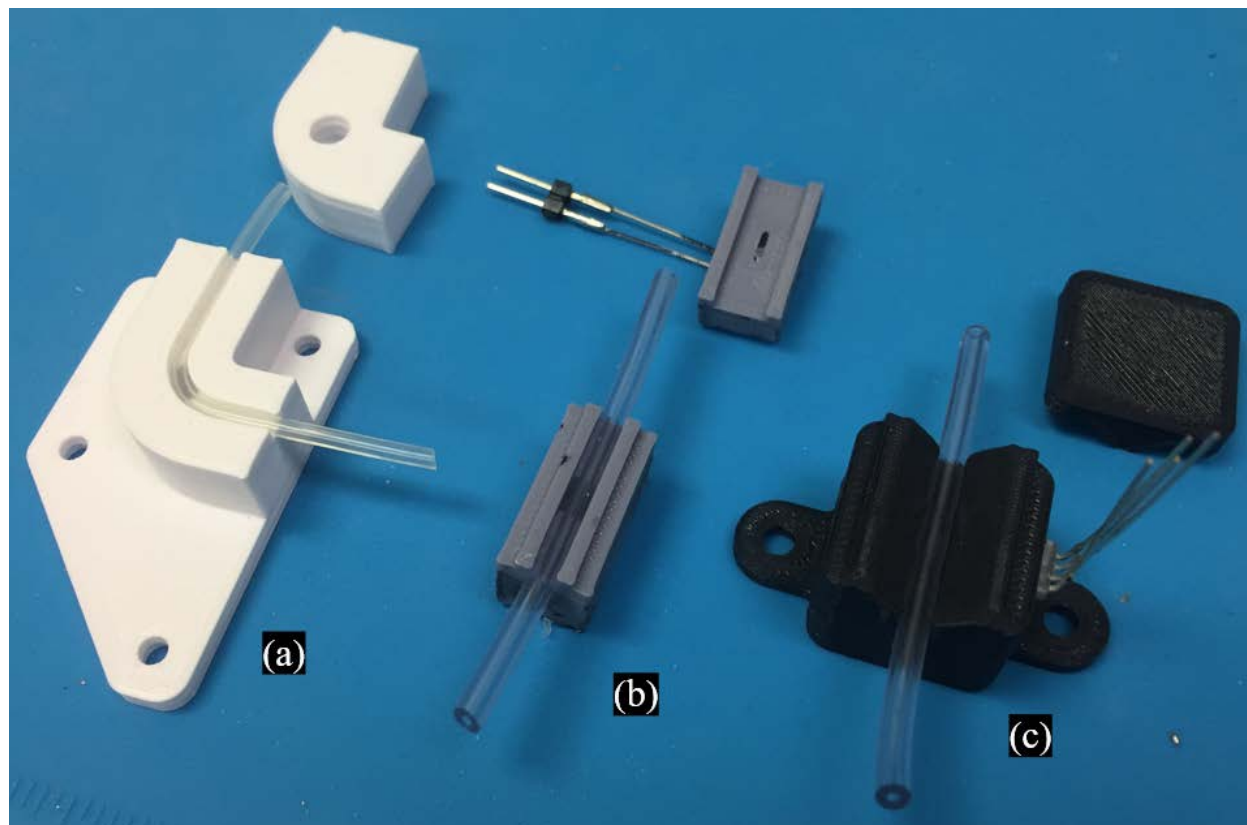


Figure 2.7. The optical evaluation sub-module passed through three prototyping iterations. Each version consisted of two parts that mated together to enclose a length of tubing containing fluidic samples. (a) The first version was a simple channel incorporating holes for placement of an LED

and a photodiode. (b) The second version included narrower slits above and below the tubing to limit the transmission of light to the internal diameter of the tubing. (c) The third version was fabricated in black plastic to exclude ambient light and incorporated a snap-fit lid.

The LED emission spectral distributions (Figure 2.8) showed sharp peaks at $\lambda = 462$ nm (blue), $\lambda = 523$ nm (green), and $\lambda = 624$ nm (red). These peaks corresponded closely to those provided in the manufacturer datasheets, with the exception of the blue peak, which was measured at 8 nm lower than the peak in the datasheet.

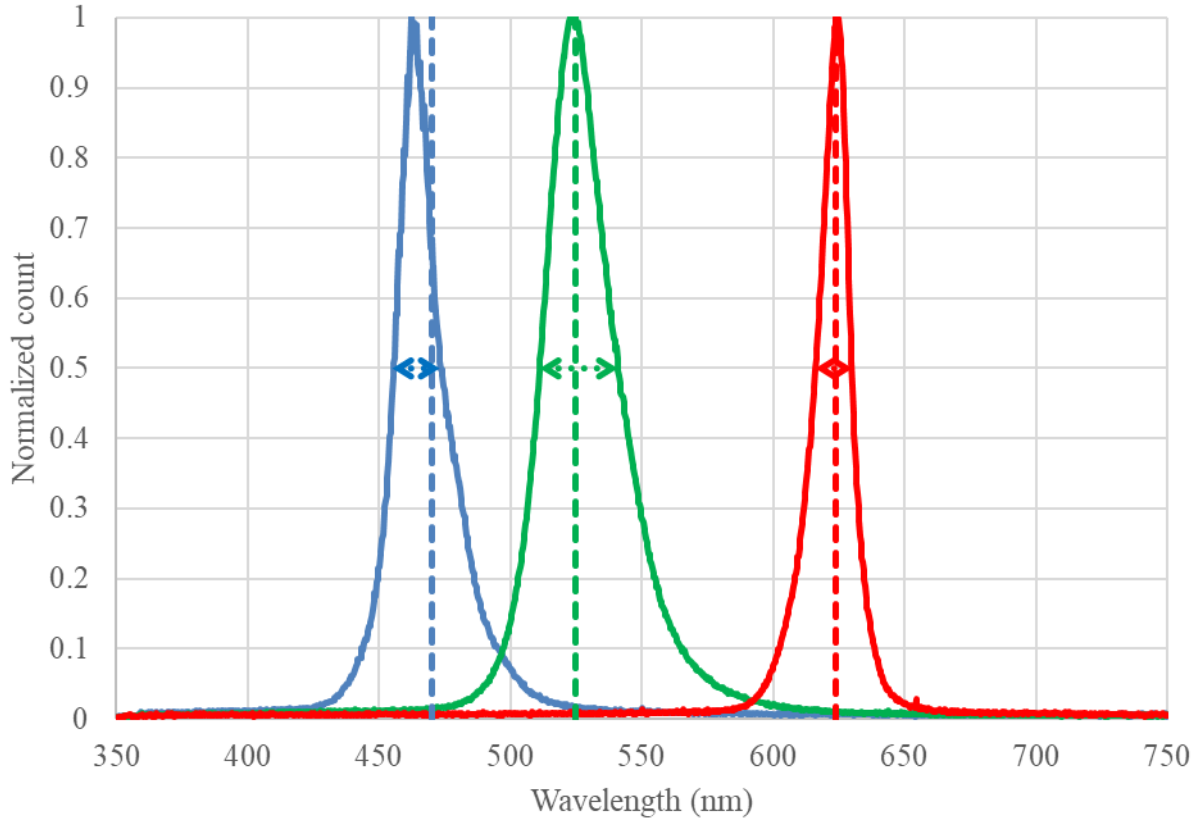


Figure 2.8. Spectral distributions of emissions from the QT-Brightek tri-color (red/green/blue) LED. Vertical dashed lines indicate the nominal peak wavelengths given by the manufacturer datasheet. Horizontal dashed lines capped with arrows illustrate the full width at half maximum (FWHM) bandwidths. Each distribution is normalized (peak emission count = 1). Blue nominal peak $\lambda = 470$ nm; measured peak $\lambda = 462$ nm; FWHM = 22 nm. Green nominal peak $\lambda = 525$ nm; measured peak $\lambda = 523$ nm; FWHM = 30 nm. Red nominal peak $\lambda = 624$ nm; measured peak $\lambda = 624$ nm; FWHM = 14 nm.

Objective 4. Evaluate the function of the assembled POEM with sperm of the channel catfish

The ten serially diluted sperm samples (Figure 2.9a) produced sensor voltages (i.e., the output voltages from the operational amplifiers) that were plotted against their concentrations (log scale; Figure 2.9b). A linear regression was fitted for all concentration values above 10^8 cells/mL. The equation of the best fit line was found to be $y = -1.9658x + 19.702$ ($R^2 = 0.9937$).

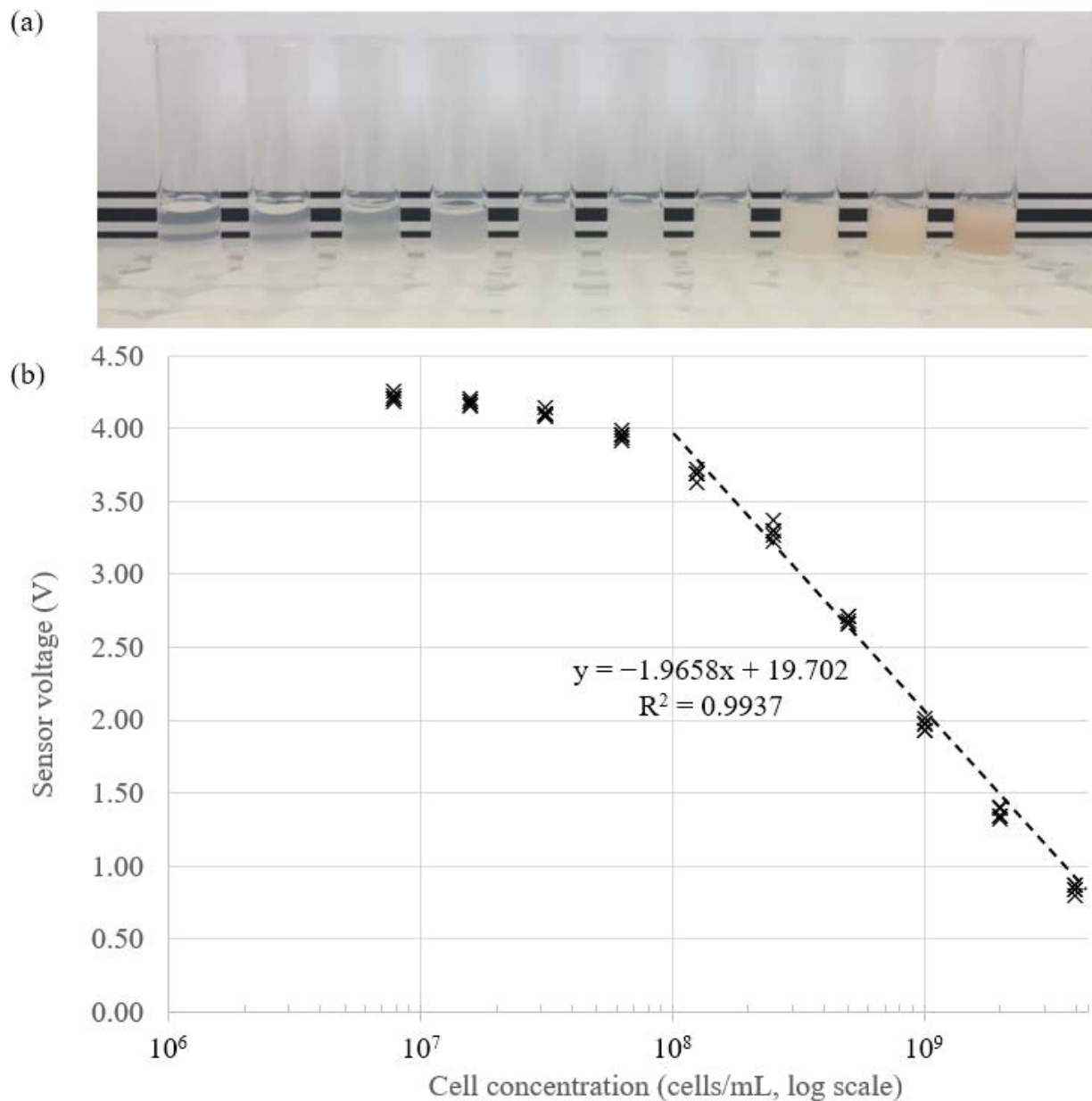


Figure 2.9. Optical measurements on the POEM of serial dilutions of channel catfish sperm allowed fitting of a regression line. (a) Serial dilutions of sperm are shown, ranging from most dilute (7.8×10^6 cells/mL) at left to the starting concentration (4.0×10^9 cells/mL) at right. A faint red discoloration is visible in the high-concentration aliquots due to blood present in the sample, a normal artifact of the collection method. A sheet of paper with black lines was placed in the background to help demonstrate the increasing opacity of the samples. (b) Sensor voltage from the POEM optical evaluation sub-module was plotted against calculated cell concentration based on serial dilutions on a log scale. All data points (5 per concentration) were plotted. A regression line was fitted to all data points $> 10^8$ cells/mL. The left-to-right order of samples in (a) matches the order of the data points in (b), but this does not reflect the order in which the samples were measured (see Methods).

In the blind concentration estimation trial, the cell concentration corresponding to each optical signal measurement was estimated from the inverse of the equation of the line derived in Figure 2.9, i.e.,

$$\text{cell concentration} = 10^{[10 - (0.508 \times \text{sensor voltage})]}$$

The records from the blind trial were opened, and the ‘known’ sperm concentration was plotted against that calculated from the POEM data (Figure 2.10). The known and calculated concentrations were found to correlate closely above a cell concentration of 10^8 cells/mL, but samples below that concentration threshold (5×10^7 cells/mL) were not clearly distinguishable from 1×10^8 cells/mL.

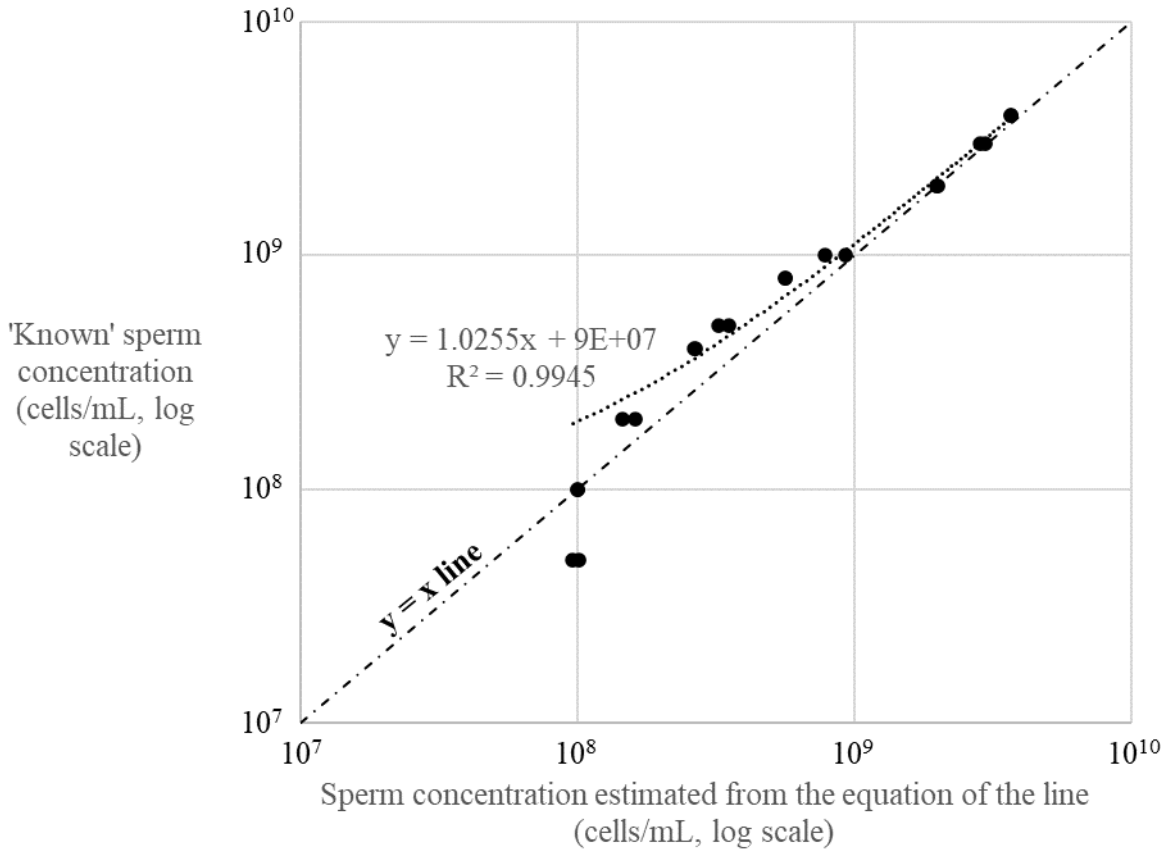


Figure 2.10. Calculated sperm concentration in a blind trial correlated closely with known concentration. A point falling exactly on the $y = x$ line would indicate an exact match between the known dilution of the sample and the value produced by calculations with data from the POEM. A linear regression was fitted to all concentrations $\geq 10^8$ cells/mL. The points corresponding to samples at 5×10^7 cells/mL appeared on the plot directly below the samples at 1×10^8 cells/mL, suggesting that the POEM may have reached the lower bound of its sensitivity at 1×10^8 cells/mL.

Discussion

The frame of the pump in early prototypes proved vulnerable to material fatigue and failure during use over several days. This was likely due in part to narrow features used in the frame, stress risers (i.e., sharp inside corners) in the design, and the constant spring force exerted on the frame. These early failures were largely rectified in later versions by designing and printing a more robust frame. Future work could test and further improve the robustness of the frame to prevent fatigue over weeks and months of use at points placed under frequent or constant stress.

The 6-roller design for the pumps permitted the tubing to enter and exit the pump on opposite sides of the roller gang, which was a desirable feature to reduce dead volume inside the pump. However, with more rollers in contact with the tubing, the force applied by each roller necessarily was less, as was the pushed volume of fluidic sample per length of tubing, in comparison to an equivalent 3-roller pump, due to the increased proportion of tubing under compression within the pump. A redesign to an intermediate number of rollers (4 or 5) could increase the pressure applied to the tubing by each roller, and so might permit the use of less forceful springs to engage the rollers with the tubing, in turn mitigating the stress and material failure problems mentioned above.

The pump stepper motor was not able to respond reliably to signal pulse trains at a frequency of greater than 100 Hz, in turn limiting the maximum fluid flow rate through the pump. This limitation might be mitigated by increasing the tubing diameter or the diameter of the rotor that drives flow through the tubing. Alternatively, other stepper motors or motor control circuitry could be investigated.

With a control signal pulse rate up to 100 Hz, the pump responded linearly to increased pulse rate while pumping water, 10% glycerol, and 20% glycerol. Glycerol is among the most viscous cryoprotectants in common use and 10–20% CPA solutions by volume are typical in cryopreservation of aquatic sperm^{49–51}. This result demonstrated that the flow rate of the pump could be controlled reliably while pumping the most viscous solutions that the pump is likely to encounter in applications in cryopreservation.

It was found while troubleshooting the digital–analog converter (DAC) that the output pin, which powers the LED, is internally limited to approximately 12 mA. The tri-color LED is rated for a typical forward current of 20 mA per color channel. Passing this higher current through the LED could be useful for measuring sperm samples of very high concentration (and therefore of low optical transmittance) by increasing the brightness of the LED. To improve the current sourcing from the DAC, one could use an operational amplifier set up as a unity gain voltage follower: that is, the operational amplifier could maintain the output voltage of the DAC while sourcing more current than is available directly from the DAC. The MCP6002 operational amplifier is a good candidate because it is already in use in this project; it can source over 20 mA. To drive a larger load, one could either buffer the MCP6002 with a transistor on the output, or pick a higher-current (but likely more expensive) operational amplifier.

The assembled POEM was evaluated with biological samples. The optical evaluation submodule was shown to be sensitive to cell concentration in a range from 1×10^8 cells/mL to 4×10^9 cells/mL. This corresponded to a useful range in the workflow for cryopreservation of sperm of fishes of biomedical and aquacultural interest^{15,27,52}. Of 60 channel catfish evaluated at the AGGRC in 2021, only three had a pre-dilution sperm concentration exceeding 5×10^9 cells/mL. At the bottom of the useful range of the POEM, the nonlinearity of signals from samples below 10^8 cells/mL was similar to that seen in previous work on photometry of oyster sperm samples⁵³. In the context of this catfish sperm evaluation and freezing work, the target

concentration for cryopreservation was 1×10^9 cells/mL after addition of extender medium and cryoprotective agents. The POEM therefore was found to cover a cell concentration range that by design allowed measurement of sperm concentration at any point throughout the collection, evaluation, and concentration adjustment workflow for sperm of the channel catfish.

The POEM has possible applications in supporting the improvement of catfish genetic lines. The Warmwater Aquaculture Research Unit (United States Department of Agriculture—Agricultural Research Service) uses cryopreserved sperm of blue catfish (*Ictalurus furcatus*), channel catfish, and hybrids of the two species to enhance efforts in traditional animal breeding and genomic selection, resulting in greater harvest body weights⁵⁴. Samples from superior sires are banked to enable future breeding work, prevent the loss of valuable genetic resources, and ultimately increase the ease and profitability of catfish farming. Hybrids cannot be produced efficiently in breeding ponds due to behavioral and physiological reproductive barriers, but rather must be produced in vitro, with the aid of hormone-induced spawning of the females and dissection of the male gonads⁵⁵. In this commercial–industrial context, increased efficiency in processing, multiplied across thousands of samples and many years of effort, can improve profits and incentivize the cryopreservation of samples from promising genetic lines. As the POEM is developed further, it could be integrated into such workflows, enabling more rapid, efficient, and standardized assessment and preparation of samples for freezing.

Conclusions

The work in this chapter showed that a 3-D printed, custom-built pumping and optical evaluation module could consistently evaluate the concentration of sperm samples of channel catfish in a range of cell concentrations that is relevant to cryopreservation workflows. This design and future derivative open designs can support standardization in the evaluation and dilution of aquatic germplasm samples. These designs can be distributed for fabrication and use by a wide community of researchers and technicians. This, in turn, can help improve the consistency, quality, and value of samples stored in repositories for aquatic germplasm.

Chapter 3 discusses the work done to integrate the POEM into a more complex device, the concentration measurement and adjustment system (CMAS), which expands the fluidic handling and concentration evaluation functions of the POEM into the active adjustment of cell concentration in preparation for cryopreservation.

Chapter 3. A Concentration Measurement and Adjustment System to Prepare Aquatic Germplasm for Cryopreservation

Introduction

Cryopreservation of animal germplasm has developed over the past half-century into a vital tool to support biomedical research and agriculture. In commercial-scale processing and human health care, strong financial and regulatory incentives have led to carefully standardized processing of cryopreserved sperm samples^{56,57}. The cattle industry is a well-developed model: frozen French straws of bull semen can be sold for thousands of dollars each, and so collection, freezing, and storage methods are well established and carefully followed⁵⁸. By contrast, in aquatic species it is common for each laboratory or sperm bank to use its own locally developed methods⁵⁹. Thus, a lack of standardization makes it difficult to reliably share samples among sites; it also greatly decreases the utility and ease of use of large collections of germplasm that are drawn from many species and contributors.

This problem is particularly severe in species that are of little utility to agriculture and industry, but that are nonetheless ecologically important. In conservation, there is a pressing need to preserve the genetic diversity of imperiled species⁶⁰, but efforts are often hampered by modest funding, lack of trained personnel, and limited access to germplasm (e.g., owing to restricted or unpredictable breeding seasons⁶¹). The usual aim, to capture the greatest possible wild genetic diversity before it is lost, is different from that of the cattle model, where technicians bank as much material as possible from a small number of desirable sires⁵⁸. In addition, very few aquatic protocols developed at the research level have been scaled up to commercial and industrial processes³. To achieve this scaling, protocols and hardware must be standardized. Development of a repository support community could produce technologies to increase the throughput and reliability of cryopreservation and its related processes.

Conservation of corals gives a concrete example of how technology can assist processing for repositories. Corals have restricted reproductive windows amounting to a few hours each year over one, two, or a few days⁶², and many species in the same geographical area may spawn on the same nights or even simultaneously^{51,63}. It thus becomes a race to cryopreserve the sperm from dozens of distinct individuals of one or more species. Each sample must be assessed for motility and concentration, diluted with cryoprotectant, distributed into containers, and frozen. These steps typically entail prolonged, manual handling. Material is often left to decline in motility before it can be processed, or it is wasted entirely. Automation of the handling steps could reduce waste, improve throughput, permit preservation from a greater number of individuals, improve the reliability and audit trail of processes, and increase the value of frozen samples.

Such challenges and opportunities cut across species and fields. Researchers working with fish and amphibian species have likewise identified the need for automation, especially in the pre-freeze processing steps, where the requirement may be for dozens of distinct samples to be evaluated and packaged into hundreds or thousands of containers in the space of a few hours. In one of a few high-throughput applications in aquatic species, the Aquatic Germplasm and Genetic Resources Center annually evaluates and cryopreserves the sperm of 50–100 channel catfish (*Ictalurus punctatus*) or blue catfish (*Ictalurus furcatus*) males over a three-day period. Executing this task requires a great deal of training, specialized equipment exceeding

US\$250,000 in total, and roughly 200 person-hours of effort. Customizable, inexpensive devices to improve efficiency and reliability are urgently needed.

The goal of the work in this chapter was to design, fabricate, and test a modular, low-cost, open-technology device to detect the concentration of a sperm sample and dilute it with an extender medium, cryoprotectant solution, or both, to a specified concentration. The specific objectives were to: 1) compose a process diagram illustrating the relationships between the components; 2) assemble the peristaltic pump and optical evaluation module (POEM, described in Chapter 2), with other components including a case, power supply, and logic and user interface components to form the concentration measurement and adjustment system (CMAS), and 3) evaluate the operation of the assembled system with biological samples. The components of the CMAS were found to operate as a cohesive device, and the CMAS was found to be capable of estimating the concentration of algal samples and diluting them as a proof-of-concept for integration in a cryopreservation workflow.

Methods

Objective 1. Design a process diagram

Key features of the cryopreservation process as carried out at the AGGRC^{15,27} and in other groups performing cryopreservation of aquatic germplasm^{14,64} were identified from the literature. Manual steps were identified that were commonly employed in the estimation and adjustment of sperm concentration in preparation for cryopreservation. A diagram illustrating the functional components needed to carry out essential sensing, pumping, and recording functions was created. This diagram informed the development process and was used as a guiding document throughout development.

Objective 2. Prototype the CMAS

The pumps, case, and optical housings to be used in the CMAS were designed in Fusion 360 CAD software (Autodesk). The 3-D designs of the pumps, case frame, and optical housings were exported in a standard format (.stl) to allow 3-D printing. The flat design patterns for the exterior panels of the CMAS case were exported from Fusion 360 to .dxf format, which contains vector data indicating the patterns to be fabricated by laser cutting.

All 3-D printed components were prepared in Cura slicing software 4.9.0 (Ultimaker, Utrecht, Netherlands) and printed on an Ultimaker 3 Extended (Ultimaker) FDM printer. All parts were printed in polylactic acid (PLA) thermoplastic (eSun, Shenzhen, China, esun3d.net). The parts were color-coded to make the changes between versions apparent: the first version was 3-D printed in white PLA, the second in gray, and the third in orange. PolySupport filament (PolyMaker, Shanghai, China) was used as an underlying raft material to improve the bed adhesion and reliability of prints (Figure 3.1). Parts were printed at 0.15-mm layer height with PolySupport support geometry where needed, such as on the pump rider arms, which had overhangs that would otherwise be unsupported.

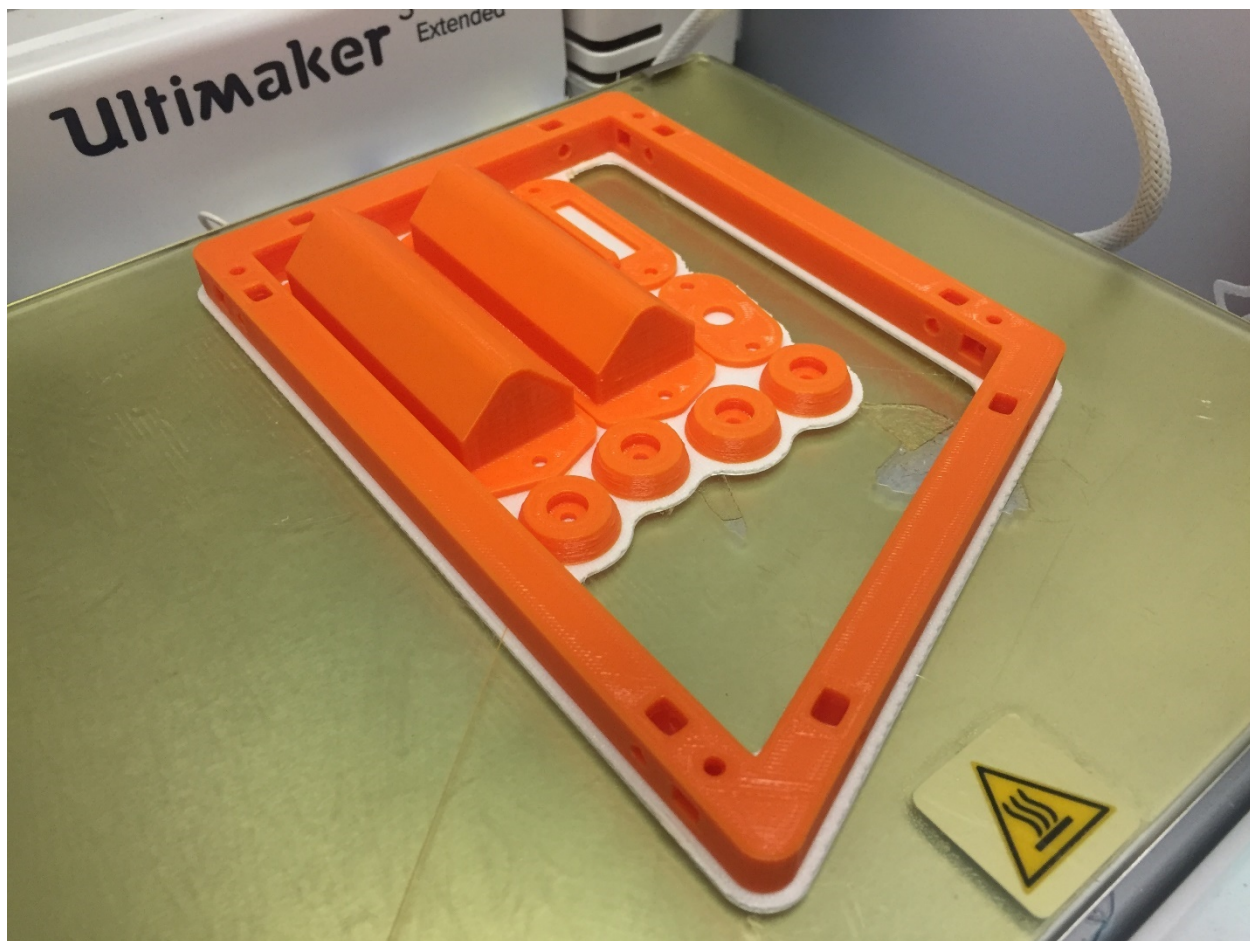


Figure 3.1. 3-D printed components for the CMAS on the build plate of an Ultimaker 3 Extended. The orange material is PLA thermoplastic, and the white material is a PolySupport filament raft.

The .dxf files were imported into Inkscape, a free vector image manipulation program, and exported from there into .pdf format, which can be used directly by the Muse 1064-nm CO₂ laser cutter (Full Spectrum Laser, Las Vegas, Nevada, USA). Parts were cut from 6-mm-thick clear polymethylmethacrylate (PMMA, generally called acrylic) in vector cutting mode. Cutting was performed with three passes at 50% speed, 100% power, and 100% current (Figure 3.2). The algorithm that determined the order of cuts presented an inadvertent problem. If the user requested that three passes be made in one cutting operation, the laser lingered on small features and carried out all three passes on the one feature consecutively. For the 3-mm holes that were used as bolt through-holes in this design, the sustained heating melted the central slug of waste material in place, preventing its removal. This was solved by running each cutting operation three times without moving the stock, rather than running a single operation with three passes. This approach allowed sufficient cooling time between passes to permit removal of waste material.

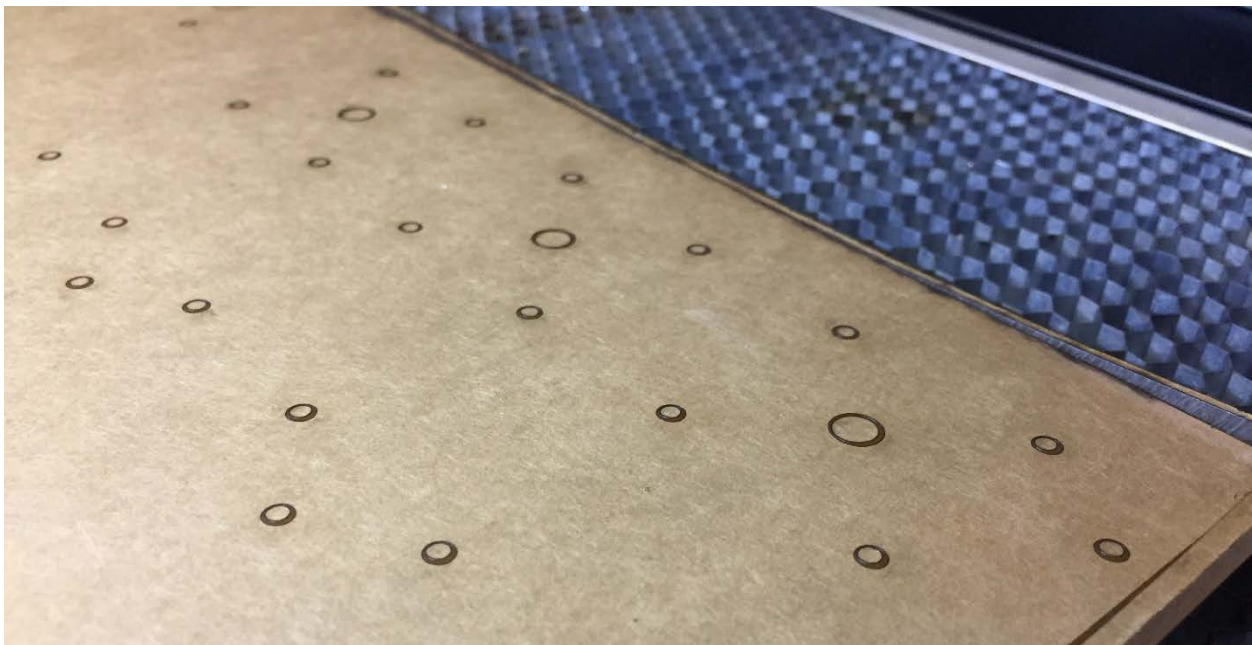


Figure 3.2. A sheet of acrylic with laser-cut features on the bed of the laser cutter.

A case for the CMAS was assembled to protect electronic components, mount pumps and tube holders, and keep wiring organized. As with the other components, the case went through a series of design iterations. The earliest version was a simple assembly of components clipped to metal DIN rails (as illustrated in Results). The second and third versions (Figure 3.3) used 3-D printed and acrylic frame components as described above.

The CMAS comprised many electronic components; the full circuit diagrams are provided in Appendix C. The electronics were assembled at first on solderless breadboard and were transferred to soldered breadboard as the design progressed (Figure 3.4). An A4988 stepper motor driver board was used to drive each NEMA 17 stepper motor. This board acted as a convenient buffer between the 5-V Arduino logic and the 12-V motor power supply. The driver board also handled the four-wire control sequence required by these stepper motors, presenting to the microcontroller a simple two-wire interface consisting of a ‘step’ line, which was pulsed to

increment the position of the motor shaft, and a 'direction' line, which directed clockwise or counter-clockwise rotation.

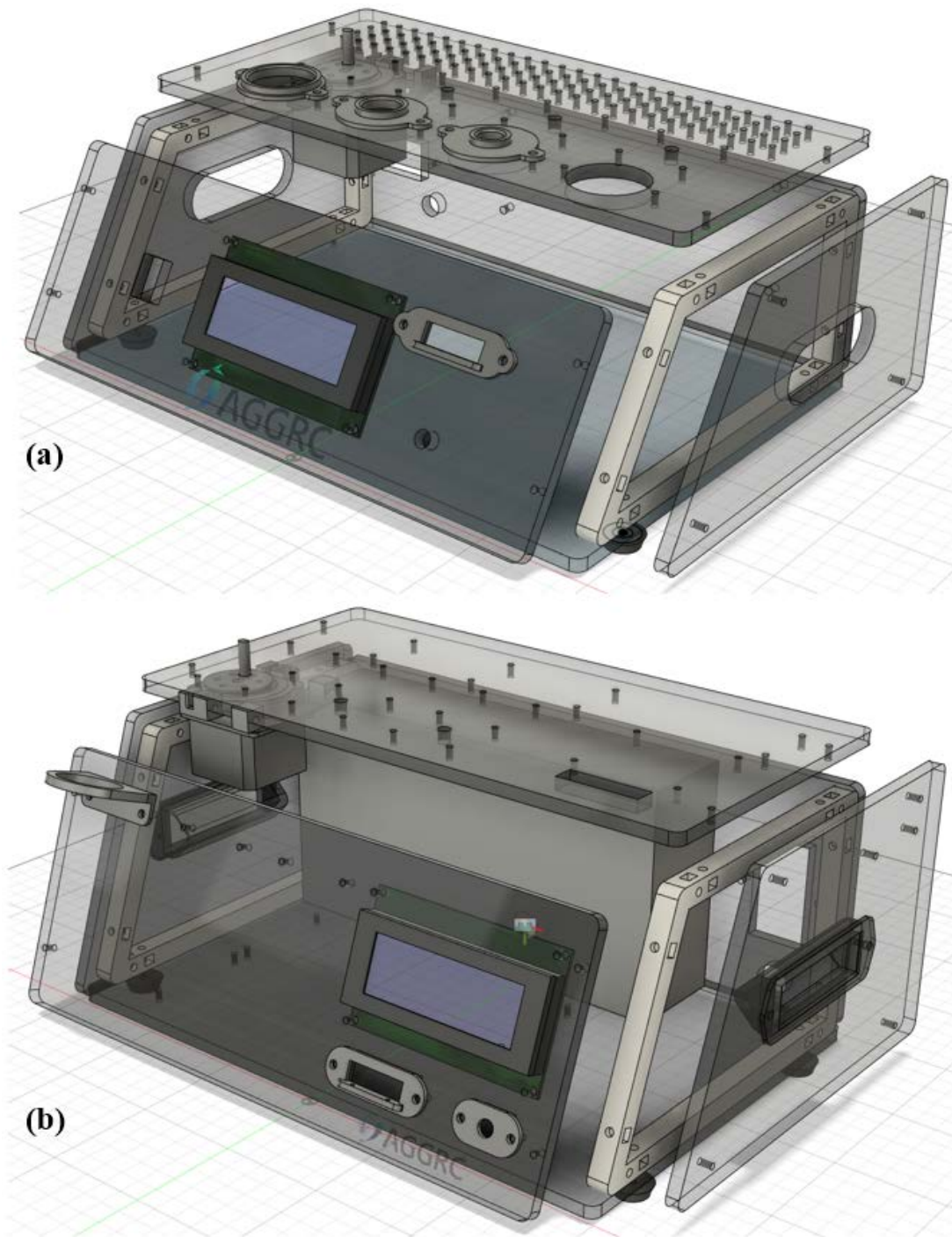


Figure 3.3. Exploded views of the (a) second and (b) third versions of the CMAS case as seen in Fusion 360 CAD software. A parametric design approach allowed for adaptation of the casing to accommodate changes in components and layout. Note the AGGRC logo on the front of the case,

which was produced by laser etching following laser cutting. The second version improved the layout of tube holders, shifted the user interface components away from the fluidics, and enclosed a power supply inside the case.

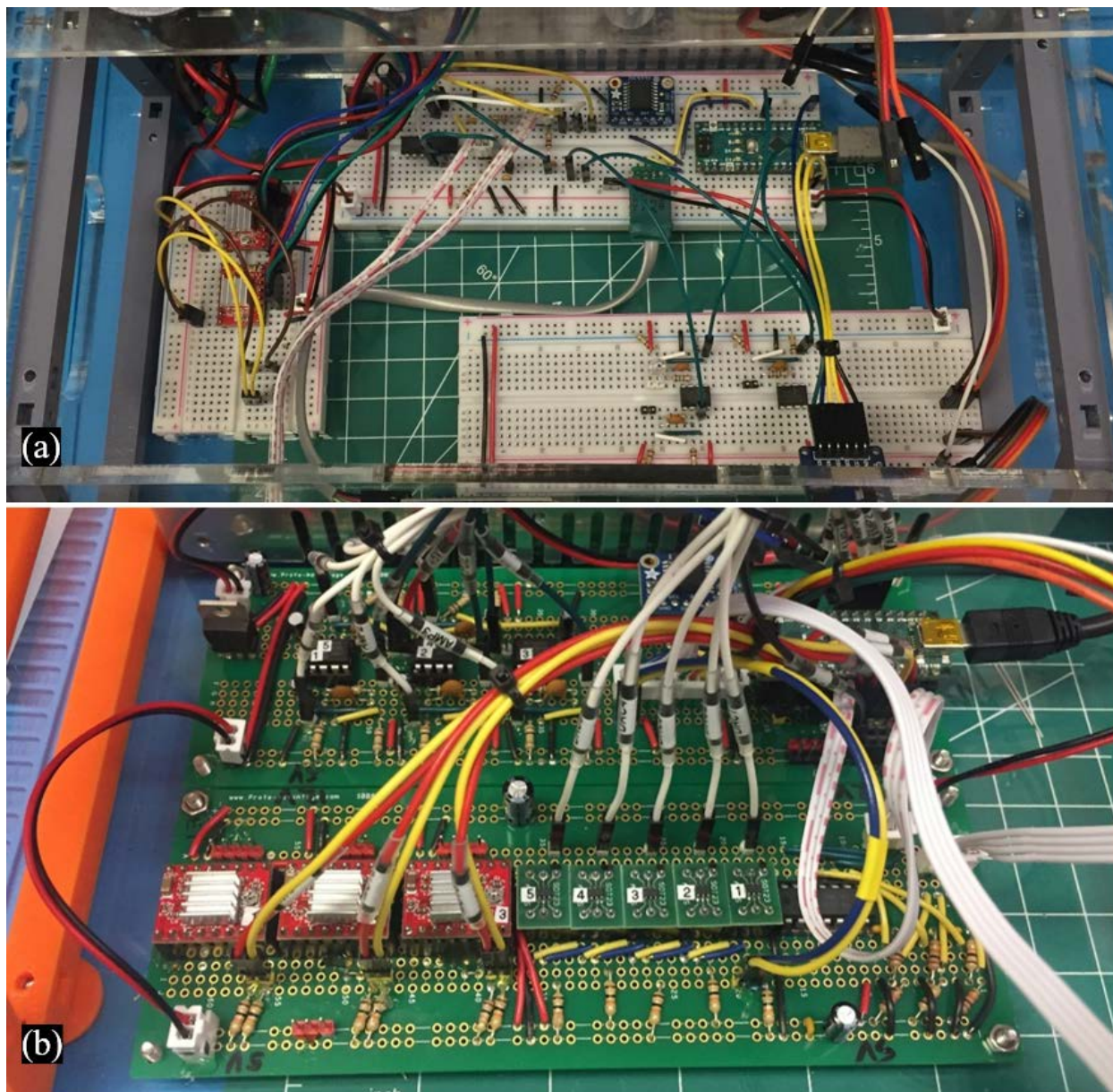


Figure 3.4. Iterative prototyping of the electronic components of the CMAS. (a) An early version was implemented on solderless breadboard, while (b) the final version described here was mounted on soldered breadboard.

To run three stepper motors along with the electronics, more power was required than could be provided by many typical consumer-level AC–DC power adapters. Power was therefore supplied by a generic 360-W (12-V, 30-A) switching power supply typically used to power 3-D printers and similar projects. One 12-V output from the power supply was connected directly to the A4988 stepper motor driver boards to power the stepper motors. A second 12-V output was routed to an LM7805 linear voltage regulator to supply 5 V to all other electronic components.

The peristaltic pump and optical evaluation module (POEM), described in Chapter 2, was integrated into the CMAS. In the implementation of the CMAS described here, only the red channel of the tri-color LEDs was used, but the other two colors were left as options for future development and experiments. It was desirable to tune the brightness of each LED. Because Arduinos have built-in analog-to-digital converters (ADC) but not digital-to-analog converters (DAC), a MCP4725 DAC IC was used to drive each LED, converting a 12-bit digital input signal from the Arduino into an analog voltage to run the LED. Each MCP4725 achieved a voltage resolution of about 1.2 mV ($5\text{ V} / 4095$, where 5 V is the supply voltage) and the input signal could take any of $2^{12} = 4096$ discrete states.

As described in Chapter 2, to receive the light signal a SFH 203 photodiode was included in a reverse bias configuration⁴⁰. An MCP6002 operational amplifier was used to amplify the photodiode signal by a factor of $A = 20$ before sending it to an ADC on the Arduino.

A DS3231 real-time clock breakout board (Adafruit Industries, adafru.it) was added to allow the logging of time-stamped events to the microSD card. This clock IC offered several advantages: a simple I²C communication interface to the microcontroller; an onboard CR1220 coin cell battery (3 V) that can run the clock for several years without external power; correction for environmental temperature; and low time drift (minutes per year).

Custom firmware for the CMAS was written to mediate among the various electronic and electromechanical components. The firmware was written in the Arduino flavor of the C++ programming language in Arduino integrated development environment software version 1.8.13 (arduino.cc/en/software). The architecture of the firmware followed finite state machine (FSM) principles (Figure 3.5) to promote modularity and to help prevent locking the software into inescapable loops during runtime. The full Arduino code is provided in Appendix D.

User interface components were included to allow the user to read data from the device and control the pumping and measurement functions. A 20×4-character LCD screen, a push-button/rotary encoder with a Schmitt trigger debounce circuit to remove mechanical button noise, and a microSD card breakout board were added as user interface components.

Objective 3. Evaluate the CMAS with biological samples

Samples of the unicellular algae *Tetraselmis chuii* were used to evaluate the overall functioning of the final version of the CMAS. Although important as larval feed for aquatic organisms, these algae were used as a stand-in for aquatic germplasm. The algal culture was obtained from Algae Research and Supply (Carlsbad, California, USA; algaresearchsupply.com). The cell concentration of a sample of the culture was evaluated in a Makler[®] chamber on an Axio Lab.A1 phase microscope (Zeiss, Oberkochen, Germany) and calculated to be 3.6×10^6 cells/mL.

The optical absorbance of the algal sample across the visible spectrum was measured on a Nanodrop 1000 spectrometer (Thermo Fisher Scientific) in UV-vis mode. The absorbance was plotted with the LED emission distributions from the POEM (originally shown in Figure 2.8).

Serial 1:1 dilutions of the algal culture were prepared with artificial seawater (32 ppt, Reef Crystals Reef Salt, Instant Ocean, instantocean.com) for a total of eight samples of concentrations 3.6×10^6 , 1.8×10^6 , 9.0×10^5 , 4.5×10^5 , 2.3×10^5 , 1.1×10^5 , 5.6×10^4 , and 2.8×10^4 cells/mL. Optical signal from the eight samples was derived in the same way as described for the channel catfish sperm samples in Ch. 2. The eight diluted samples were pumped through the CMAS (one ‘pull’ from each sample tube from highest to lowest concentration, and this series was repeated four times) and the resulting signals were recorded.

Between samples, artificial seawater was used to flush the tubing. A linear regression was fitted to allow the calculation of the corresponding inverse function, and so to allow the determination of an unknown cell concentration from its optical signal.

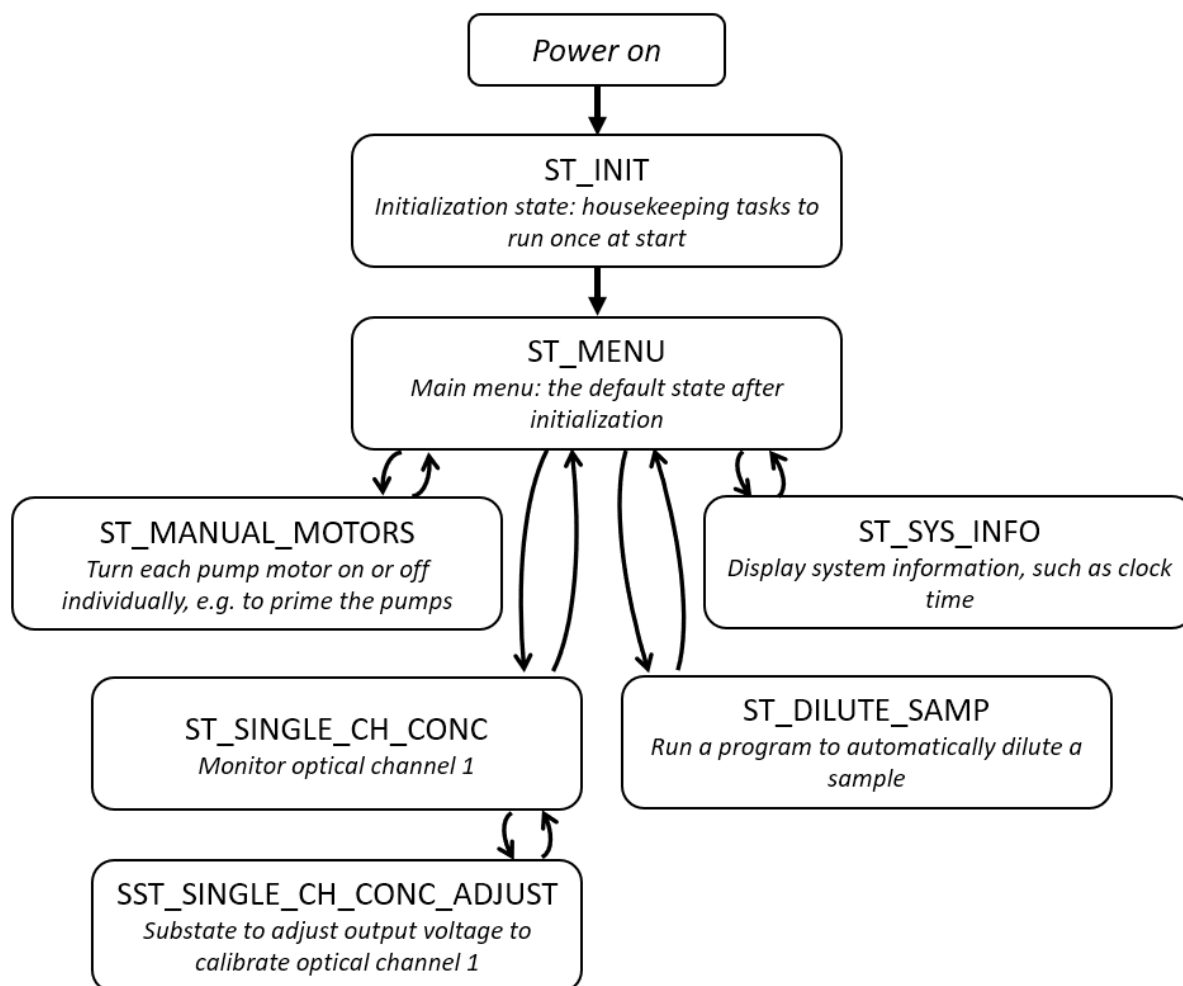


Figure 3.5. The finite-state machine logic flow that controlled the CMAS. Capital letters indicate the names of states (ST) and substates (SST) as used in the Arduino firmware. Arrows indicate permitted transitions between states. For example, the firmware may transition directly from ST_SYS_INFO to ST_MENU, but not from ST_SYS_INFO to ST_DILUTE_SAMP, except via ST_MENU.

To allow comparison of the optical performance of the CMAS to that of an existing commercial instrument, the absorbance of the same eight serially diluted samples was measured on a Nanodrop 1000 spectrophotometer at $\lambda = 625$ nm, corresponding closely to the $\lambda = 624$ nm peak of the red channel of the LED provided on the CMAS.

To allow the automatic adjustment of cell concentration, the CMAS firmware was hard-coded to actively calculate the concentration of samples pumped through a POEM installed in the CMAS. The function required to calculate the concentration was determined on a personal computer in Excel (Microsoft) software, rather than on the CMAS itself. The CMAS was equipped with a POEM and an additional peristaltic pump sub-module. The CMAS was configured to automatically dilute an algal sample to a concentration of 1×10^6 ; the POEM was

used to pump and evaluate the incoming sample, the CMAS calculated the appropriate pumping ratio between the two fluid flows required to reach the final desired concentration, and the peristaltic pump sub-module was used to add artificial seawater to the sample. The function of this basic workflow was evaluated by drawing an aliquot of the original sample (3.6×10^6 cells/mL) into the CMAS; this was repeated for a total of five trials. A 1:1 dilution of the original sample was prepared by pipetting, for a starting concentration of 1.8×10^6 cells/mL; this was also repeated for a total of five trials. The resulting ten diluted samples were evaluated by eye in a Makler® chamber on an Axio Lab.A1 phase microscope to determine the final concentrations, and these concentrations were plotted.

Results

Objective 1. Design a process diagram

The concept design of the CMAS was based on the concentration measurement and fluidic dilution functions normally performed manually in germplasm processing at the AGGRC²⁷ and elsewhere^{14,64}. A diagram (Figure 3.6) was composed to show the flow of data and the flow of fluids necessary to perform essential germplasm evaluation and dilution functions. The user was intended to interact with the device through a user interface (UI) consisting of a screen (UI output) and buttons or a rotary encoder (UI input). The UI was to interact with a microcontroller that mediated between the user and the fluidic and sensing components of the device.

In this design, the fluidic flow consisted of an input reservoir containing the sample to be evaluated and diluted, diluent reservoirs containing extender medium or cryoprotectant medium, an output reservoir for the final, diluted sample, tubing to connect these, and pumps (not shown in Figure 3.6) to move fluid through the tubing.

Concentration measurement systems were provided at the beginning and end of the fluidic flow process to evaluate the concentration of samples before and after dilution. Evaluation at the beginning of flow was necessary because it was meant to determine a mixing ratio to drive the pump flow rates to achieve a final target dilution. Evaluation at the end of flow was considered optional; it may be added in future work as a quality control measure to verify whether the target concentration has been achieved.

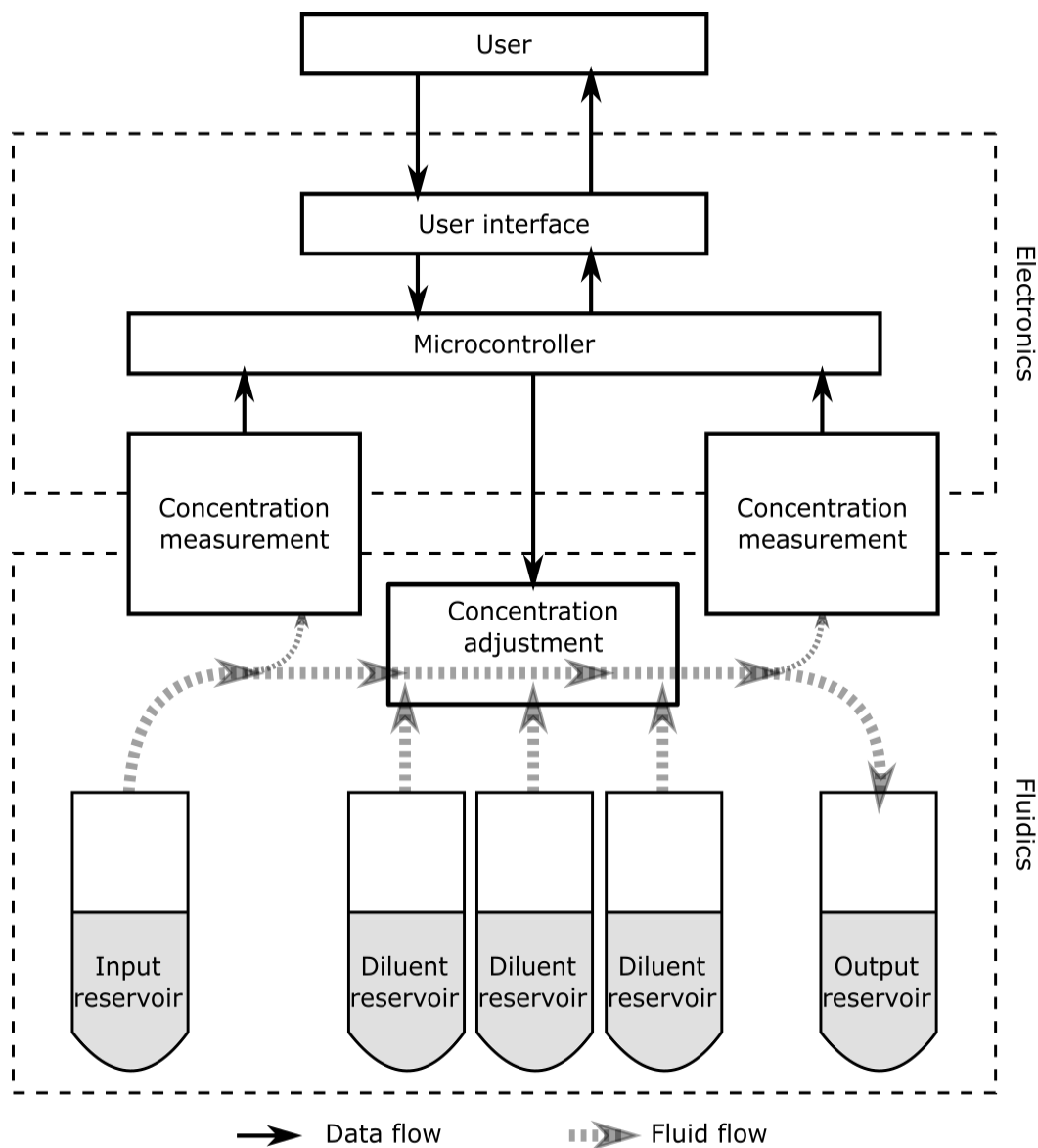


Figure 3.6. Design concept for the CMAS. A fluidic sample flows from the input to the output reservoir, with the addition of diluents and the measurement of sample concentration along the way. The microcontroller mediates between the user (through user interface components) and the sensing and electromechanical components that drive fluid flow and evaluate concentration.

Objective 2. Prototype the CMAS

The first assembled prototype of the CMAS (Figure 3.7) was a simple proof-of-concept comprising only the essential components, such as pumps and basic electronic circuits. These were mounted to aluminum DIN (German Institute for Standardization, din.de) rails, which are common in network hardware boxes for mounting of standardized components. Adapters were designed and 3-D printed to sturdily connect motors, breadboards, and an LCD screen to the custom DIN rail assembly.

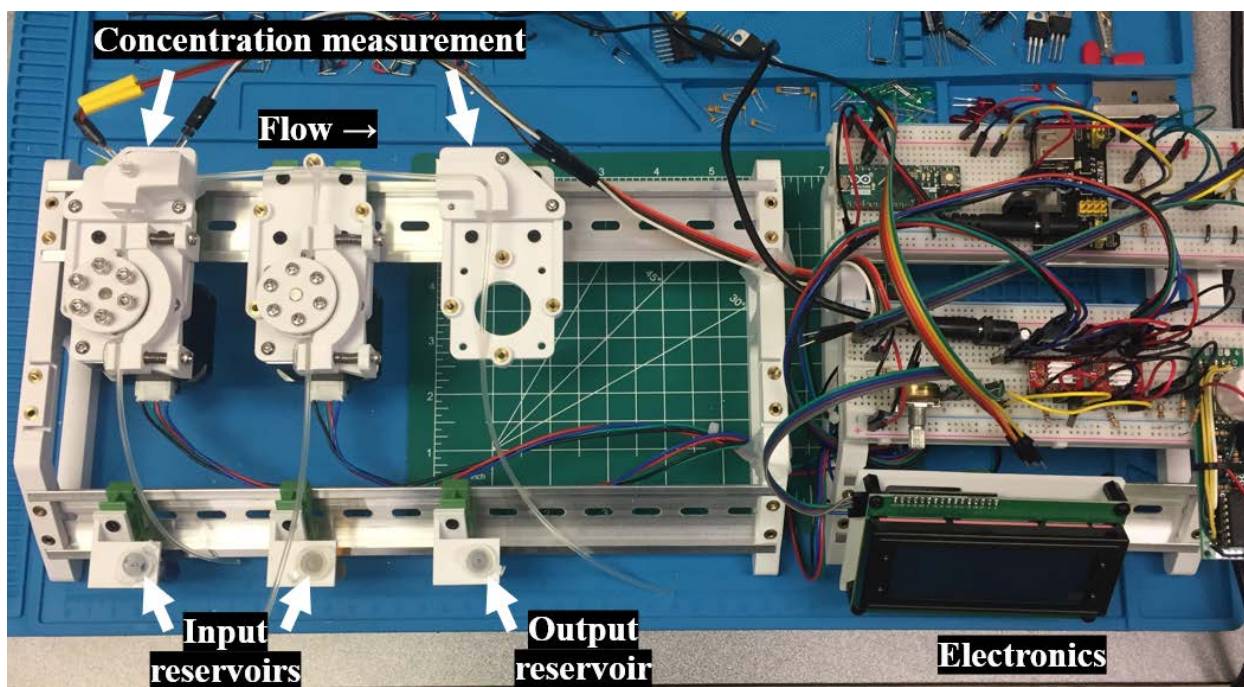


Figure 3.7. The first prototype of the CMAS. In this version, components were individually mounted on aluminum DIN rails to allow for easy reconfiguration.

The first prototype was used to evaluate simple pumping with the custom peristaltic pumps and mixing of the pumped fluid (Figure 3.8).

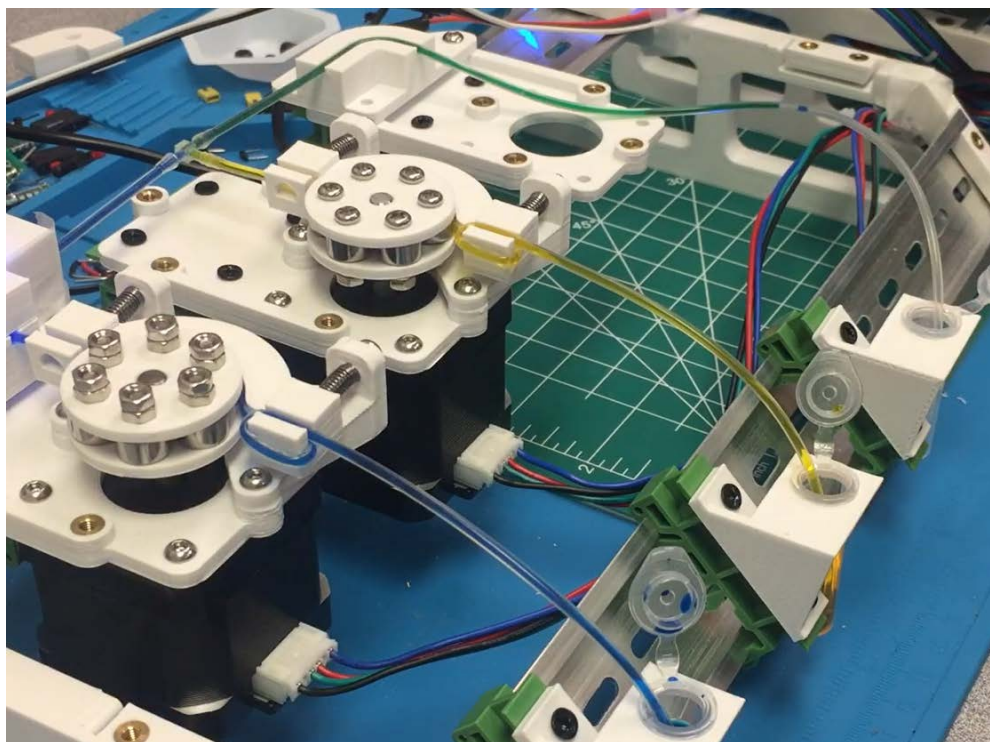


Figure 3.8. Demonstration of fluidic pumping and mixing in the first prototype of the CMAS, before addition of optical sensors. Blue and yellow food dyes, diluted in water, were drawn from

reservoir vials and pumped to a T-junction. The resulting mixed green fluid was produced into the output vial at top right. The loops in the lengths of tubing containing blue and yellow dye were meant to prevent the tubing from being drawn into the pumps as the pump rollers rotated. This problem was solved with a small tubing clamp in the third (orange) prototype.

The second prototype (Figure 3.9) introduced a solid enclosure of PMMA panels built onto a 3-D printed frame. This approach combined the flexible design options allowed by 3-D printing with the rapid fabrication allowed by laser cutting. A completely 3-D printed enclosure of equivalent size and durability would have taken more than 24 h to print on most consumer-grade printers, whereas this enclosure was fabricated in under 6 h, including printing and laser-cutting time. Components such as the bases of the pumps, the mount for the rotary encoder, and the brackets for the sample tubes were adapted to mount to this new frame.

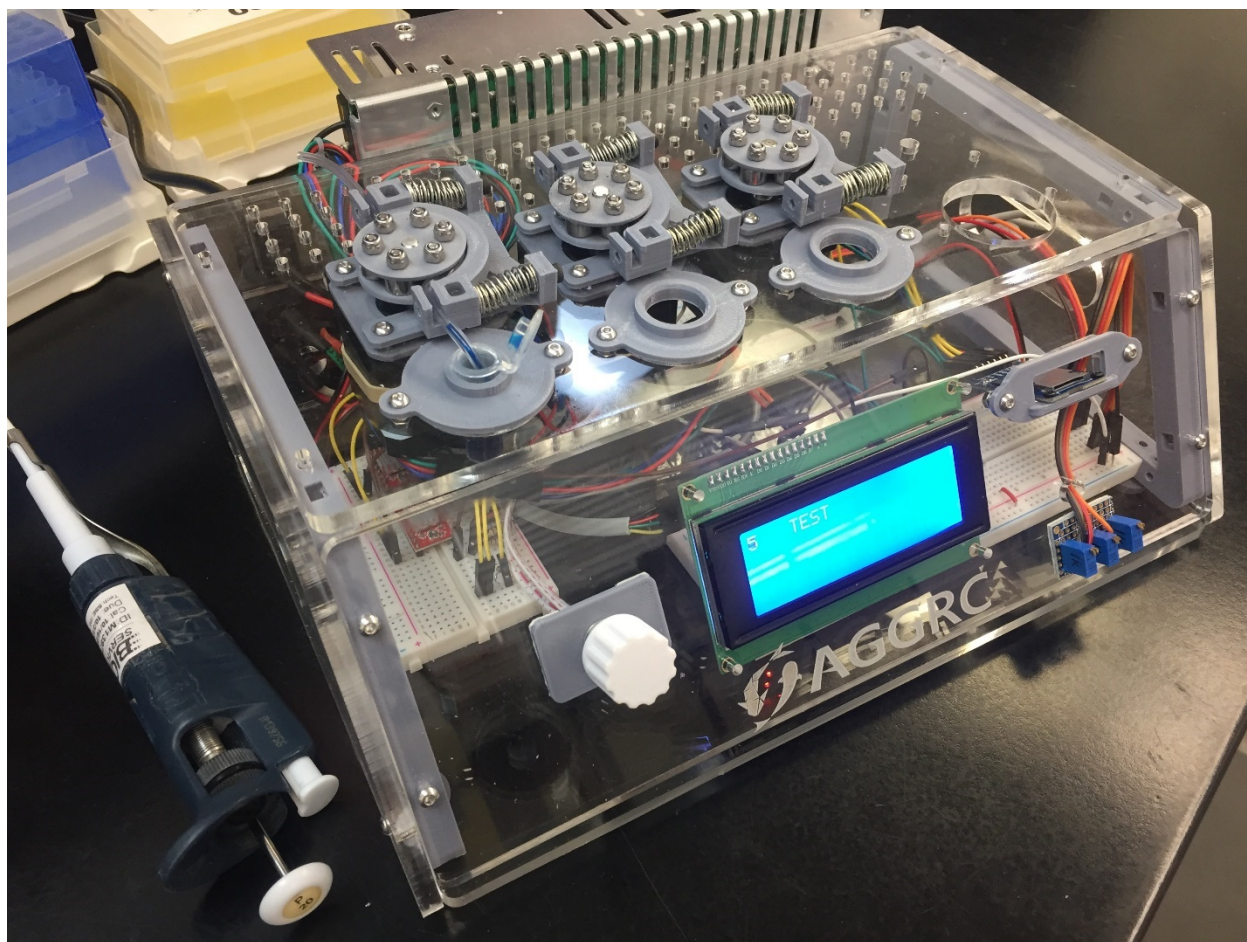


Figure 3.9. The second prototype of the CMAS. New features included an acrylic case, custom seating points for different sample tube sizes, and an integrated power supply. Clear acrylic was used to allow viewing of the internal components.

The third, final prototype (Figure 3.10) included many refinements. Some changes from the second prototype were planned from the outset. Soldered breadboards were prepared for the electronics once they had been tested and improved. The power supply was moved to the inside of the enclosure to protect it, which in turn required that the case be enlarged to accommodate it. Carefully labeled wire bundles were prepared to run between the various electronic components both inside and outside the case. The five black optical evaluation sub-module housings can be seen mounted to the top of CMAS case. However, only the leftmost submodule was populated with an LED and photodiode; a more complex workflow with multiple optical evaluation steps can be evaluated in future work.

Other changes were made in response to problems discovered in prototyping. The design of the peristaltic pumps was refined, with a more robust base to prevent material fatigue and failure, and with small modifications to the shape of the rotors to have them ride more smoothly on the tubing. The optical modules were provided with mounting points to secure them permanently to the case. Finally, the brackets for the sample tubes were moved to the outside of the enclosure to prevent spilled sample fluid from entering the case.

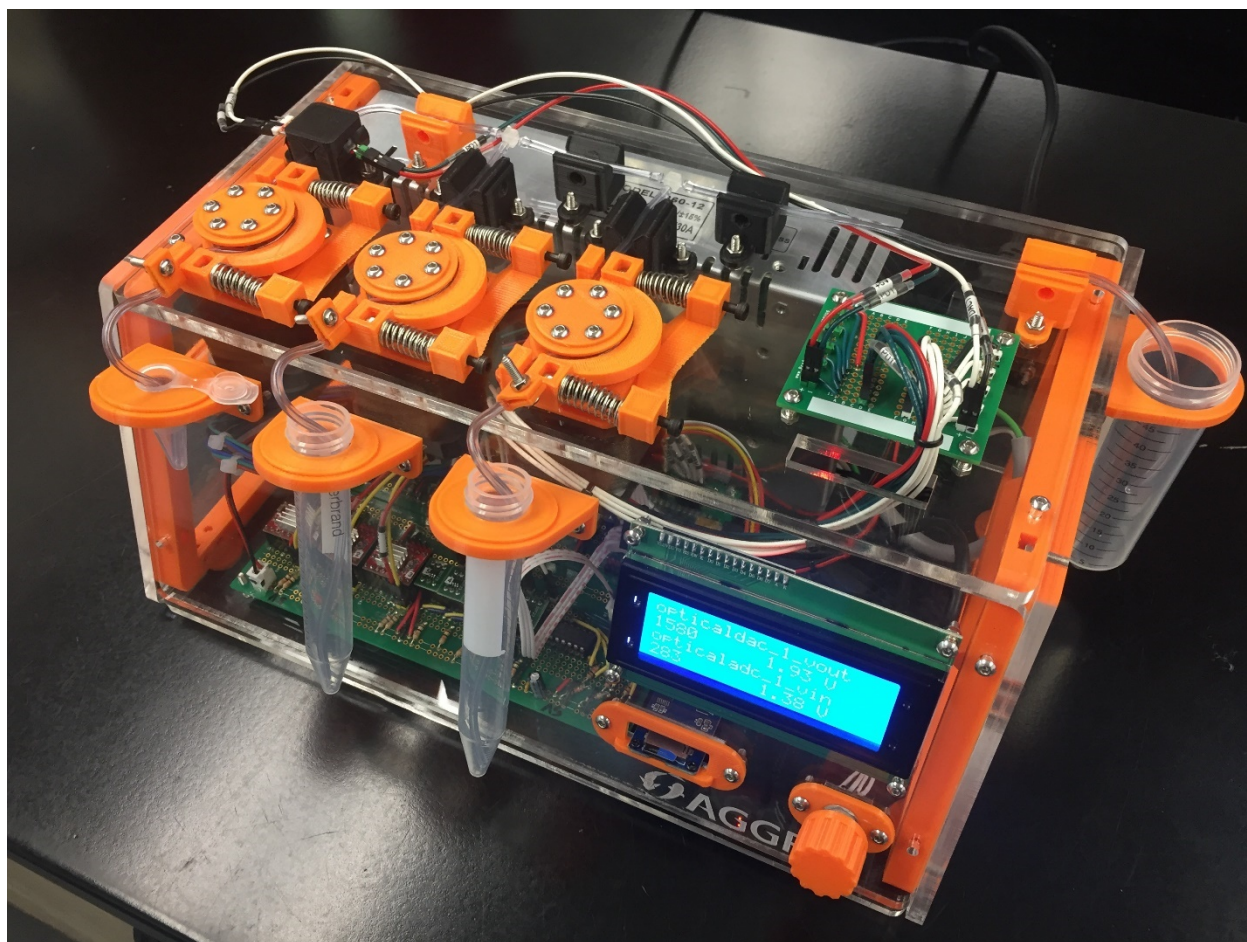


Figure 3.10. The third prototype of the CMAS. New features included moving the power supply into the slightly larger case, transferring the electronics onto soldered breadboards, and moving all fluidics and sample tubes to the outside of the case. Changes of these types improved the safety and function of the device.

Objective 3. Evaluate the CMAS with biological samples

The algal absorbance profile as measured by the Nanodrop 1000 (Figure 3.11) showed no prominent peaks but declined gradually from the UV into the visible spectrum.

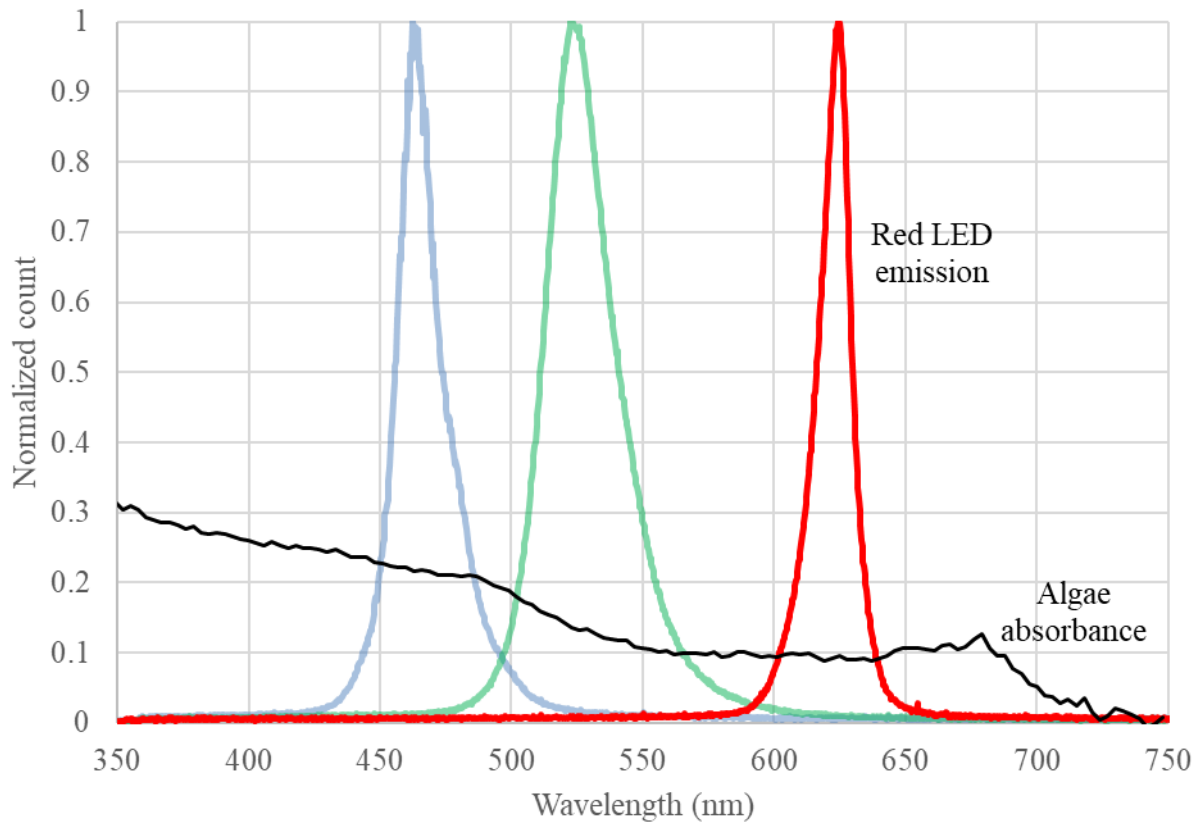


Figure 3.11. Spectral absorbance of a sample of the algae *Tetraselmis chuii* (3.6×10^6 cells/mL) measured on a Nanodrop 1000 spectrophotometer. The emission distributions of the LED used in the CMAS are shown for comparison. All distributions are normalized (peak value = 1). The peak absorbance wavelength of the algal sample is not shown ($\lambda = 229$ nm).

The optical signals from the serially diluted algal samples were plotted (Figure 3.12) and the best-fit regression line was determined to be $y = -2.9698x + 20.94$ ($R^2 = 0.9812$). The CMAS was hard-coded with the ability to calculate the corresponding inverse function:

$$\text{cell concentration} = 10^{[7.05 - (0.337 \times \text{sensor voltage})]}$$

This allowed the CMAS to calculate the cell concentration of samples, with the aim of finding a suitable dilution ratio for the sample and adjusting to a target concentration.

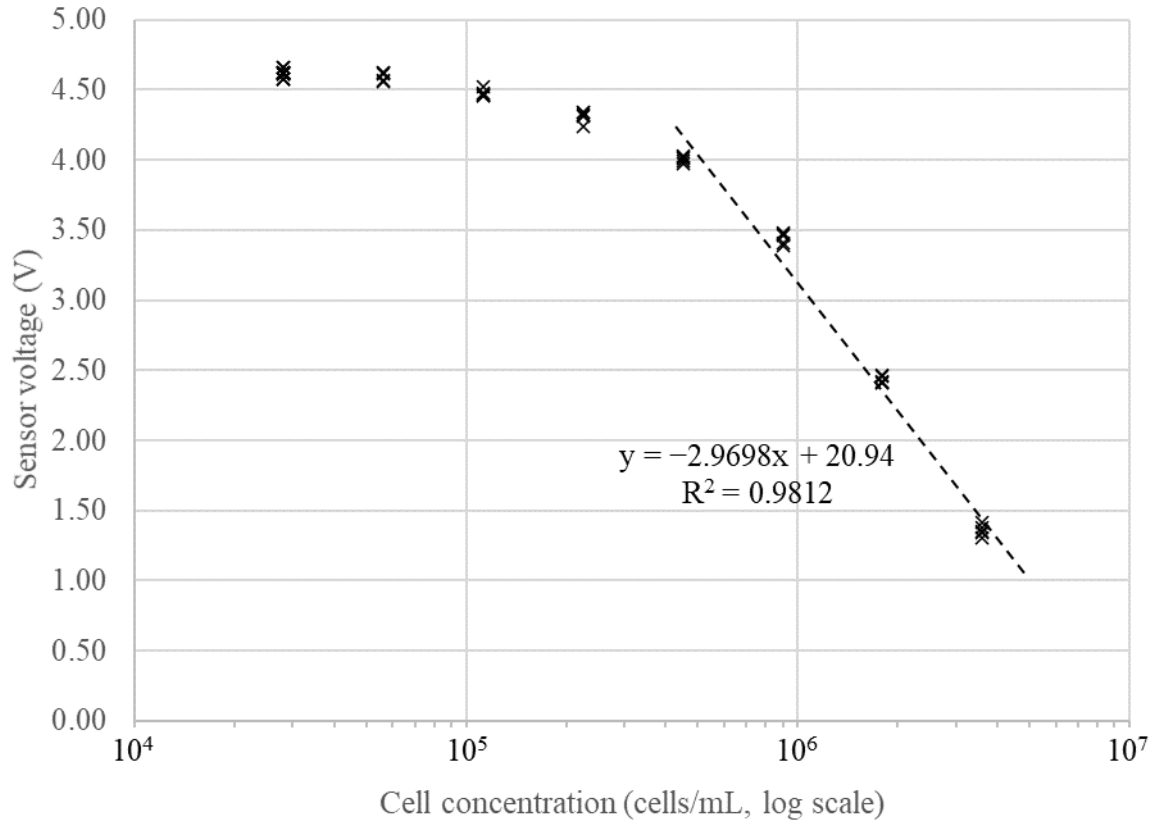


Figure 3.12. The optical signals from algal samples evaluated on the CMAS of concentration $> 3 \times 10^5$ cells/mL were fitted by linear regression.

The optical absorbances of the eight serial dilutions of algal samples, as measured on the Nanodrop 1000, were plotted against cell concentration (Figure 3.13).

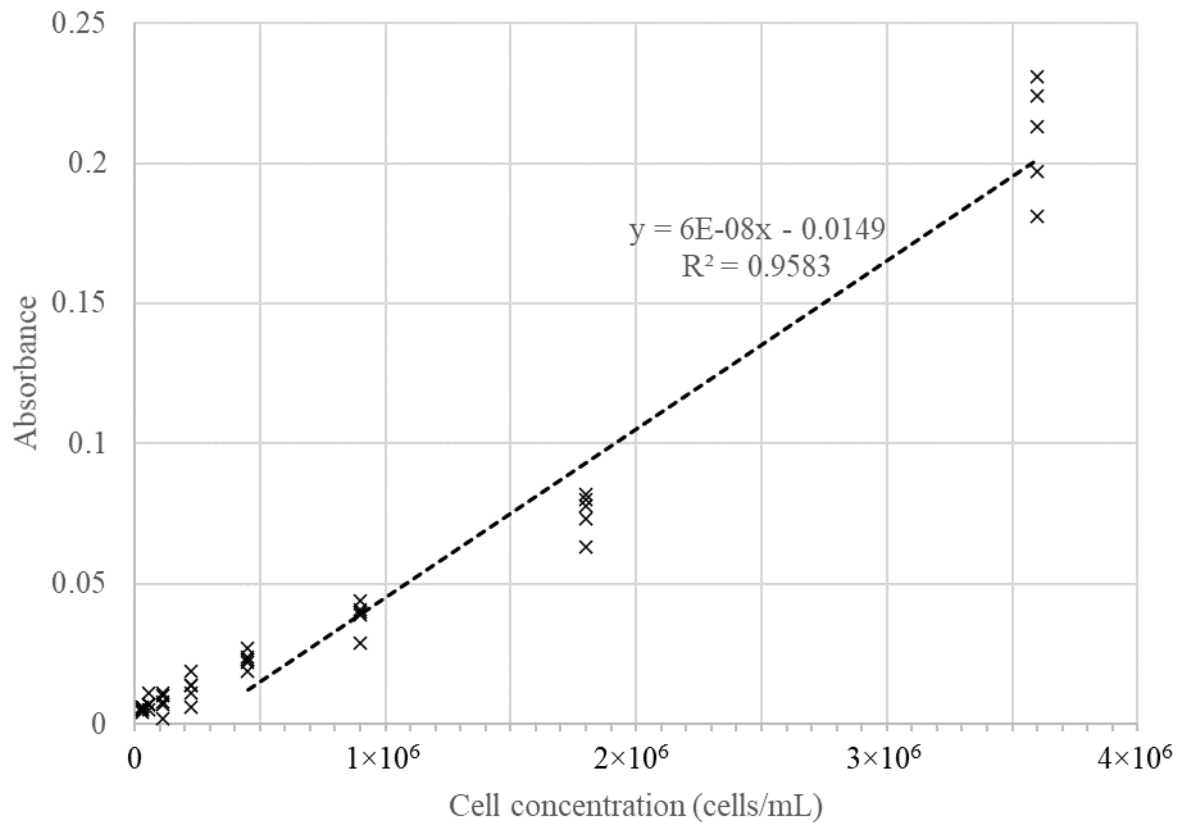


Figure 3.13. The optical absorbance of the same algal samples as in Figure 3.11, evaluated on a Nanodrop 1000 spectrophotometer ($\lambda = 625$ nm). All samples of concentration $> 3 \times 10^5$ cells/mL were fitted to a linear regression.

Algal cell concentrations resulting from automatic dilution by the CMAS were plotted (Figure 3.14). The target concentration in all cases was 1×10^6 cells/mL. Starting from the higher initial concentration (3.6×10^6 cells/mL), the CMAS produced an adjusted concentration of $7.1 \pm 0.5 \times 10^5$ cells/mL (mean \pm SD). Starting from the lower initial concentration (1.8×10^6 cells/mL), the CMAS produced an adjusted concentration of $8.9 \pm 1.1 \times 10^5$ cells/mL (mean \pm SD).

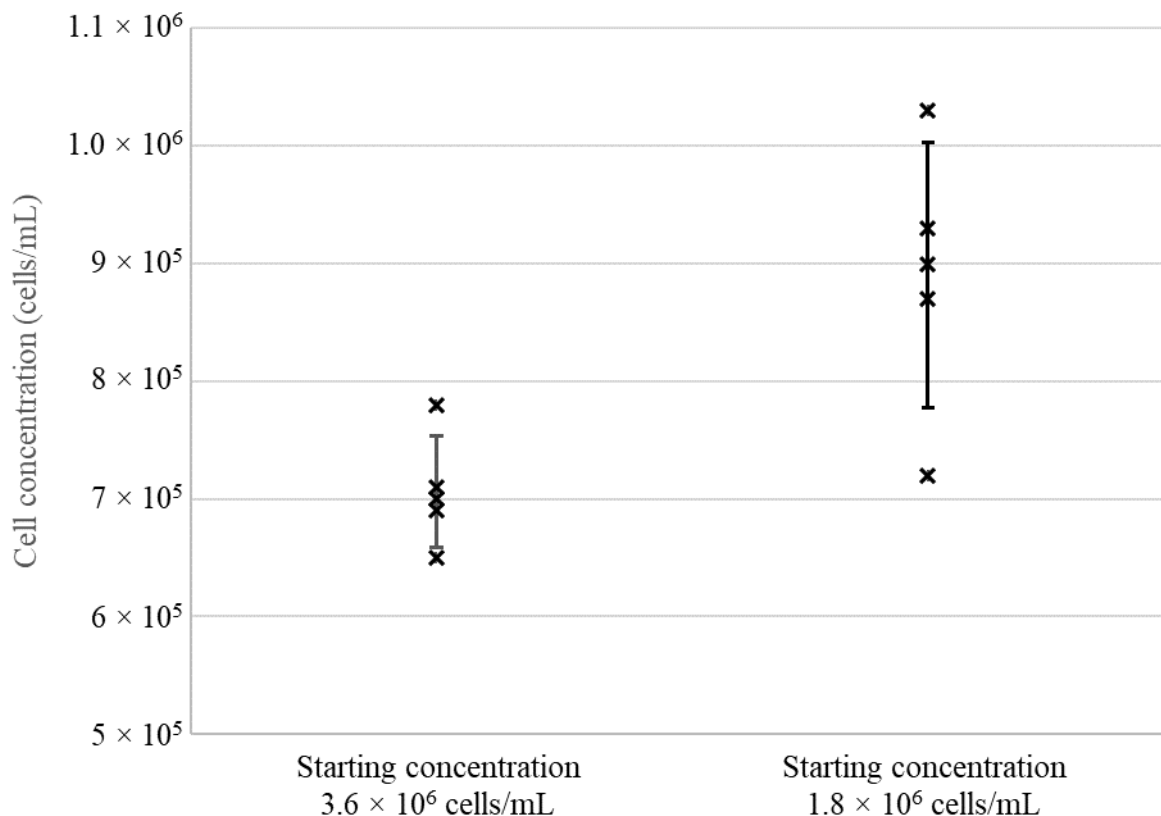


Figure 3.14. Results of automatic dilutions by the CMAS of algal samples. The target concentration from both starting concentrations was 1.0×10^6 cells/mL. The symbol x indicates individual data points; vertical bars indicate one standard deviation from the mean.

Discussion

The overlay of the algal absorbance distribution with the LED emission spectra showed that the algae had no sharp absorbance peak in the visible light spectrum. This suggests that the three colors of light from the LED may allow for similar optical sensitivity in the CMAS. However, algal absorbance is slightly greater at shorter wavelengths; therefore, if increased sensitivity is necessary in future work, the blue LED channel may be a better option than the red channel used here.

As was true of the catfish sperm samples evaluated in Ch. 2, the algal samples allowed for a close linear regression fit only in a limited range of concentration (from 4.5×10^5 to 3.6×10^6 cells/mL). Cryopreservation protocols have not yet been determined for these algae, therefore it is not possible to comment on whether this range is directly relevant to cryopreservation.

However, the CMAS may at least be of general use in adjusting the concentration of algal samples drawn directly from a dense culture, as was the case for the sample used here.

The optical sensitivity of the CMAS in detecting cell concentration compared favorably to that of the Nanodrop 1000. The regression lines obtained for the CMAS ($R^2 = 0.9812$) and the Nanodrop 1000 ($R^2 = 0.9583$) for the same range of concentrations were calculated based on different optical parameters: the CMAS data effectively represented light transmittance, while the Nanodrop data represented absorbance. From the perspective of programming a microcontroller, performing calculations directly with the CMAS sensor voltage without converting to absorbance was simpler but nonetheless gave a satisfactory result, as shown by the goodness-of-fit of the linear regressions for both catfish sperm (Ch. 2) and algae.

Evaluation of the concentration adjustment function showed that the components of the CMAS can work together to estimate and adjust the cell concentration of a sample. The trials with algal samples demonstrated reasonable precision in production of adjusted concentrations (in the two trials, $\pm 6.7\%$ and $\pm 12.6\%$) but low accuracy (the trials produced mean cell concentrations that were 71% and 89% of the target concentration, i.e., 41% and 12% below the target). If in future trials it is found that the CMAS consistently dilutes to a lower concentration than the target, it may be necessary to compensate for this tendency directly in software.

Fabrication

The CMAS was designed with flexibility of open fabrication methods in mind. Certain components, such as the peristaltic pumps, can be fabricated by printing with FDM (thermoplastic) or SLA/MSLA (resin) 3-D printers, or by machining from stock plastic or metal. Others, such as the frame, can be 3-D printed, laser-cut, or cut and drilled with traditional machine tools such as a bandsaw and drill press. Providing the design files in multiple, flexible formats (i.e. .f3d/.f3z, .stl, and .dxf) allows for fabrication with a wide variety of technologies.

The cost of materials to build the CMAS is detailed in Appendix B, CMAS Bill of Materials, and was estimated for a single CMAS (as of 2021) to be US\$560, not including taxes, shipping, tools, or fabrication equipment. If purchase of all tools and fabrication equipment were included, the cost was \$4569. The bulk of this amount would be to buy a laser cutter (\$3524), which is not strictly needed. With the use of alternative fabrication techniques that may already be available (e.g., drill press and table saw) to fabricate the panels that constitute the case of the CMAS, the one-time cost of tools and equipment is reduced to \$483.

Benefits in the laboratory

The benefits of the CMAS to laboratory workflow will depend in part on the volume and number of samples to be processed. According to existing workflow modeling⁶⁵, estimation of the motility and concentration of one catfish sperm sample and adjustment to a target concentration requires on average 288 s (i.e., 12.5 samples/h). This manual throughput depends strongly on the number of samples to be processed, but it is little affected by the volume of each sample; the timing is dominated by assessment and calculation.

Processing time with the CMAS, in contrast, depends on number of samples and on sample volume. A tubing replacement (if necessary to prevent cross-contamination between samples) required approximately 30 s, and priming the tubing of the CMAS with sample required ~ 20 s. If the peristaltic pump that draws sample could be run at maximum flow rate (1.1 mL/min), processing of a single sample would require $(50 + 55V)$ s, where V is the volume of the sample

in mL. The processing time for a 4.3-mL sample (final adjusted volume 8.6 mL) on the CMAS (287 s) would be therefore similar to the equivalent manual processing time (288 s). The CMAS would result in a time savings for samples < 4.3 mL, but an increase in processing time for samples > 4.3 mL. The comparison is not exact because the manual process includes estimation of motility, a function not provided by the CMAS. However, this comparison serves as a starting point to estimate the time savings provided, and could be refined based on laboratory-specific needs and practices.

Future improvements

In future work, the CMAS could be improved in several respects. To adequately compress the chosen tubing in the peristaltic pumps, substantial spring force was needed. A choice of softer tubing could permit the use of weaker springs and could improve the pump efficiency. For example, replacement of tubing in the pumps would be made easier. However, it would also require remeasurement of flow rates. The electronics, which are currently laid out on soldered breadboard, could be adapted to a printed circuit board design: in particular, an efficient surface-mount design would greatly reduce the physical footprint of the electronics and allow for a more compact form factor⁶⁶. The casing could also be better sealed to prevent the incursion of fluids, which can be a common risk in a laboratory or hatchery environment. These improvements would improve the utility, safety, and reliability of the device.

There is provision in the current design of the CMAS to mount up to three pumping sub-modules and five optical evaluation sub-modules in all. This could allow, for example, the dilution of an evaluated sample (pumped by one pumping sub-module) with a first-stage extender (pumped by a second sub-module), followed by a cryoprotectant solution (pumped by a third sub-module). All three fluids could be measured before mixing, each by its own optical evaluation sub-module; another evaluation could be made after the mixing of the sample and the extender; and a final evaluation could be made at the end of the workflow to verify the final concentration achieved.

The CMAS could be integrated with other devices to improve the efficiency of cryopreservation workflows for aquatic germplasm: for example, an open hardware version of a filler–sealer device for French straws, which are widely used as containers for animal germplasm. This device would be an obvious candidate for integration as a processing step immediately downstream from the CMAS. It could be a productive technology development project to connect the fluidic output of the CMAS to the fluidic input of the French straw filler–sealer and coordinate the action of the two devices.

Conclusions

The CMAS was designed and fabricated as an open-technology platform that can serve as a starting point for further refinement and for future technology development. A basic concentration evaluation and dilution workflow was evaluated with a sample of unicellular algae and a single diluent solution.

The integration of the POEM into the CMAS provides an opportunity to increase the reach of open technologies in the aquatic germplasm community. The CMAS is a design amenable to open, distributed fabrication by 3-D printing, laser cutting, and hand-soldering. It has been demonstrated in this work that such a device can effectively evaluate cell concentration in fluidic samples and dilute them to a target concentration. These activities are essential features of the

cryopreservation process, and they are targets for improvements in efficiency and throughput such as those offered by the CMAS. Encouraging laboratories to engage in the open-technology community, and in particular to fabricate their own versions of open-technology tools and devices such as the CMAS, can improve the quality of germplasm samples, increase cryopreservation throughput through distributed processing, and strengthen aquatic germplasm repositories globally.

Chapter 4. Identifying Opportunities for Microfabrication with Low-Cost Resin Printing

Introduction

The concentration measurement and adjustment system (CMAS) described in the previous two chapters works with sample volumes that are appropriate to some species, such as the channel catfish, *Ictalurus punctatus*, which produces volumes of sperm in the tens of milliliters per male. However, these sample volumes are not appropriate to small-bodied species, such as the zebrafish, *Danio rerio*, which produces 0.5–2 μL per male of sperm when stripped⁶⁷. It would be desirable to extend the CMAS into the microliter sample regime in future work. To achieve this reduction of scale, it would be necessary to evaluate inexpensive fabrication technologies that allow the rapid prototyping of sub-millimeter geometric features, fluidic channels, and connectors.

Microfabricated devices enable a wide range of experiments and assays across biology, medicine, and engineering. Prototyping of these devices has traditionally relied on expensive and technically difficult microfabrication techniques such as photolithography, micro-milling, and hot embossing⁶⁸. Recent development of industrial and commercial resin 3-D printers has enabled rapid microfabrication with photo-curable resins, and this practice is now widespread in research^{33,69,70}. The 3-D printing approach for microfabrication provides prototyping possibilities with less investment in equipment and expertise than is necessary for traditional techniques³⁴. However, commercial laser-based stereolithographic printers have represented a major investment (thousands of US dollars) for non-specialist laboratories. In the past three years, mask-based stereolithography (MSLA) printers have emerged on the consumer market. For as little as US\$250, prototyping can be performed at the microfabrication scale.

Handling and thorough mixing at millifluidic scales (i.e., in channels < 1 mm across) is a difficult and longstanding problem. Human intuition, which deals mainly with fluids on the scale of a cup of coffee, or that of a flowing river, tells us that two different liquid solutions coming into contact will mix readily. On sub-millimeter and smaller scales, however, laminar flow predominates: fluids slide past one another, or flow alongside one another, rather than mix freely, as is the case in larger-scale flows. Mixing between fluidic samples in the laminar flow regime is achieved mainly by the slow, passive diffusion of molecules across the interface between the two fluids.

To mix fluids on the order of microliters, it is therefore necessary to design mixing geometries that will promote turbulent flow at small scales. Such designs are traditionally created by way of photolithography. This is a technically sophisticated and time-consuming method in which a 2-dimensional design is inscribed by a photolithographic process as thin, 3-dimensional geometry on a silicon wafer. The finished wafer is used as a mold onto which a flexible silicone called polydimethylsiloxane (PDMS) is cast. The PDMS is removed and bonded to a glass slide, creating closed channels into which fluidic samples may be injected. Handling, connective, and mixing geometries are commonly incorporated into channels fabricated in this way. For example, logarithmic spiral geometries^{71,72} promote mixing of microfluidic flows, and ‘herringbone’ repeated chevron geometries⁷³ are a commonly used feature with the same purpose. Both approaches aim to ‘fold’ fluid streams on one another, inducing turbulence in the flow path and producing a thoroughly mixed solution.

To adapt the CMAS to germplasm samples from zebrafish and similar small-bodied fishes, it will be necessary to handle, evaluate, and mix germplasm samples at such millifluidic and microfluidic scales. However, photomasks used to carry out photolithography can take days to be printed by a commercial provider and shipped, and the PDMS casting process can take several hours, even when carried out by an experienced user. 3-D resin printing may offer an alternative rapid prototyping approach.

Resin 3-D printing technologies

Laser stereolithography (laser SLA) has been, until recently, the dominant technology in resin 3-D printing. It relies on the precise aiming of an ultraviolet (UV) laser to cure each voxel (“volumetric element,” or “3-dimensional pixel”) of the printed geometry, or on the use of a digital micromirror device (DMD), similar to those used in digital light projection (DLP) projectors, to project a pattern of UV light onto a layer of uncured resin. Both approaches have proven expensive: these printers usually run in the thousands to tens of thousands of US dollars. This is a substantial improvement on the usual equipment, facility, and staffing costs of microfluidic prototyping, but it still represents a serious barrier to entry into such prototyping for small research groups with limited or inflexible funding structures, or with limited access to institutional core facilities that offer stereolithography as a service. Nonetheless laser SLA has been applied to many problems in microfluidic rapid prototyping and world-to-chip interfaces, with promising results⁷⁴.

In recent years, a new approach to resin 3-D printing has emerged. Mask-based stereolithography (MSLA) has repurposed existing liquid crystal display (LCD) screens to form cured layers of resin in a manner similar to the DLP/DMD approach. However, LCD-based systems are far cheaper than DLP/DMD systems. The realization of this technology has opened the world of resin printing to the mass consumer market: for as little as US\$250, a user can get started with a resin printer capable of a single-voxel resolution of $50 \times 50 \times 10 \mu\text{m}$. The associated consumable materials (replacement fluorinated ethylene propylene (FEP) film, resins, and post-processing supplies) are available at modest cost. Resins, for example, start around US\$20/L.

As resin printers have found a wider market, the production of dedicated LCD screens has become economically feasible. Whereas earlier machines such as the Anycubic Photon repurposed red-green-blue (RGB) LCDs with 2k ($50\text{-}\mu\text{m}$ or $47.25\text{-}\mu\text{m}$ pixel width) resolution, more recent offerings such as the Phrozen Sonic Mini 4k have improved to monochrome-pixel LCDs with a $35\text{-}\mu\text{m}$ pixel width that is virtually invisible to the naked eye. In comparison to RGB LCDs, these ‘mono’ screens pass far more UV light. Because the cure time per layer depends on the UV light flux into the resin, the print time of a component has substantially decreased: by roughly 40% in practice. As a side effect of the decreased light blocking, the lifespan of the LCD has also increased.

It was the goal of the work in this chapter to demonstrate that recently developed low-cost, consumer-grade UV resin 3-D printers offer opportunities in microfabrication that may be applicable to future development of the CMAS into a microliter sample regime. The specific objectives were to: 1) introduce the resolution and quality of geometric features that were found to be possible with consumer-grade LCD-based MSLA printers, and 2) identify post-processing methods that maximized the potential of these printers. The features produced by inexpensive MSLA printers approached the quality and scale possible with conventional microfabrication techniques. This offers an opportunity to extend the rapid prototyping process associated with the

development of the CMAS into milliliter volumes, greatly expanding the utility of the CMAS in research and sample processing.

Methods

Objective 1. Resolution and quality of geometric features

A microfluidic channel feature was designed in Fusion 360 (Autodesk) to be fabricated by MSLA printing, laser SLA printing, and photolithography.

The MSLA print was prepared in ChituBox software v1.8.1 (chitubox.com). The design was printed on a Phrozen Mini 4K MSLA printer (Phrozen, Taiwan; phrozen3d.com) in Blu Clear v2 UV resin (Siraya Tech; siraya.tech). In addition, the laser SLA print was fabricated on a Form 3 laser SLA printer (Formlabs, Somerville, Massachusetts, USA; formlabs.com) by the Advanced Manufacturing and Machining Facility (Department of Mechanical and Industrial Engineering, Louisiana State University). The MSLA and laser SLA prints were cleaned and UV-cured following the instructions provided by the printer manufacturers.

The photolithographic geometry was fabricated in PDMS with a conventional microfabrication approach⁷⁵. A silicon wafer was spin-coated with SU-8 photoresist. An opaque mask printed with the desired geometry was laid over the photoresist and the photoresist was exposed to UV light. The unexposed photoresist was washed away with acetone, leaving a mold pattern of cured SU-8 on the silicon wafer. Polydimethylsiloxane (PDMS) was prepared according to manufacturer directions and cast onto the wafer mold, producing the desired channel geometry in cured PDMS, which was peeled away cleanly from the mold.

The three geometries to be evaluated were sputter coated with platinum and evaluated by profilometry and scanning electron microscopy (SEM).

Objective 2. Post-processing choices

Duplicates of a test 3-D geometry were printed in Siraya Tech Blu Clear v2 resin on a Phrozen Sonic Mini 4K printer. One copy was washed in isopropyl alcohol (IPA) following the printer manufacturer directions and cured under UV light in air for 3 min. The second test geometry underwent a process that differed from manufacturer directions: it was washed and cleaned by ultrasonication in IPA for 3 min, and cured under UV light for 3 min while still submerged in IPA.

Results

Objective 1. Resolution and quality of geometric features

The MSLA print and PDMS cast (Figure 4.1a and c) presented smooth surface profiles in profilometry, while the laser SLA print (4.1b) presented a rough surface with distinct parallel striations. Scanning electron microscopy (4.1g–i) showed that the PDMS cast was smoothest, the MSLA print had distinct but uniform striations, and the laser SLA print had rough, inconsistent striations.

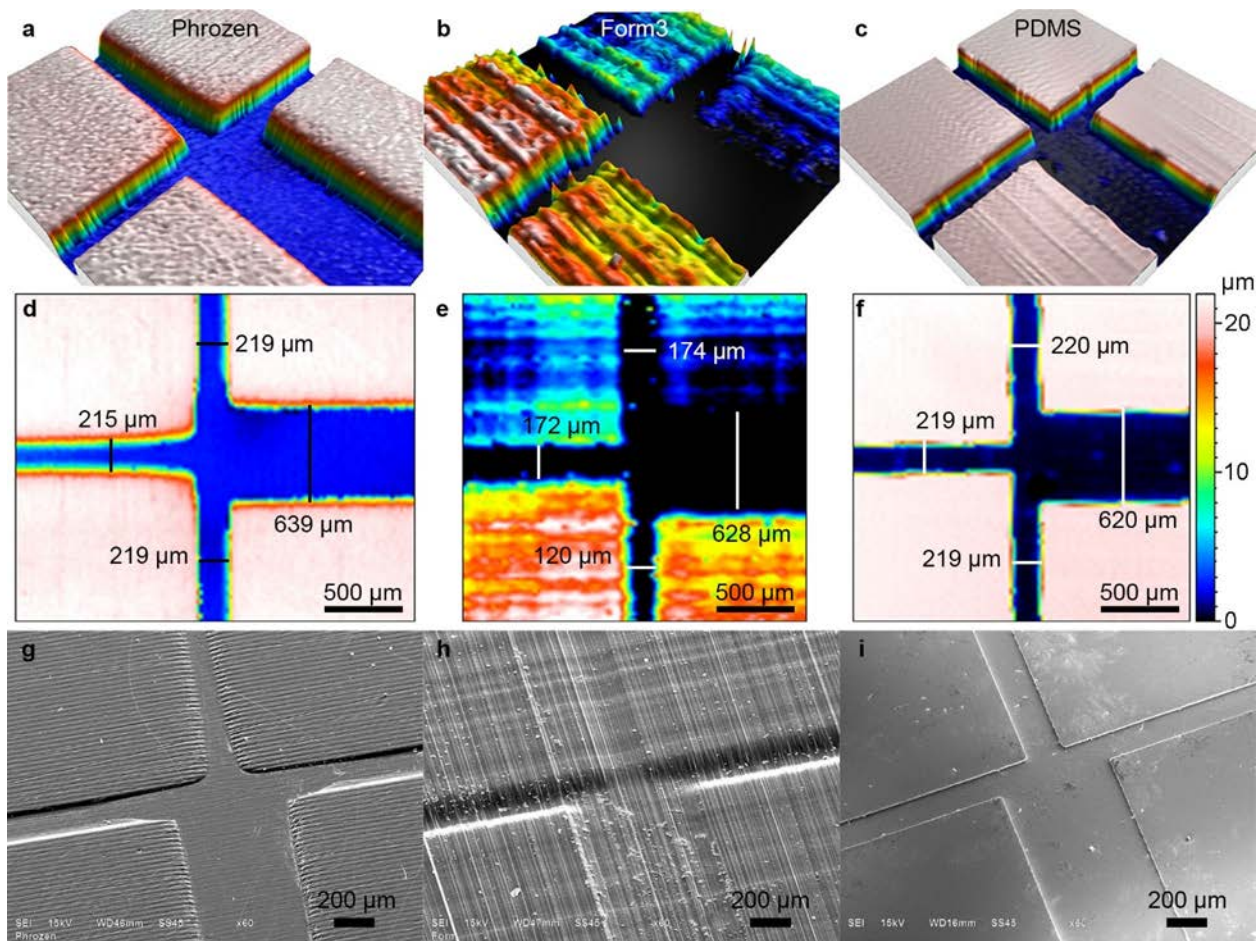


Figure 4.1. MSLA resin 3-D printing produced geometries comparable to traditional microfluidic fabrication with photolithography. Comparison of a microfluidic channel using different fabrication tools: Phrozen Mini 4K (a, d, and g), Form 3 (b, e, and h), and a PDMS cast from a silicon wafer (c, f, and i). The channels were sputter coated with platinum for surface profiling (a-c) and scanning electron (SEM) microscopy images (g-i). Profiled images were used to dimension the channel widths (d-f), with designed channel widths of 220 μm for the three inlet channels and 620 μm for the outlet channel. Images by J. Belgodere.

Objective 2. Post-processing choices

The first post-processing method (as recommended by the manufacturer) showed considerable residual, uncured resin on the part (Figure 4.2). The second method (ultrasonication and UV curing under IPA) showed clean, distinct features without visible residual resin.

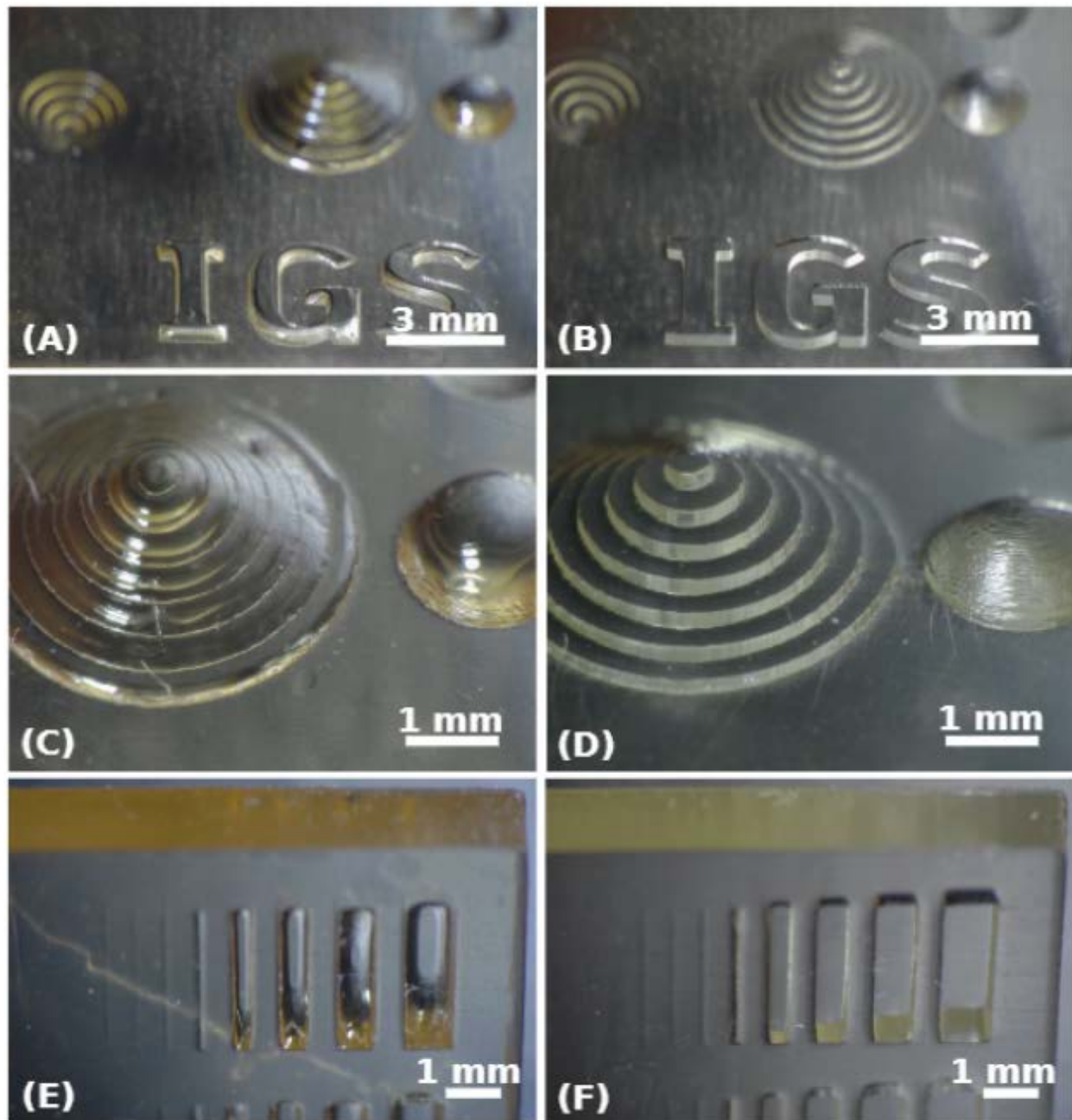


Figure 4.2. Specific post-processing steps greatly improved the results of MSLA printing. a), c), e): A test geometry printed in Siraya Tech Blu Clear v2 resin on a Phrozen Sonic Mini 4K printer was printed, washed, and cured following the printer manufacturer directions. b), d), f): An identical test geometry was washed with the aid of ultrasonication and cured with UV light in an isopropanol bath. Images by I. Semmes.

Discussion

Based on profilometric data and SEM imagery, fabrication by MSLA 3-D printing produced a smooth, clean channel geometry that approached the quality of a PDMS channel cast from a wafer fabricated by conventional photolithography for microfabrication.

The MSLA fabrication approach also represented a significant qualitative improvement in smoothness over the features produced on a laser SLA printer following procedures recommended by the manufacturer. Resolution is difficult to compare between MSLA and laser-based SLA because the former cures resin in small, discrete voxels and the latter cures with a laser spot. However, in one respect at least the MSLA approach is superior: it can cure areas as small as a single pixel, or 35 μm to a side, while laser-based SLA systems have a usual minimum laser spot size of $\sim 140\text{ }\mu\text{m}$ diameter.

Applying straightforward cleaning techniques in post-processing can result in a clean, sharp geometry with little residual resin. This is likely to reduce toxic interactions with biomaterials and to promote curing of materials such as silicone that may be cast onto the geometry.

The work presented here showed that there is considerable opportunity to produce microfabrication-scale geometry with inexpensive MSLA printers. The newfound accessibility of this approach to microfabrication could be applied to future prototypes of the CMAS that reach into the millifluidic or microfluidic scale. Pumping and evaluation functions that could be applied to germplasm of small-bodied fishes are likely to require the design and fabrication of sub-millimeter features such as mixing and observation chambers with dimensions in the tens or hundreds of microns. Such fine features are difficult to fabricate by conventional FDM printing. Inexpensive MSLA printers have the potential to join the arsenal of other ‘maker’ technologies such as FDM printers and consumer-grade laser cutters, and to extend projects such as the CMAS into a new, far smaller scale.

The wide availability of MSLA printing is likely to be highly disruptive. It greatly lowers the bar to entry, easily converting users, who normally function as customers of prototyping services, into makers, without the need for deep pockets or experience in the field. Researchers no longer need depend on a single precious prototype fabricated at considerable cost.

The recent and rapid shifts by manufacturers from RGB LCDs to monochrome LCDs and from 2K to 4K screens are indicative of the rapid pace of progress in MSLA. With fierce competition and rapid headway into the consumer market, innovation in MSLA printing is likely to develop quickly in the near future. Opportunities for low-cost microfluidics will quickly expand as printing costs diminish, the resolution and quality of finished prints improve, and specialty techniques to implement 3-D printed geometries in microfluidics are developed.

Conclusions

It was the goal of this chapter to demonstrate that low-cost, consumer-grade UV resin 3-D printers offer opportunities in microfabrication to support further development of the CMAS into the microliter scale of sample handling. It was shown that fabrication by MSLA resin printing approaches traditional photolithography in scale and quality, and that careful choices in post-processing can maximize the potential of the MSLA printing approach. It is anticipated that inexpensive consumer-grade resin printing will be a great boon to research groups looking to expand their in-house prototyping and research capabilities.

Chapter 5. Summary and Conclusions

It was the goal of this thesis to standardize the concentration of sperm samples prior to cryopreservation through a low cost, open-technology approach. The specific objectives were addressed each in a chapter:

Ch. 2. A custom peristaltic pump and optical evaluation module to estimate aquatic sperm concentration

Prototypes of a custom peristaltic pump module and an optical evaluation module (POEM) were designed, fabricated, and evaluated. The prototypes were mounted together to form the POEM, and this assembled unit was evaluated with sperm samples from the channel catfish *Ictalurus punctatus*.

Ch. 3. A concentration measurement and adjustment system to prepare aquatic germplasm for cryopreservation

A prototype of the modular, open-technology concentration measurement and adjustment system (CMAS) was fabricated and tested. The CMAS integrated the POEM into the context of a complex, multi-technology device fabricated with 3-D printed and laser-cut parts, soldered electronics, and an Arduino microcontroller. It was found that the CMAS was able to dilute a sample of unicellular algae with an extender medium, showing that the various components of the CMAS were integrated into a single, functional device.

Ch. 4. Identifying opportunities for microfluidics with low-cost resin printing

Opportunities were identified to extend the use of the CMAS to microliter volumes by prototyping with inexpensive resin 3-D printing. It was found that low-cost, consumer-grade resin stereolithography offered feature resolutions approaching those of conventional microfabrication.

Design for Open Fabrication

The goal of the work in this conclusory chapter was to find applications for this thesis work in the open-technology and aquatic germplasm communities. The specific objectives were to: 1) identify design strategies in this thesis that can be applied to future open fabrication efforts, and 2) propose an addition to the AGGRC conception of the open-technology prototyping process.

The CMAS was designed for fabrication by a broad audience of developers and makers. The considerations for this fabrication mode are different from those for Design for Manufacturing (DfM), a common industrial design approach to the creation of products that may be injection molded, automatically assembled, laser-cut, or otherwise produced at scale, with maximum cost efficiency per unit and with planning for quality assurance⁷⁶. In Design for Open Fabrication (DfOF), the emphasis is on fabrication processes that are inexpensive or readily available, enabled by plans and instructions that are readily understood, easily distributed, and easily customized to meet new needs.

Three approaches to specific open fabrication problems encountered in the development of the CMAS are proposed here to enable DfOF efforts.

DIN rail prototyping

The first prototype of the CMAS was a proof of concept, with partial functionality and loose organization. The priority at that stage was on speed of work and interchangeability of parts. A mounting system based on DIN rails (commonly used in network and electrical cabinets), 3-D printing, and heat-set inserts was therefore developed (Figure 5.1) to enable rapid, robust prototyping with solderless breadboards, user interface components, and mounts for stepper motors and custom peristaltic pumps. This design approach can be widely applied in other open fabrication projects, particularly in the early stages of prototyping. It allows the rapid assembly of diverse components onto a solid, standardized frame.

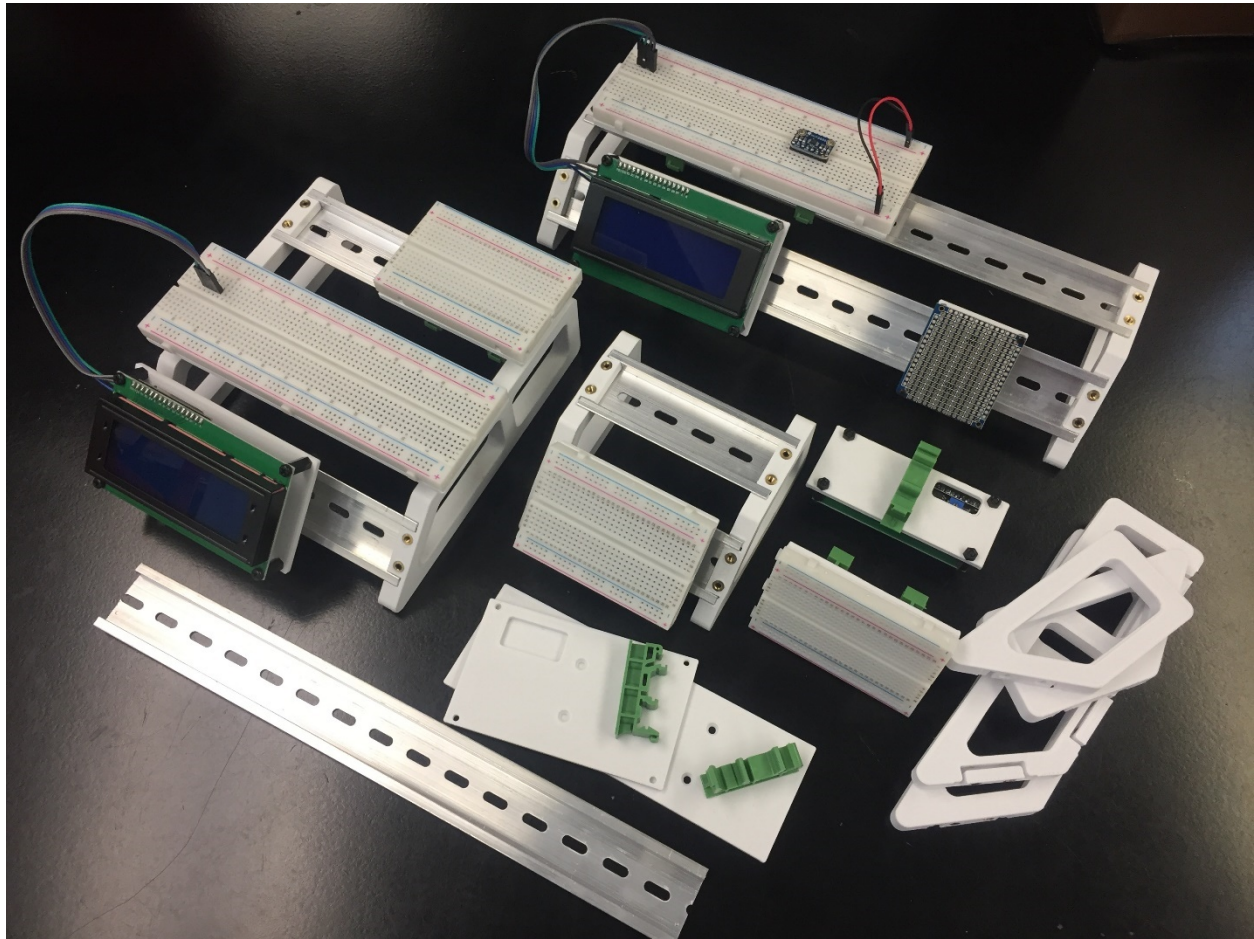


Figure 5.1. A DIN rail mounting system based on 3-D printing and heat-set threaded inserts. This system allows the snap-assembly of breadboards and user interface components for rapid prototyping.

The CMAS form factor

In developing the second prototype of the CMAS (i.e., the first version that was encased in acrylic), a need became apparent for a flexible case design that could be rescaled as components were added, removed, and redesigned. The case was therefore designed parametrically in Fusion 360. For example, the overall length, width, depth, and front face angle were all set as parameters that could be updated according to need. These parameters were set to propagate

through the design history, so that a simple change of a parameter would produce the correct laser-cutting and 3-D printed part files for immediate fabrication. In the event, there was indeed a need for the third CMAS prototype to be taller than the second, with a steeper front face. Updating the design to meet this need required less than 10 min of work.

To lower the barrier to entry for prototyping of other new devices, a simplified version of this parametric case (Figure 5.2) was produced as a Fusion 360 (.f3d) design file. This design, referred to as the CMAS form factor, has none of the cut-outs or mounting points that are specific to CMAS components. Instead, it is a stripped-down case form factor that may be resized for different applications. Eleven parameters, from overall dimensions to diameters for machine screw through-holes, can be adjusted by a user with little CAD knowledge, and the files for laser cutting and 3-D printing can quickly be produced. A more advanced user could customize the design further, adding cutouts, mounting points, and other components for fabrication. A guide to the CMAS form factor and to the use of the corresponding .f3d file is provided as appendix E of this thesis.

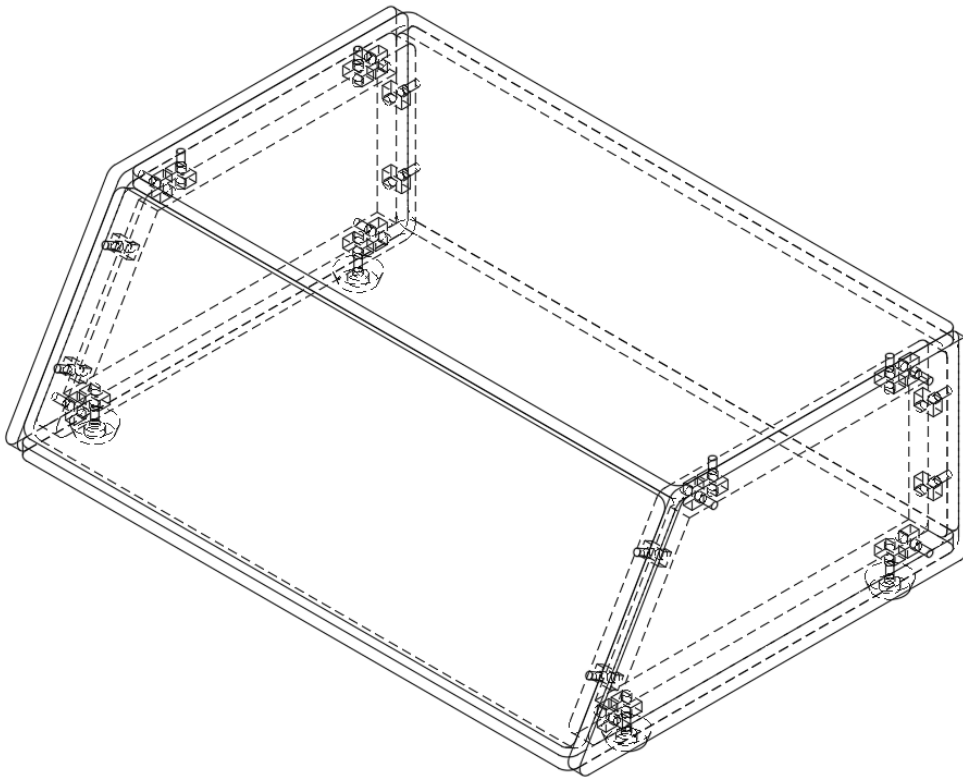


Figure 5.2. The CMAS form factor. This is a stripped-down parametric case design meant for use in the development of open technology projects.

Shrink-tube labelling of wires

In an electronic system with many wires running between components, it is necessary to label the wires clearly and permanently without creating obstructions. A first attempt at labelling, in which labels were simply folded onto the wires, produced poor results. These labels obstructed ongoing work and tended to peel apart and fall off the wires. A second attempt, adopting an approach similar to one used in commercial electronics, proved superior. A first layer of heat-shrink tubing was applied to increase the diameter of the 22 AWG wire, a label was applied, and

a length of clear heat-shrink tubing was applied (Figure 5.3). The process was time-consuming, but the result was low-cost, permanent, and professional in appearance. It also allowed secondary identification of wires by varying the color of the heat-shrink tubing or of the label. This approach can find wide application in open-fabrication projects where many wire runs are necessary and simply color-coding wires does not identify them sufficiently.

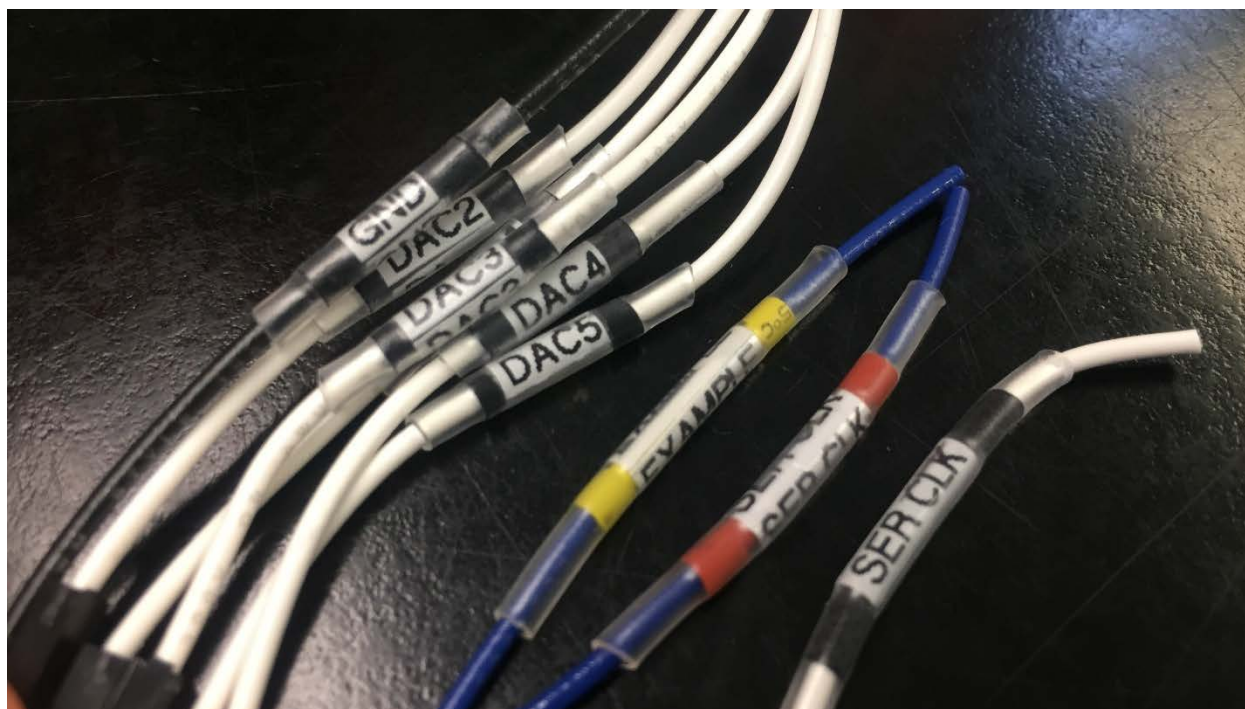


Figure 5.3. Labeling wires with color-coded shrink tubing.

Variations on the AGGRC Prototyping Process

As outlined in the preface, the development of the CMAS spanned the component and operation prototyping phases of the AGGRC technology development process, with some biological testing to establish feasibility of this open technology in the aquatic cryopreservation workflow. This prototyping process was conceived with thermoplastic (FDM) 3-D printing in mind as the principal fabrication method. Most tools and devices currently in development at the AGGRC follow this method, such as the positional cooling platform device (PCPD) and shipping dewar positional cooling device (SDPCD), which are meant to improve the ease and reliability of freezing French straws in cryogenic nitrogen vapor. For these devices, current efforts aim to add electromechanical control, feedback, and recording functions to the existing designs. However, in the case of the CMAS, the project was conceived with integration of electronics and multiple fabrication technologies from the beginning. The development of the CMAS therefore serves as a starting point for future complex open-technology projects at the AGGRC and elsewhere.

The community members participating in the development and use of such a device may be categorized as developers, makers, or users. Developers create novel ideas, designs, and instructions. Makers produce copies and modifications of the designs supplied by developers. Finally, users apply finished products to real-world problems in research and industry. A participant in the community may fall into more than one category. The AGGRC, for example, is a group that encompasses all three activities, from generation of ideas, to prototyping and testing,

to application in an aquatic germplasm workflow. As developers they integrate under one roof theory and practice, prototyping and testing, and they are uniquely positioned to approach prototyping from a user and a maker perspective early in the design process. An elaboration of the AGGRC prototyping process is therefore proposed, accommodating complex multi-technology projects with an early focus on adopting different roles (developer, maker, user) and adapting the design based on experience from these perspectives.

The *operation prototyping* phase is particularly ripe for extension because it is the first phase in which the diverse components are brought together as a single, integrated device. It is at this stage that software must interact with hardware, components must communicate with one another, and conflicts or flaws that involve interference between components may come to light. In the case of the CMAS, this is the stage at which the pump sub-modules were first controlled by the firmware, the optics produced signals that could be interpreted by the user, and electrical power was drawn for all components from a single central supply. An extension to the operation prototyping phase is therefore proposed (Figure 5.4) in which the developer explicitly steps into other roles.

The typical developer at the AGGRC works regularly with aquatic germplasm, which affords an opportunity to do rudimentary device testing, or at least to consider the steps that a user must adopt to include the device in a workflow. The developer may not collect meaningful data with respect to the handled germplasm (given that this will be a device early in development), but may benefit immensely from simulating, and perhaps timing, the activities that a user will carry out at the laboratory bench, with an early prototype of the device on hand. The ‘user evaluation’ activity conventionally comes later in the development process (early and late test product phases); here, it is emphasized that user interaction is fundamental to the design from early in the process. After all, if the end user cannot make effective use of the device, it has not met its purpose.

Likewise, the developer may normally have access to ample fabrication technologies, but must explicitly consider the maker’s perspective. The developer might attempt to fabricate the prototype device under restrictive conditions: for example, with an inexpensive 3-D printer and limited tools, or with limitations of time in the fabrication and assembly from raw materials to a finished device. A peer developer might equally adopt this role and fabricate the prototype, approaching it as an external maker, following verbal or simple written instructions. These exercises could help to reveal difficulties in fabrication and assembly that would not otherwise become apparent until the test product was sent out in a later phase of development.

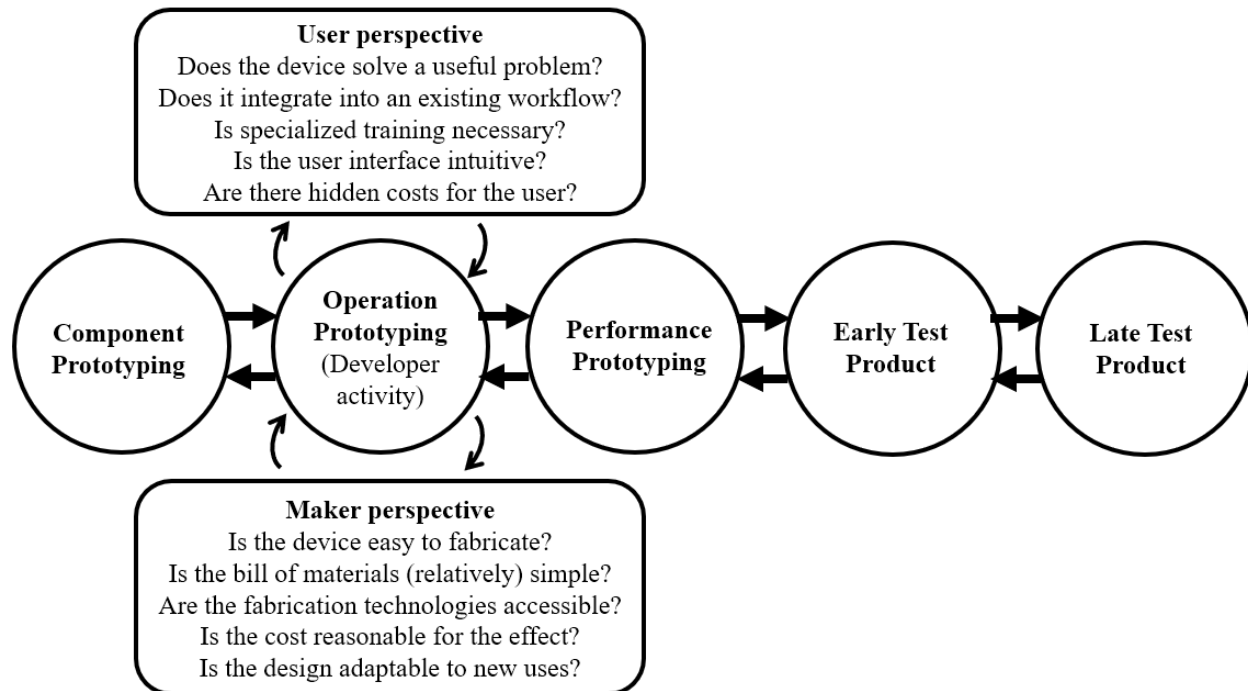


Figure 5.4. A possible elaboration of the operation prototyping phase of device development. Heavy horizontal arrows indicate the main, existing prototyping workflow. Lighter, curved arrows indicate excursions into new considerations during operation prototyping. All activities in the main workflow are intrinsically developer activities, although in the existing conception they may involve users and makers in the later stages.

Conclusions

The prototyping of the CMAS was a step to address some of the many problems in the standardization of workflows for the cryopreservation of aquatic germplasm. As sophisticated fabrication methods fall in cost and the maker movement spreads more widely, opportunities will grow to distribute technology to laboratory groups around the world. In the context of the protection and use of genetic resources, these opportunities can translate into open technology that can reduce costs, improve the efficiency of technical work, and improve the standardization of samples, and so too improve their consistency, quality, and value. In this way, open-technology approaches can support the development of repositories for genetic resources, which can come to rely on aggregate throughput and distributed processing. With the open distribution of ideas, designs, and fabrication methods, local efforts can be made into fruitful collaborations, and collaborations can be applied to help solve global problems.

Appendix A. Guide to Fabrication and Assembly of the Concentration Measurement and Adjustment System

Overview

The CMAS was fabricated using three technologies: 3-D printing, laser cutting, and soldering. It is expected that the maker will have some familiarity with each of these or will be willing to learn independently. Concise fabrication instructions are provided here with the more experienced maker or developer in mind. Many tutorials are available online that introduce these fabrication technologies. Three starting points are suggested here.

3-D printing: hubs.com/knowledge-base/introduction-fdm-3d-printing

Laser cutting: hubs.com/blog/laser-cutting


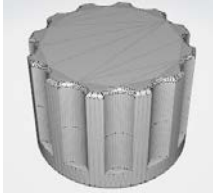
Soldering: makerspaces.com/how-to-solder

3-D printing of the .stl files

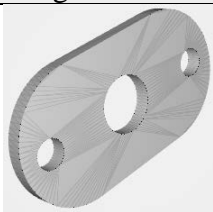




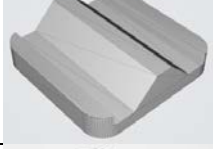



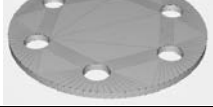
The 3-D printing files are provided in .stl ('stereolithography') format, a simple mesh representation of 3-D geometry made up entirely of triangular faces. These files contain no information specific to one 3-D printer or material, nor do they explicitly include dimensions (although they are implicitly measured in mm, which is the usual unit for 3-D printing software). The maker must use software called a *slicer* to convert the .stl files into a format that the 3-D printer will be able to use.

The files provided herein (Table A.1) were processed in Cura slicing software 4.9.0 (Ultimaker, Utrecht, Netherlands) and 3-D printed with polylactic acid (PLA) thermoplastic (eSun, Shenzhen, China, esun3d.net) on an Ultimaker 3 Extended (Ultimaker) 3-D printer (Figure A.1). However, it should be possible to produce the necessary parts on any common 3-D printer. Note that the optical enclosures should be printed in black or another dark, opaque filament to help exclude light.

Table A.1. 3-D printed components. These parts can be printed in any color of filament except where otherwise noted.

| Component | Quantity | Note | Image |
|--------------|----------|------|---|
| Card slot | 1 | |  |
| Encoder knob | 1 | |  |

(table cont'd.)

| Component | Quantity | Note | Image |
|----------------------|----------|--|---|
| Encoder slot | 1 | |  |
| Frame brace | 2 | |  |
| Frame foot | 4 | |  |
| Frame handle | 2 | |  |
| Optics base | 7 | 5 should be printed in black (for opacity); the other 2 can be any color |  |
| Optics cap | 5 | 1 printed in black for each populated optics group |  |
| Pump base | 3 | |  |
| Pump motor spacer | 3 | |  |
| Pump rider | 3 | |  |
| Pump rotor cap plate | 3 | |  |

(table cont'd.)

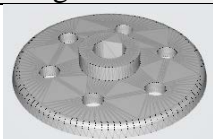

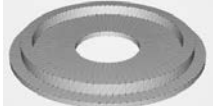

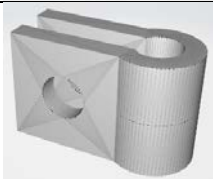
| Component | Quantity | Note | Image |
|----------------------------|----------|--|---|
| Pump rotor half | 6 | |  |
| Tube holder | 4 | |  |
| Tube adapter insert 1.5-mL | 4 | Only print if needed |  |
| Tube adapter insert 15-mL | 4 | Only print if needed |  |
| Tubing clamp | 3 | Keeping several spares is recommended to help with changing out tubing |  |

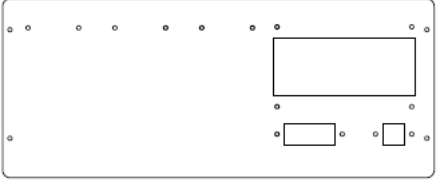
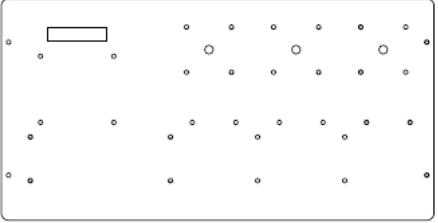

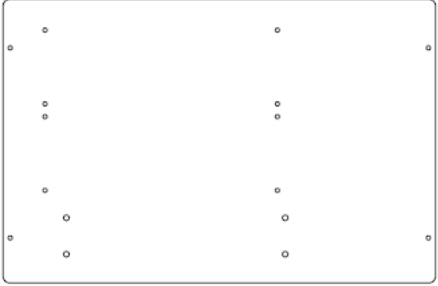
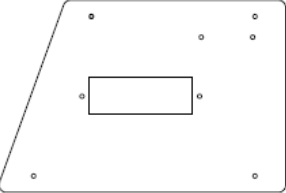


Figure A.1. An assortment of CMAS parts printed on the Ultimaker 3 Extended 3-D printer.

Laser cutting the body panels

The body panels of the CMAS are designed to be cut from 1/4" (6 mm) acrylic (PMMA). The exact method for cutting will vary according to the laser used. This work used a Muse 1064-nm CO₂ laser cutter (Full Spectrum Laser, Las Vegas, Nevada, USA) with a 12 × 20" cutting bed, which allowed cutting of multiple panels from a single sheet of material. The panels were cut completely through with three passes of the laser at 50% speed, 100% power, and 100% current (as set in the custom firmware that runs the laser cutter). As an aid in planning and splitting material for cutting, the dimensions and quantities of each panel are summarized in Table A.2.

Table A.2. Body panels to cut. The given dimensions are the maximum dimensions of each panel, *i.e.* the dimensions of the rectangular bounding box containing the panel.

| Panel | Dimensions (mm) | Dimensions (in) | Quantity | Image |
|--------|-----------------|-----------------|----------|--|
| Front | 298.0 × 123.4 | 11.74 × 4.86 | 1 |  |
| Top | 298.0 × 152.2 | 11.74 × 6.00 | 1 |  |
| Back | 298.0 × 118.0 | 11.74 × 4.65 | 1 |  |
| Bottom | 298.0 × 195.2 | 11.74 × 7.69 | 1 |  |
| Side | 195.2 × 130.0 | 7.69 × 5.12 | 2 |  |

Other fabrication methods are possible, although more laborious, without access to a laser cutter. For example, the panels could be cut with a bandsaw and a drill press. In this case, the provided patterns (in .dxf format) could be printed out on plain office paper and glued with spray adhesive to the acrylic. The cuts and holes could be made following the printed patterns. Nor must the panel material be acrylic: fiberboard or thin plywood should serve equally well.

Assembling the electronics

Fabricating the electronics requires several skills: reading circuit diagrams, identifying electronic components, soldering, and crimping wire connectors.

Layout

A pin-by-pin layout of the breadboards is not provided here, but full circuit diagrams are provided in Appendix C. A possible layout is provided (Figure A.2) to guide planning of breadboard space.

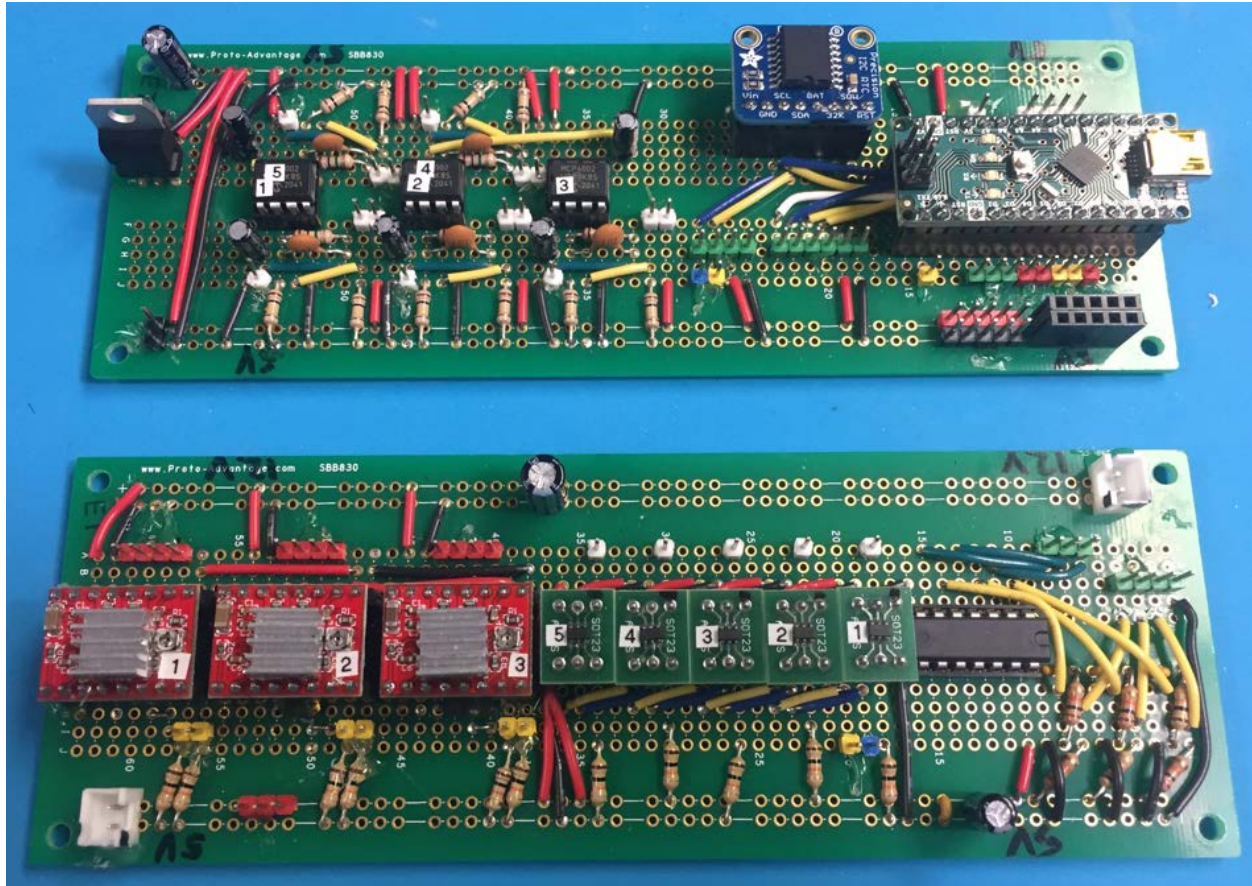


Figure A.2. The two main breadboards of the CMAS.

Soldering

Most soldering for the CMAS is conventional through-hole soldering. However, the DAC ICs are only available in a surface-mount package (Figure A.3). It was therefore necessary to

solder the DACs to 6-pin 0.1" SOT-23 adapter boards, which matched the pitch of standard through-hole breadboards. This can be done by hand with drag soldering or a similar technique. This is made easier by the careful selection of a soldering tip (a drag soldering tip is suggested in the Bill of Materials, Appendix B) and a generous application of flux to prevent solder bridging.

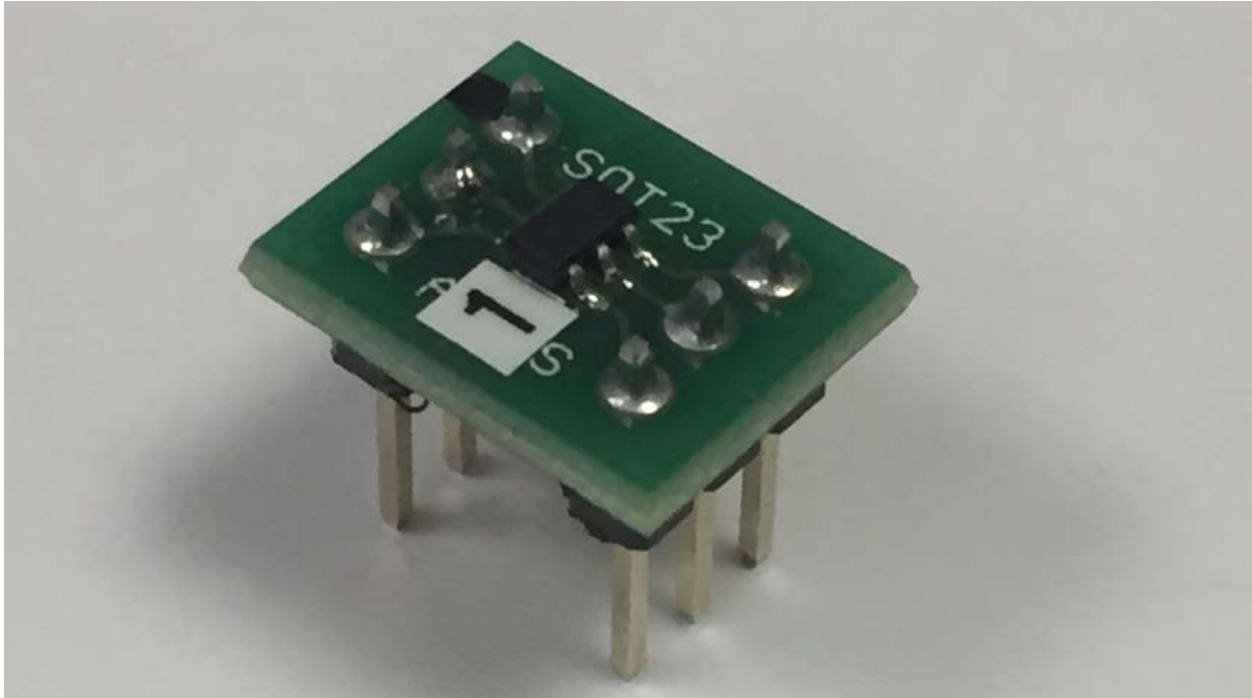


Figure A.3. A DAC IC in a SOT-23 package soldered to an adapter board.

Wiring and labeling

This design can include a large number of wires to connect power and data to the various components. For assembly and later troubleshooting, it is best to consistently and cleanly label each wire as it is cut and crimped. One possible approach to this labelling is suggested in Ch. 5. The exact wiring configuration (Figure A.4) will be up to the individual maker and the available wiring supplies, although some Dupont crimp terminals and a crimper are suggested in the Bill of Materials.

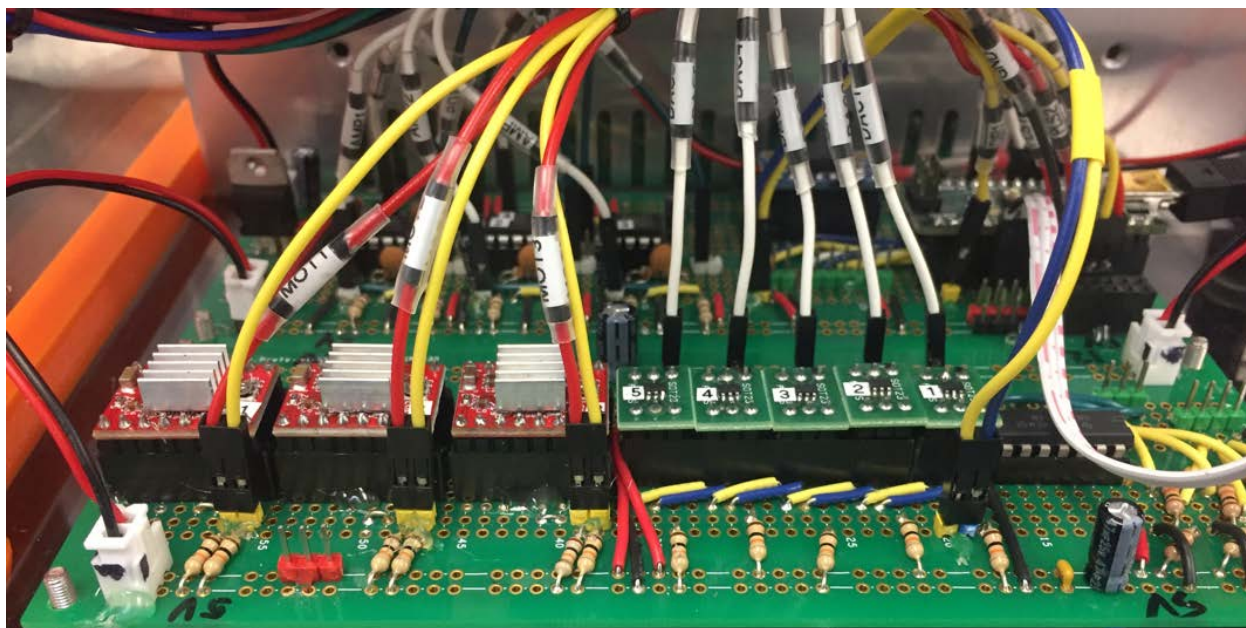


Figure A.4. An example of wiring in the CMAS.

Assembling the frame

It is easiest to assemble the frame by installing the power supply and frame braces onto the bottom panel first (Figure A.5a). Doing so before installing the back panel allows access to the power supply distribution terminals for connection of external power (A.5b).

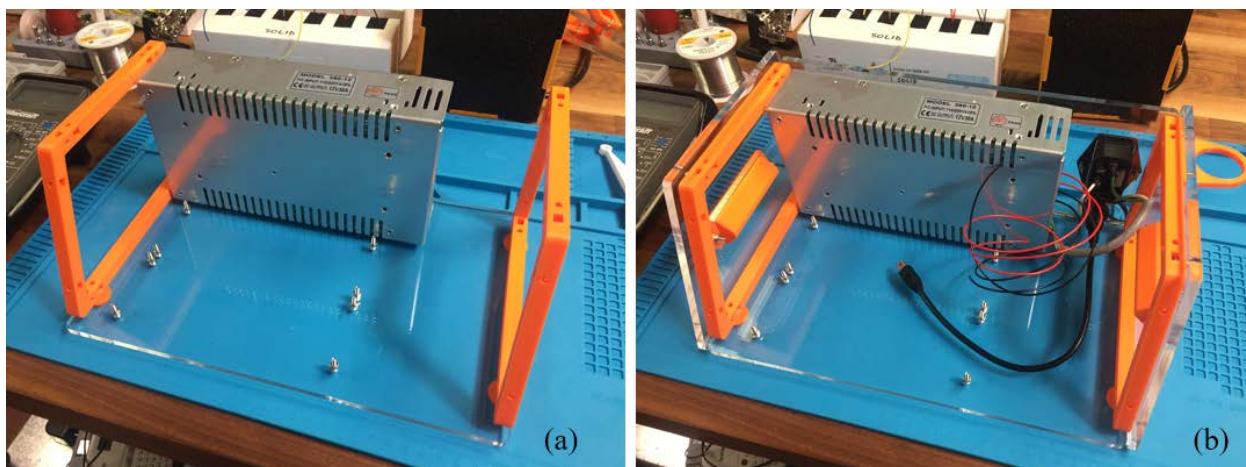


Figure A.5. Assembling the frame. (a) Installation of the power supply and frame braces on the bottom panel. (b) Connection of external power, and installation of the back and side panels.

The top and front panels, including the pumps, optics, and user interface components, are meant to be easily removed (Figure A.6), and are best installed last (Figure A.7).

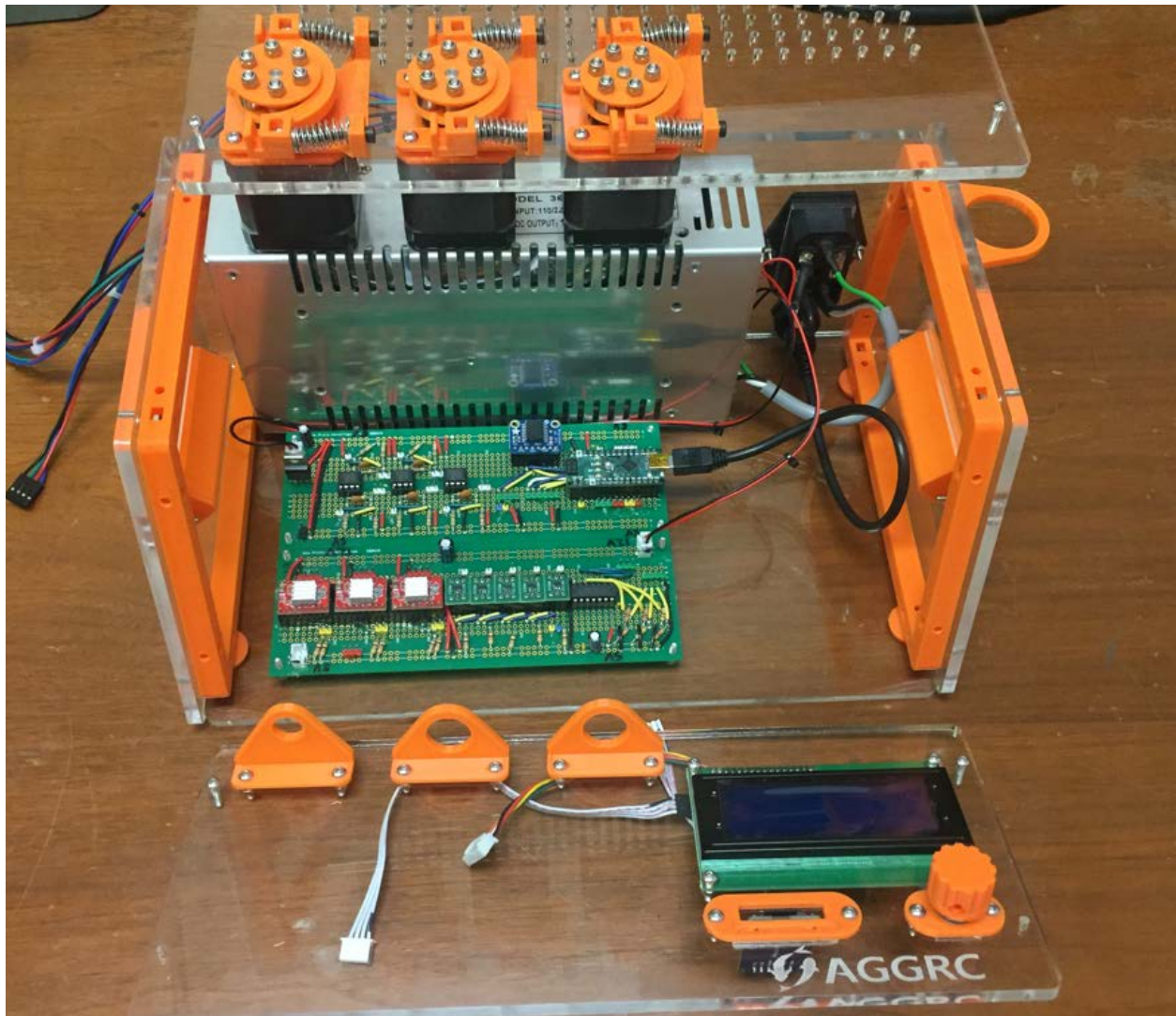


Figure A.6. Assembly of the top and front panels. Installation of the breadboards onto the bottom panel.

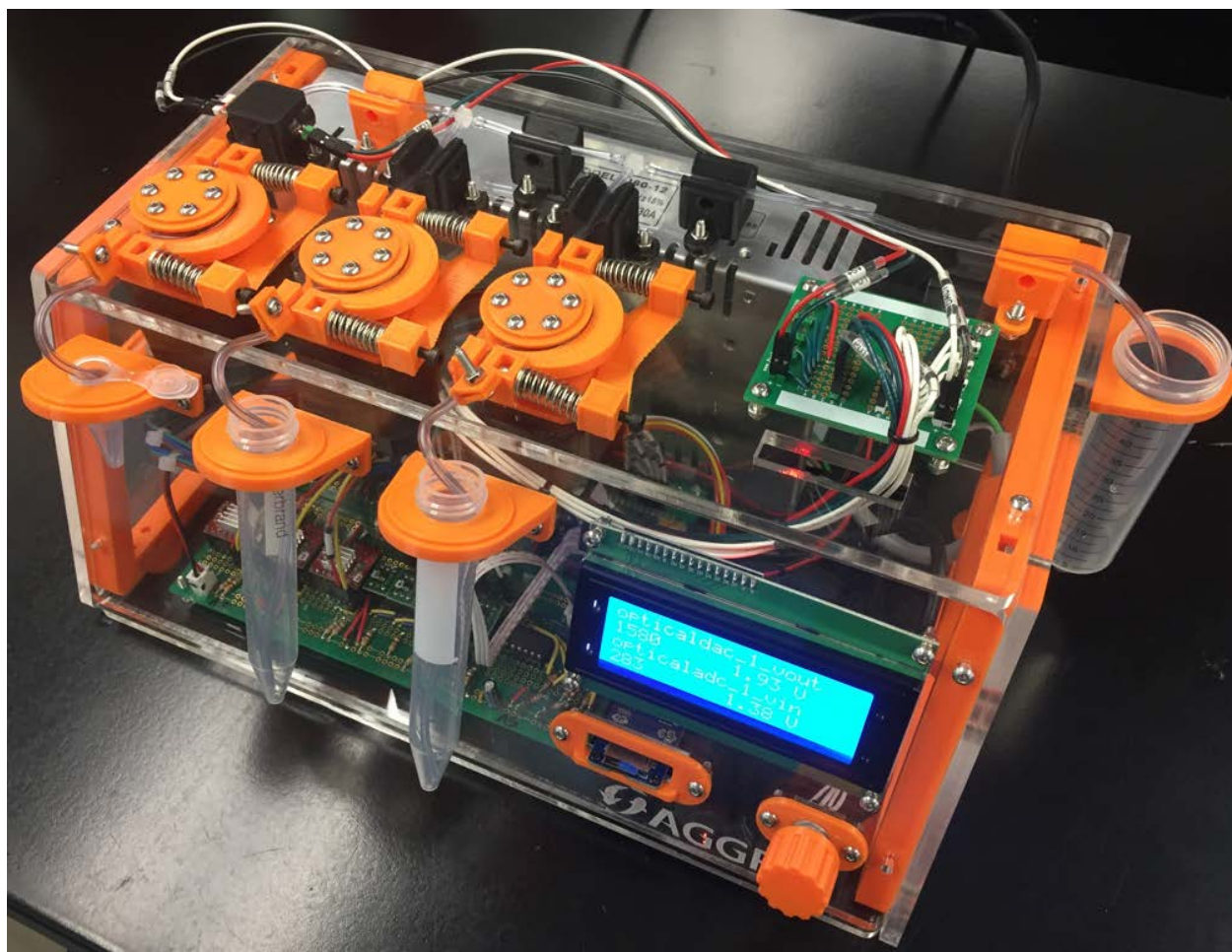


Figure A.7. The assembled CMAS.

Appendix B. CMAS Bill of Materials

Quantities for certain bulk purchases are given as follows: “1 (10)” means the item is available as a package of 10, but only 1 is used in the project. The cost given is for the full package of 10. “3 (3)” means that 3 are required, and the cost given is for a pack of 3. Costs are estimates in US dollars as of 2021. No tax or shipping is included. “Ext.” is the extended cost, i.e., (cost × quantity). Many items, especially the tools, are listed only as suggestions and may be substituted with another brand. For example, the Ender 3 3-D printer is only one of many entry-level 3-D printers offered; likewise with the Hakko FX888D soldering station. Many items are available from other vendors; the links listed are provided for convenience.

Table B.1. Fabrication technologies and tools.

| Item | Comment | Link | Cost | Quantity | Ext. |
|-----------------------------------|--|---|---------|----------|---------|
| 3-D printer | | amazon.com/dp/B07BR3F9N6 | 174.99 | 1 | 174.99 |
| Muse CO ₂ laser cutter | | fslaser.com/musecore/ | 3524.00 | 1 | 3524.00 |
| Hakko FX888D soldering station | | amazon.com/dp/B00ANZRT4M | 104.95 | 1 | 104.95 |
| T18-D16 soldering chisel tip | General-purpose tip | amazon.com/dp/B004OR9BV4 | 8.99 | 1 | 8.99 |
| T18-CF15 soldering bevel tip | For surface-mount components | amazon.com/dp/B004OR9BLO | 9.99 | 1 | 9.99 |
| Solder | | amazon.com/dp/B08RHMPJW3 | 8.99 | 1 roll | 8.99 |
| Flux pen | | amazon.com/dp/B07B53LNGX | 7.95 | 1 | 7.95 |
| Fine tweezers | For surface-mount components | amazon.com/dp/B00FZPESTY | 16.07 | 1 | 16.07 |
| Solder wick | | amazon.com/dp/B0195UVWJ8 | 9.74 | 1 roll | 9.74 |
| Flush cutters | | amazon.com/dp/B00FZPDG1K | 7.47 | 1 | 7.47 |
| Lighter | To heat shrink tubing | amazon.com/dp/B086R3LFBW | 11.98 | 1 (10) | 11.98 |
| Screwdrivers, metric hex set | 2.0 mm for M3 screws; 2.5 for M4 and M3 smooth shaft | amazon.com/dp/B000NZ5QE2 | 19.43 | 1 set | 19.43 |

(table cont'd.)

| Item | Comment | Link | Cost | Quantity | Ext. |
|----------------------|---|---|-------|-----------------|-------|
| Needle nose pliers | | amazon.com/dp/B093K71F9F | 13.99 | 1 | 13.99 |
| Parallel-jaw pliers | Not required, but useful for gripping hex nuts | amazon.com/dp/B01FSV4PME | 19.95 | 1 | 19.95 |
| Wire strippers | To strip wire insulation | amazon.com/dp/B0000302WS | 11.99 | 1 | 11.99 |
| Small zip ties | To keep wire bundles neat | amazon.com/dp/B075F78RX5 | 11.99 | As needed (500) | 11.99 |
| Hot glue gun | Used as a soldering aid | amazon.com/dp/B095C32T5C | 9.99 | 1 | 9.99 |
| Label maker | To mark wires, (a pen and masking tape will work) | amazon.com/dp/B013DG2FNW | 34.99 | 1 | 34.99 |
| Wire bender | 3-D printed | thingiverse.com/thing:1274814 | - | 1 | - |
| Resistor lead bender | 3-D printed | thingiverse.com/thing:4191881 | - | 1 | - |
| IC lead straightener | 3-D printed | thingiverse.com/thing:3121797 | - | 1 | - |

Table B.2. Hardware and raw fabrication materials.

| Item | Comment | Link | Cost | Quantity | Ext. |
|---|---------------------------------------|---|-------|-----------|-------|
| 6-mm acrylic sheet | Any color | amazon.com/dp/B07H9NQP8G | 22.99 | 2 | 45.98 |
| M3 machine screw 14 mm | | amazon.com/dp/B08H2HQ3VZ | 5.99 | 105 (100) | 11.98 |
| M3 half thread socket cap machine screw 40 mm | For peristaltic pump rider assemblies | amazon.com/dp/B076XKGNDB | 10.99 | 6 (20) | 10.99 |
| M3 hex nut | | amazon.com/dp/B082D6M295 | 5.99 | 75 (200) | 5.99 |
| M3 nylock hex nut | | amazon.com/dp/B0865NLJNN | 7.99 | 24 (100) | 7.99 |

(table cont'd.)

| Item | Comment | Link | Cost | Quantity | Ext. |
|--|--|---|-------|---------------|-------|
| M4 machine screw 12 mm | To attach power supply | amazon.com/dp/B084Q45BGR | 6.91 | 4 (100) | 6.91 |
| Mini self-tap screws M2 6 mm | To secure microSD card reader | amazon.com/dp/B081DVZMHH | 12.29 | 2 (60) | 12.29 |
| PLA 3-D printing filament | Any color works, but optical enclosures are printed in black | amazon.com/dp/B01EKEMDA6 | 22.99 | 1 kg roll | 22.99 |
| PolySupport 3-D printing filament | Not needed, but useful for dual extrusion. Link is for 2.85 mm | amazon.com/dp/B07XP75M2Y | 39.99 | 750 g roll | 39.99 |
| Ball bearings 3 × 9 × 5 mm | | amazon.com/dp/B082PQNVF7 | 8.89 | 18 (10) | 17.78 |
| Assorted springs | Use 6 of (7/32 × 1 1/2") and 6 of (23/64 × 1 3/8") | amazon.com/dp/B000K7M36W | 10.99 | 12 (20) | 10.99 |
| Plastic barbed tube fitting for food & beverage, 1/16" tube ID | | mcmaster.com/5116K183/ | 6.06 | 30 (10) | 18.18 |
| Continuous-flex soft plastic tubing, 1 mm ID 3 mm OD | | mcmaster.com/3774N1/ | 31.50 | 50 ft (50 ft) | 31.50 |

Table B.3. Electronic components.

| Item | Comment | Link | Cost | Quantity | Ext. |
|--|------------------------|---|-------|----------|-------|
| Arduino Nano | | amazon.com/dp/B0097AU5OU | 19.80 | 1 | 19.80 |
| Mini USB case-mount plate and extension | | amazon.com/dp/B082J1BL6H | 9.99 | 1 | 9.99 |
| USB cable | | amazon.com/dp/B00NH13S44 | 5.87 | 1 | 5.87 |
| NEMA 17 stepper motor | | amazon.com/dp/B07LCK19D5 | 27.99 | 3 (3) | 27.99 |
| A4988 stepper motor driver module | | amazon.com/dp/B01FFGAKK8 | 10.99 | 3 (5) | 10.99 |
| Wall-socket-to-C14 power cable | Or regional equivalent | amazon.com/dp/B072BYGKZZ | 8.99 | 1 | 8.99 |
| C14 panel mount power socket | | amazon.com/dp/B082ZFRV1B | 8.49 | 1 (3) | 8.49 |
| 12-V 30-A power supply | | amazon.com/dp/B01EWG6YT8 | 17.98 | 1 | 17.98 |
| I ² C 20×4 LCD module | | amazon.com/dp/B01GPUMP9C | 12.99 | 1 | 12.99 |
| Resistor 10 kΩ ¼ W | | digikey.com/short/20n1pdq9 | 0.10 | 27 | 2.70 |
| Resistor 100 kΩ ¼ W | | digikey.com/short/0wnhpnrf | 0.10 | 10 | 1.00 |
| Solderable breadboard 400 point | | digikey.com/short/8cjwbjmt | 3.99 | 1 | 3.99 |
| Solderable breadboard 830 point | | digikey.com/short/rb8jt0q8 | 6.49 | 2 | 12.98 |
| Pin header assortment, male & female | | amazon.com/dp/B07RRPYZCT | 9.99 | 1 pack | 9.99 |
| Dupont connector assortment with crimping tool | | amazon.com/dp/B07PCQ5VMV | 26.89 | 1 pack | 26.89 |

(table cont'd.)

| Item | Comment | Link | Cost | Quantity | Ext. |
|---|--|---|-------|----------------|-------|
| Solid 22 AWG wire, assorted colors | For use directly on soldered breadboard | digikey.com/short/885h54hn | 16.95 | 1 pack | 16.95 |
| Stranded 22 AWG wire, assorted colors | For use in running between components | digikey.com/short/n8df2p9n | 16.95 | 1 pack | 16.95 |
| JST-XH cables | | amazon.com/dp/B07DVFTGSL | 7.99 | As needed (50) | 7.99 |
| MCP6002 dual op-amp | | digikey.com/short/8pn2j7t4 | 0.38 | 3 | 1.14 |
| 74HC14 hex inverting Schmitt trigger IC | | digikey.com/short/hv82f71d | 0.61 | 1 | 0.61 |
| Ceramic capacitor 100 pF | | digikey.com/short/rhntn9bv | 0.26 | 5 | 1.30 |
| Ceramic capacitor 0.1 μ F | | digikey.com/short/t22bpcz9 | 0.23 | 6 | 1.38 |
| Electrolytic capacitor 100 μ F | | digikey.com/short/2v0f9pvv | 0.28 | 2 | 0.56 |
| IC socket (14-pin) | May be swapped out for two 8-pin sockets | digikey.com/short/b9v5wzzn | 0.27 | 1 | 0.27 |
| IC socket (8-pin) | | digikey.com/short/m9t4fm04 | 0.20 | 3 | 0.60 |
| 7805 linear voltage regulator | | digikey.com/short/t5nqcw8t | 0.89 | 1 | 0.89 |
| Photodiode SFH 203 P | | digikey.com/short/4rfq94dp | 1.15 | 5 | 5.75 |
| LED, tri-color QBL8RGB-60D0-2897 | | digikey.com/short/zpt12zdd | 1.05 | 5 | 5.25 |
| DAC: A0 variant | | Mouser: MCP4725A0T-E/CH | 1.01 | 2 | 2.02 |

(table cont'd.)

| Item | Comment | Link | Cost | Quantity | Ext. |
|-------------------------------|--------------------------------|--|-------|--------------------|-------|
| DAC: A1 variant | | Mouser: MCP4725A1T-E/CH | 1.01 | 2 | 2.02 |
| DAC: A2 variant | | Mouser: MCP4725A2T-E/CH | 1.01 | 1 | 1.01 |
| SOT-23 0.1” pitch adapter | | Mouser: 535-LCQT-SOT23-6 | 4.49 | 5 | 22.45 |
| Rotary encoder | | digikey.com/short/95tnfvv7 | 2.34 | 1 | 2.34 |
| 3-conductor mains power cable | Salvage from an old power cord | - | - | 20 cm | - |
| Shrink tubing assortment | To insulate wire connections | amazon.com/dp/B072PCQ2LW | 6.49 | As needed (1 pack) | 6.49 |
| microSD card breakout board | | amazon.com/dp/B07MTTLF75 | 8.99 | 1 (5) | 8.99 |
| microSD card 32 GB | | amazon.com/dp/B073JWXGNT | 9.72 | 1 | 9.72 |
| DS3231 real-time clock module | | amazon.com/dp/B0718XYTBT | 17.56 | 1 | 17.56 |
| CR1220 battery | For real-time clock | amazon.com/dp/B0751YTGST | 4.27 | 1 (10) | 4.27 |

Table B.4. Total costs to build the CMAS.

| | |
|--|----------------|
| B.1. Fabrication technologies and tools | 4007.45 |
| B.2. Hardware and raw fabrication materials | 243.56 |
| B.3. Electronic components | 317.15 |
| | |
| Total excluding fabrication technologies and tools (sum of tables B.2 and B.3) | 560.71 |
| GRAND TOTAL (sum of tables B.1, B.2, and B.3) | 4568.16 |

Appendix C. CMAS Circuit Diagrams

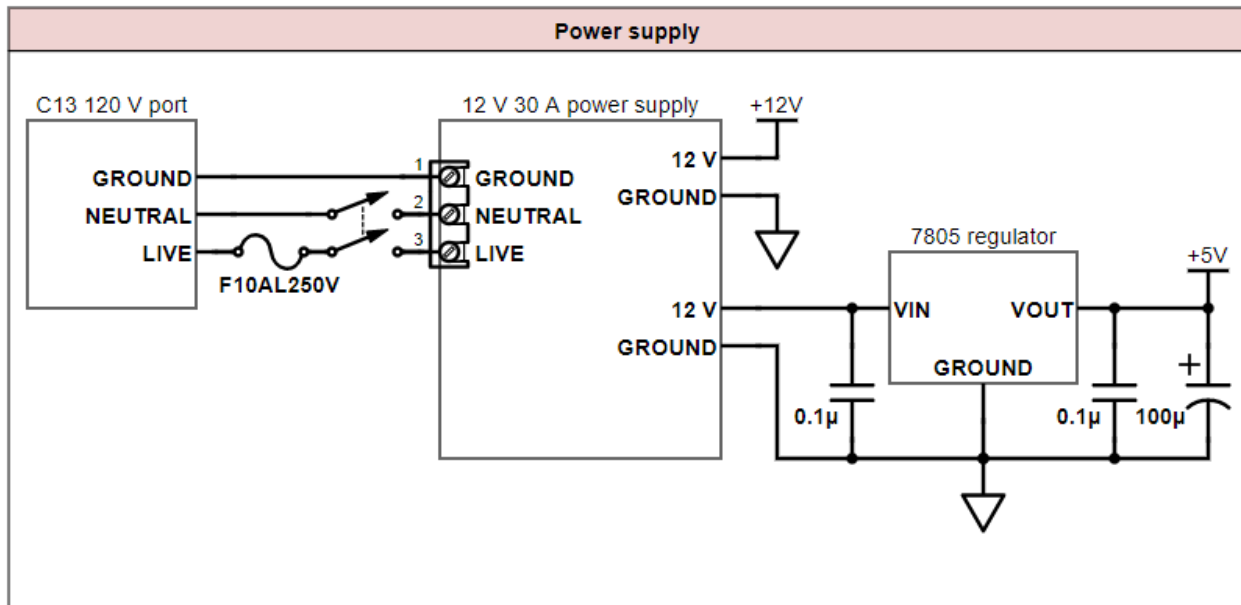


Figure C.1. Circuit diagram of the power supply.

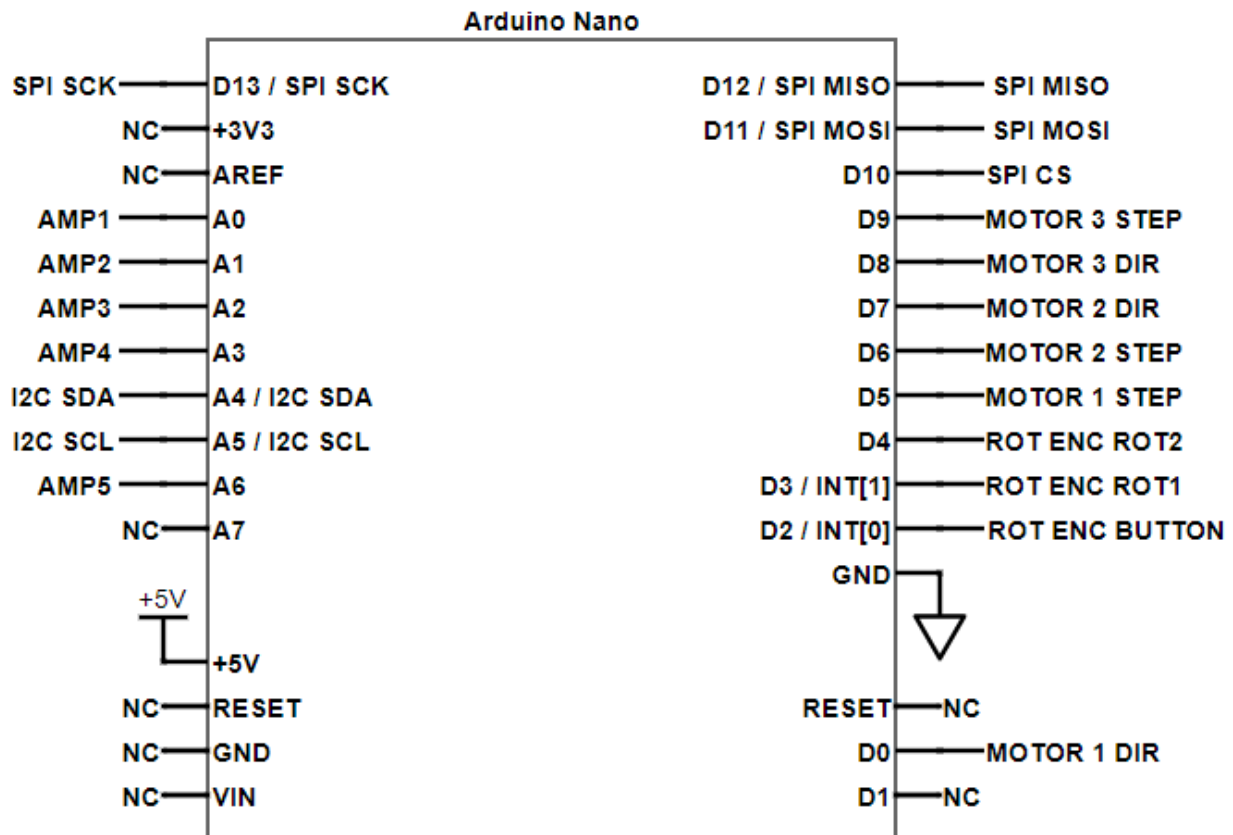


Figure C.2. Pinout of the Arduino Nano microcontroller platform. NC: no connection.

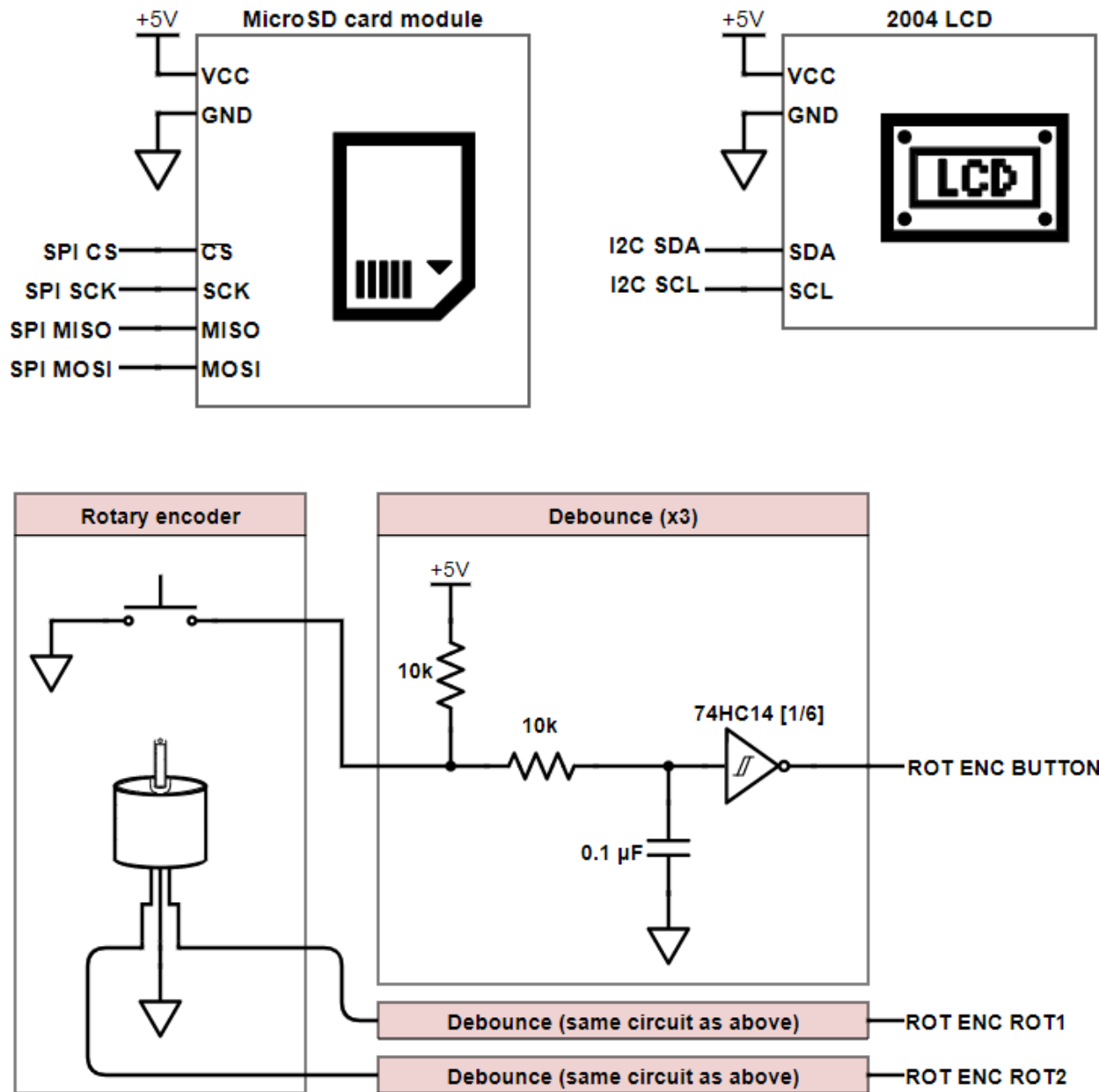


Figure C.3. Pinouts and circuit diagrams of the MicroSD card module, 2004 LCD module, and rotary encoder. One debounce circuit is needed for each rotary encoder output. The rotary encoder is a single electromechanical component incorporating a pushbutton (two pins) and a quadrature encoder (three pins). These two elements of the rotary encoder are shown separately in the “Rotary encoder” panel to clarify the electrical connections.

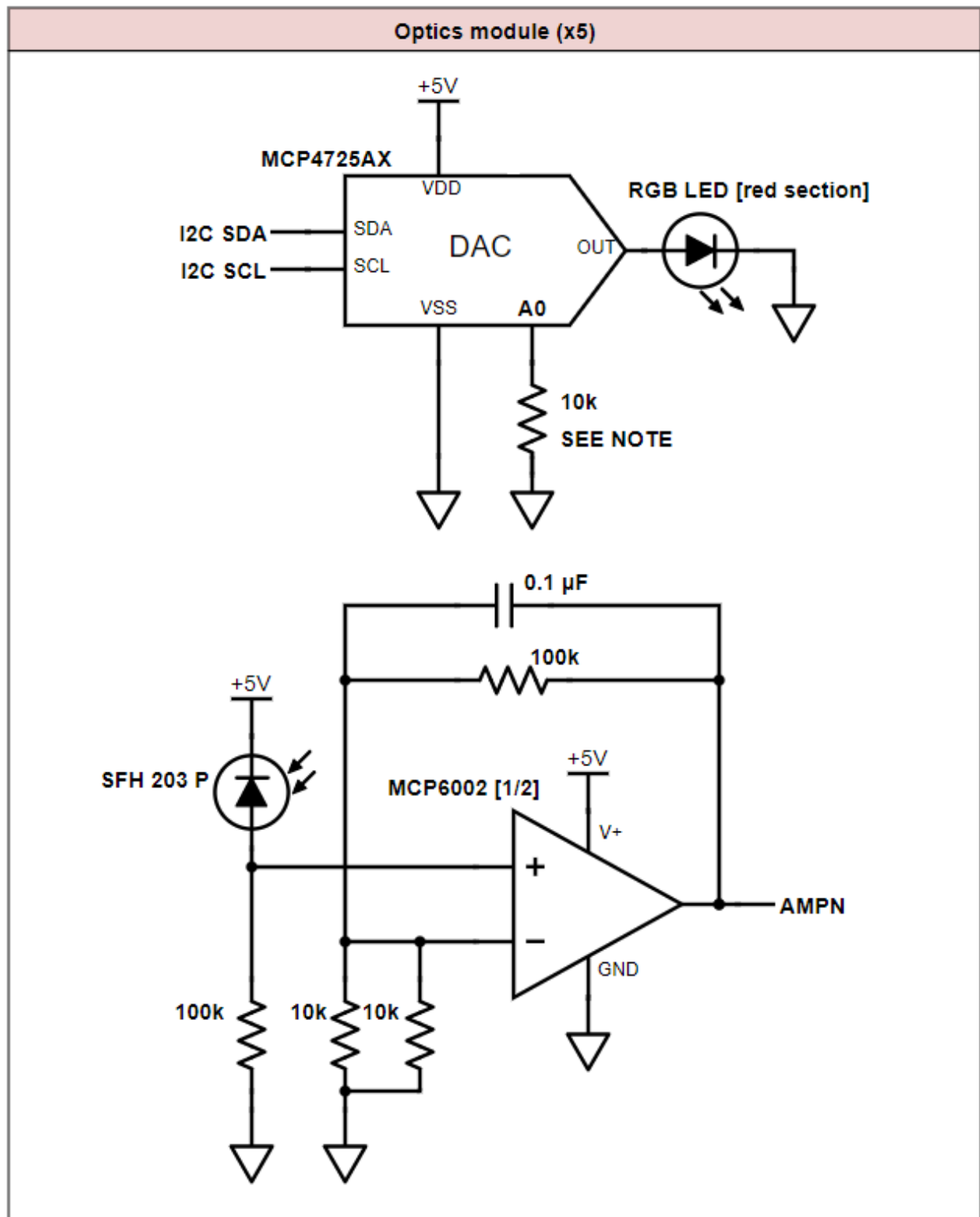
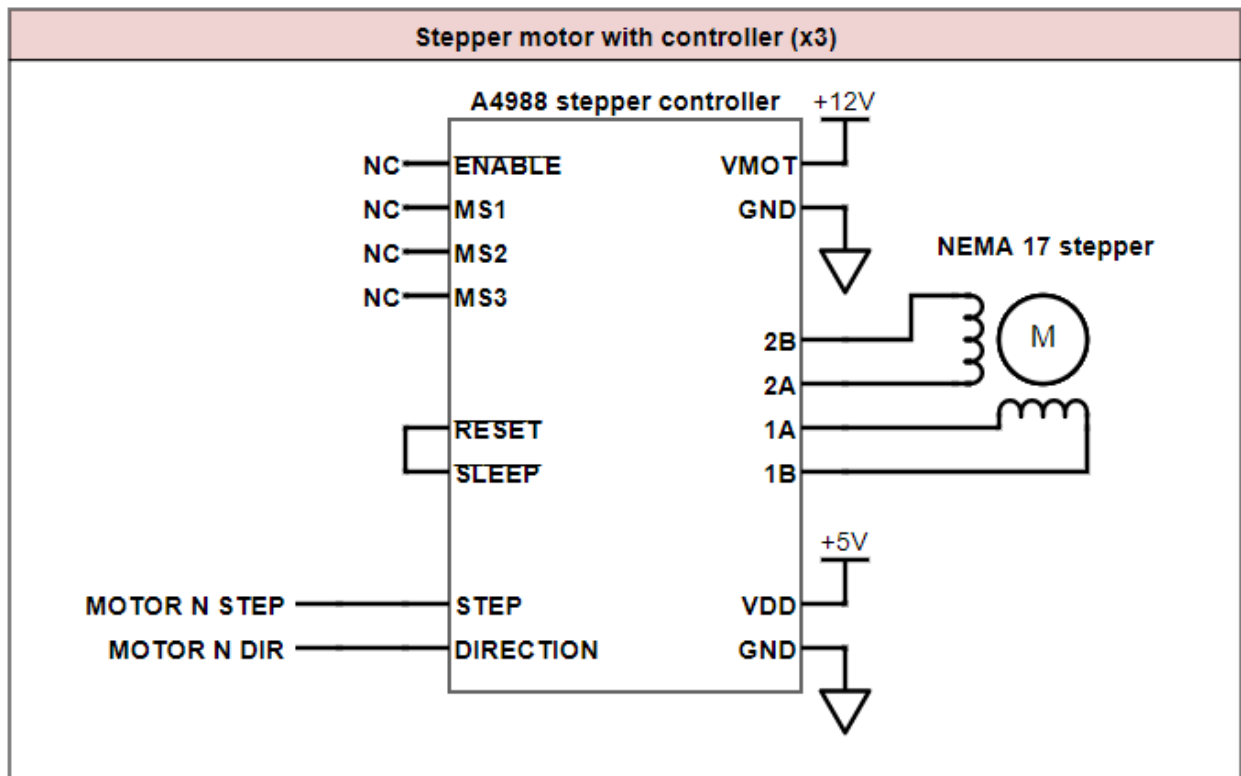


Figure C.4. Circuit diagram of an optics module. A module comprises an LED, the Digital–Analog Converter (DAC) supporting the LED, a photodiode, and the operational amplifier circuit supporting the photodiode. Up to five optics modules may be fitted to the CMAS. The five MCP4725 DAC ICs must each have a unique I²C bus address to prevent conflict. This IC comes

in four variants, each of which has two possible addresses set by pin A0. The base address of each variant is different and is set at the factory. The variants differ only in their base address and in no other way. This design uses two of the A0 variant, two of the A1 variant, and one of the A2 variant. Pull pin A0 on each IC up to +5V via a 10 k Ω resistor or down to ground via a 10 k Ω resistor as follows. (Confusingly, variants A0, A1, and A2 all have a pin A0, which is the address set pin).



Appendix D. CMAS Arduino Code

```
/*
  LAST UPDATE 2021-08-10
  VERSION 1.0

  Firmware for the Concentration Measurement and Adjustment System (CMAS.)
  Developed at the Aquatic Germplasm and Genetic Resources Center,
  Louisiana State University Agricultural Center, by Nikolas Zuchowicz.
  aquaticgermplasm.com
  nikolas.z@outlook.com

  Intended for use with an Arduino Nano in the assembled CMAS.

  ====

  LIBRARY ATTRIBUTIONS AND LICENSES

  AccelStepper.h is by Mike McCauley
  (http://www.airspayce.com/mikem/arduino/AccelStepper/index.html)
  and is distributed under the GPL V3 license (GNU General Public License.)

  TimerOne.h is by Paul Stoffregen
  (https://github.com/PaulStoffregen/TimerOne)
  and is distributed under the CC BY 3.0 US license (Creative Commons
  Attribution 3.0.)
*/

#include <Wire.h> // General communication
#include <LiquidCrystal_I2C.h> // LCD screen
#include <Adafruit_MCP4725.h> // Digital-analog converter (DAC)
hardware
#include <SPI.h> // SPI communication protocol for SD
memory card
#include <SD.h> // SD memory card
#include <RTCLib.h> // Real-time clock
#include <AccelStepper.h> // Stepper motor control (for the
peristaltic pumps)
#include <TimerOne.h> // Stepper command scheduling

// Peristaltic pump motor control pins
#define PIN_MOTOR1_STEP 5
#define PIN_MOTOR1_DIR 0
#define PIN_MOTOR2_STEP 6
#define PIN_MOTOR2_DIR 7
#define PIN_MOTOR3_STEP 9
#define PIN_MOTOR3_DIR 8

// Analog-digital conversion input pins from the optics
#define PIN_OPTICALIN_1 A0
#define PIN_OPTICALIN_2 A1
#define PIN_OPTICALIN_3 A2
#define PIN_OPTICALIN_4 A3
#define PIN_OPTICALIN_5 A6

// Analog-digital conversion input pins from the optics
```



```

#define PIN_ROTENC_BUTTON 2
#define PIN_ROTENC_ROT1 3
#define PIN_ROTENC_ROT2 4

// Device select pin for the SD memory card
#define PIN_SD_SELECT 10

// I2C object instances
LiquidCrystal_I2C lcd(0x27, 20, 4);
Adafruit_MCP4725 opticaldac_1;
Adafruit_MCP4725 opticaldac_2;
Adafruit_MCP4725 opticaldac_3;
Adafruit_MCP4725 opticaldac_4;
Adafruit_MCP4725 opticaldac_5;
RTC_DS3231 rtc;

File SD_logfile;

// Voltage out for DACs to drive optics
int opticaldac_1_vout = 0;
int opticaldac_2_vout = 0;
int opticaldac_3_vout = 0;
int opticaldac_4_vout = 0;
int opticaldac_5_vout = 0;

// Voltage in from ADCs from optics
int opticaladc_1_vin = 0;
int opticaladc_2_vin = 0;
int opticaladc_3_vin = 0;
int opticaladc_4_vin = 0;
int opticaladc_5_vin = 0;

// State machine refresh timers
unsigned long currentMillis = 0;

unsigned long dac_previousMillis = 0;
const long dac_interval = 500;

unsigned long lcd_previousMillis = 0;
const long lcd_interval = 500;

unsigned long rtc_previousMillis = 0;
const long rtc_interval = 1000;

// Current cursor position on the LCD
int cursor_position = 0;

// Create stepper motor control objects for the three peristaltic pumps
AccelStepper motor1(AccelStepper::DRIVER, PIN_MOTOR1_STEP, PIN_MOTOR1_DIR);
AccelStepper motor2(AccelStepper::DRIVER, PIN_MOTOR2_STEP, PIN_MOTOR2_DIR);
AccelStepper motor3(AccelStepper::DRIVER, PIN_MOTOR3_STEP, PIN_MOTOR3_DIR);

// States for the finite state machine
enum state {ST_INIT, ST_MENU, ST_MANUAL_MOTORS, ST_SINGLE_CH_CONC,
SST_SINGLE_CH_CONC_ADJUST, ST_DILUTE_SAMP, ST_SYS_INFO};
enum state current_state = ST_INIT;

```

```

// Interrupt service routine flags
volatile bool flag_encoderButtonPressed = false;
volatile int flag_encoderRotated = 0;

void setup() {

    pinMode(PIN_ROTENC_BUTTON, INPUT);
    pinMode(PIN_ROTENC_ROT1, INPUT);
    pinMode(PIN_ROTENC_ROT2, INPUT);

    // Connect rotation and button push on the rotary encoder to interrupt
    service routines
    attachInterrupt(digitalPinToInterrupt(PIN_ROTENC_BUTTON), encoderButtonISR,
    RISING);
    attachInterrupt(digitalPinToInterrupt(PIN_ROTENC_ROT1), encoderRotISR,
    RISING);

    // Initialize the five DACs with separate I2C addresses
    opticaldac_1.begin(0x60);
    opticaldac_2.begin(0x61);
    opticaldac_3.begin(0x62);
    opticaldac_4.begin(0x63);
    opticaldac_5.begin(0x64);

    opticaldac_1.setVoltage(0, false);
    opticaldac_2.setVoltage(0, false);
    opticaldac_3.setVoltage(0, false);
    opticaldac_4.setVoltage(0, false);
    opticaldac_5.setVoltage(0, false);

    // Initialize the LCD
    lcd.init();
    lcd.backlight();
    lcd.home();
    lcd.print("CMAS firmware v1.0");

    // Initialize the SD memory card
    lcd.setCursor(0, 1);
    if (!SD.begin(PIN_SD_SELECT)) {
        lcd.print("SD init failure");
        lcd.setCursor(0, 2);
        lcd.print("Check SD card");
    } else {
        lcd.print("SD init success");
    }

    lcd.setCursor(0, 3);
    if (!rtc.begin()) {
        lcd.print("Cannot find RTC");
    } else {
        DateTime time = rtc.now();
        lcd.print(time.timestamp());
    }

    delay(4000);
    lcd.clear();
}

```

```

}

void loop() {

    // The main loop runs a finite state machine.
    // The code for each state is devolved to a separate function.

    currentMillis = millis();

    switch (current_state) {

        case ST_INIT: // Initialization
            current_state = runstate_INIT();
            break;

        case ST_MENU: // Main menu to access other functions
            current_state = runstate_MENU();
            break;

        case ST_MANUAL_MOTORS: // Activate and deactivate pumps
            current_state = runstate_MANUAL_MOTORS();
            break;

        case ST_SINGLE_CH_CONC: // Measure input on a single optical channel
            current_state = runstate_SINGLE_CH_CONC();
            break;

        case SST_SINGLE_CH_CONC_ADJUST: // Adjust optical output on a single
optical channel
            current_state = runsubstate_SINGLE_CH_CONC_ADJUST();
            break;

        case ST_DILUTE_SAMP: // Run a dilution program (dilutes 1 sample fluid
with 1 extender fluid)
            current_state = runstate_DILUTE_SAMP();
            break;

        case ST_SYS_INFO: // Show system information, e.g. real time clock
timestamp
            current_state = runstate_SYS_INFO();
            break;

    }

}

state runstate_INIT() {

    // Maximum motor pulsetrain of 100 Hz, above which linear control breaks
down
    motor1.setMaxSpeed(100);
    motor1.setSpeed(0);
    motor2.setMaxSpeed(100);
    motor2.setSpeed(0);
    motor3.setMaxSpeed(100);
    motor3.setSpeed(0);

```

```

    // This timer interrupt runs once per millisecond to make sure that the
    stepper motors run smoothly
    // and concurrently with other operations such as the I2C LCD refresh.
    Without this, the motors
    // pause for the duration of each LCD refresh.

    // Set motor refresh to 1000 Hz
    Timer1.initialize(1000);
    Timer1.attachInterrupt(pollMotors);

    // DAC output voltage of (1580/4095)*5 = 1.93 V places the ADC input to
    around 1.50 V.
    // This needs adjustment on the fly, but this is close to what is needed.
    opticaldac_1_vout = 1580;
    opticaldac_1.setVoltage(opticaldac_1_vout, false);

    transition_to_state_MENU();
    return ST_MENU;
}

void transition_to_state_MENU() {

    flag_encoderRotated = 0;

    lcd.clear();
    lcd.setCursor ( 0, 0 );
    lcd.print(" Run motors manually");
    lcd.setCursor ( 0, 1 );
    lcd.print(" Single-chan. conc.");
    lcd.setCursor ( 0, 2 );
    lcd.print(" Dilute sample");
    lcd.setCursor ( 0, 3 );
    lcd.print(" System info");

    lcd_refresh_cursor();

}

state runstate_MENU() {

    if (flag_encoderRotated != 0) {
        cursor_position += flag_encoderRotated;
        if (cursor_position < 0) cursor_position = 3;
        if (cursor_position > 3) cursor_position = 0;
        flag_encoderRotated = 0;
        lcd_refresh_cursor();
    }

    if (flag_encoderButtonPressed) {

        flag_encoderButtonPressed = false;
        switch (cursor_position) {
            case 0:
                transition_to_state_MANUAL_MOTORS();
                return ST_MANUAL_MOTORS;
            case 1:

```

```

        transition_to_state_SINGLE_CH_CONC();
        return ST_SINGLE_CH_CONC;
    case 2:
        transition_to_state_DILUTE_SAMP();
        return ST_DILUTE_SAMP;
    case 3:
        transition_to_state_SYS_INFO();
        return ST_SYS_INFO;
    }

} else {
    return ST_MENU;
}

}

void transition_to_state_MANUAL_MOTORS() {

    lcd.clear();
    lcd.setCursor ( 0, 0 );
    lcd.print(" Run motor 1");
    lcd.setCursor ( 0, 1 );
    lcd.print(" Run motor 2");
    lcd.setCursor ( 0, 2 );
    lcd.print(" Run motor 3");
    lcd.setCursor ( 0, 3 );
    lcd.print(" Exit to main menu");

    cursor_position = 0;
    lcd_refresh_cursor();

}

state runstate_MANUAL_MOTORS() {

    if (flag_encoderRotated != 0) {
        cursor_position += flag_encoderRotated;
        if (cursor_position < 0) cursor_position = 3;
        if (cursor_position > 3) cursor_position = 0;
        flag_encoderRotated = 0;
        lcd_refresh_cursor();
    }

    if (flag_encoderButtonPressed) {

        flag_encoderButtonPressed = false;
        switch (cursor_position) {
            case 0:
                if (motor1.speed() != 0) {
                    motor1.setSpeed(0);
                } else {
                    motor1.setSpeed(100);
                }
                break;
            case 1:
                if (motor2.speed() != 0) {
                    motor2.setSpeed(0);

```

```

        } else {
            motor2.setSpeed(100);
        }
        break;
    case 2:
        if (motor3.speed() != 0) {
            motor3.setSpeed(0);
        } else {
            motor3.setSpeed(100);
        }
        break;
    case 3:
        cursor_position = 0; // sets correct cursor position in menu
        transition_to_state_MENU();
        return ST_MENU;
    }

} else {
    return ST_MANUAL_MOTORS;
}
}

void transition_to_state_SINGLE_CH_CONC() {

    lcd.clear();
    lcd.setCursor ( 0, 0 );
    lcd.print(" Single-chan. conc.");
    lcd.setCursor ( 0, 1 );
    lcd.print(" OUT          V");
    lcd.setCursor ( 6, 1 );
    lcd.print(opticaldac_1_vout);
    lcd.setCursor ( 11, 1 );
    lcd.print((float)opticaldac_1_vout / 4095 * 5);
    lcd.setCursor ( 0, 2 );
    lcd.print(" IN          V");

    cursor_position = 0;
    lcd_refresh_cursor();

}

state runstate_SINGLE_CH_CONC() {

    if (currentMillis - dac_previousMillis >= dac_interval) {
        dac_previousMillis += dac_interval;
        read_adcs();
        lcd.setCursor ( 6, 2 );
        lcd.print(opticaladc_1_vin);
        lcd.setCursor ( 11, 2 );
        lcd.print((float)opticaladc_1_vin / 1023 * 5);
    }

    if (flag_encoderRotated != 0) {
        cursor_position += flag_encoderRotated;
        flag_encoderRotated = 0;
        if (cursor_position < 0) cursor_position = 1;
        if (cursor_position > 1) cursor_position = 0;
    }
}

```

```

    lcd_refresh_cursor();
}

if (flag_encoderButtonPressed) {
    flag_encoderButtonPressed = false;
    switch (cursor_position) {
        case 0:
            cursor_position = 1; // sets correct cursor position in menu
            transition_to_state_MENU();
            return ST_MENU;
            break;
        case 1:
            transition_to_substate_SINGLE_CH_CONC_ADJUST();
            return SST_SINGLE_CH_CONC_ADJUST;
            break;
    }
} else {
    return ST_SINGLE_CH_CONC;
}

}

void transition_to_substate_SINGLE_CH_CONC_ADJUST() {

    lcd.setCursor ( 1, 1 );
    lcd.print(">");

}

state runsubstate_SINGLE_CH_CONC_ADJUST() {

    if (currentMillis - dac_previousMillis >= dac_interval) {
        dac_previousMillis += dac_interval;
        read_adcs();
        lcd.setCursor ( 6, 2 );
        lcd.print(opticaladc_1_vin);
        lcd.setCursor ( 11, 2 );
        lcd.print((float)opticaladc_1_vin / 1023 * 5);
    }

    if (flag_encoderRotated != 0) {
        opticaldac_1_vout += flag_encoderRotated;
        flag_encoderRotated = 0;
        if (opticaldac_1_vout < 0) opticaldac_1_vout = 0;
        if (opticaldac_1_vout > 4095) opticaldac_1_vout = 4095;
        opticaldac_1.setVoltage(opticaldac_1_vout, false);
        lcd.setCursor ( 6, 1 );
        lcd.print(opticaldac_1_vout);
        lcd.setCursor ( 11, 1 );
        lcd.print((float)opticaldac_1_vout / 4095 * 5);
    }

    if (flag_encoderButtonPressed) {
        flag_encoderButtonPressed = false;
        transition_to_state_SINGLE_CH_CONC();
        cursor_position = 1;
        lcd_refresh_cursor();
    }
}

```



```

        return ST_SINGLE_CH_CONC;
    } else {
        return SST_SINGLE_CH_CONC_ADJUST;
    }
}

void transition_to_state_DILUTE_SAMP() {

    lcd.clear();
    lcd.setCursor ( 0, 0 );
    lcd.print(" Dilute sample");

    cursor_position = 0;
    lcd_refresh_cursor();

}

state runstate_DILUTE_SAMP() {

    // Currently set with regression-based concentration calculation for an
    // algae sample
    long conc = (long)pow((float)10,((((float)opticaladc_1_vin / 1023 * 5)-
20.94)/(-2.9698)));
    lcd.setCursor ( 0, 1 );
    lcd.print(conc);
    lcd.print(" cells/mL");

    lcd.setCursor ( 0, 2 );
    if (conc <= 1000000) {
        lcd.print("Conc. too low to dilute");
    } else {
        int motor1_target;
        int motor2_target;

        if (conc <= 2000000) {
            motor1.setSpeed(100);
            motor2.setSpeed(((float)conc - (float)1000000) / (float)10000);

            lcd.print("P1 ");
            lcd.print(100);
            lcd.setCursor ( 0, 3 );
            lcd.print("P2 ");
            lcd.print(((float)conc - (float)1000000) / (float)10000));
        } else {
            motor1.setSpeed(((float)100 / (((float)conc - (float)1000000) /
(float)1000000)));
            motor2.setSpeed(100);

            lcd.print("P1 ");
            lcd.print(((float)100 / (((float)conc - (float)1000000) /
(float)1000000)));
            lcd.setCursor ( 0, 3 );
            lcd.print("P2 ");
            lcd.print(100);
        }
    }
}

```

```

if (flag_encoderButtonPressed) {
    flag_encoderButtonPressed = false;

    motor1.setSpeed(0);
    motor2.setSpeed(0);

    cursor_position = 2; // sets correct cursor position in menu
    transition_to_state_MENU();
    return ST_MENU;
} else {
    return ST_DILUTE_SAMP;
}
}

void transition_to_state_SYS_INFO() {

    lcd.clear();
    lcd.setCursor ( 0, 0 );
    lcd.print(" Exit to main menu");
    lcd.setCursor ( 0, 1 );
    lcd.print(" Reset clock");
    lcd.setCursor ( 1, 2 );
    DateTime time = rtc.now();
    lcd.print(time.timestamp());

    cursor_position = 0;
    lcd_refresh_cursor();

}

state runstate_SYS_INFO() {

    if (currentMillis - rtc_previousMillis >= rtc_interval) {
        rtc_previousMillis += rtc_interval;
        lcd.setCursor ( 1, 2 );
        DateTime time = rtc.now();
        lcd.print(time.timestamp());
    }

    if (flag_encoderRotated != 0) {
        cursor_position += flag_encoderRotated;
        if (cursor_position < 0) cursor_position = 1;
        if (cursor_position > 1) cursor_position = 0;
        flag_encoderRotated = 0;
        lcd_refresh_cursor();
    }

    if (flag_encoderButtonPressed) {

        flag_encoderButtonPressed = false;
        switch (cursor_position) {
            case 0:
                cursor_position = 3; // sets correct cursor position in menu
                transition_to_state_MENU();
                return ST_MENU;
                break;

```

```

        case 1:
            rtc.adjust(DateTime(F(__DATE__), F(__TIME__)));
            break;
    }

    } else {
        return ST_SYS_INFO;
    }

}

void encoderButtonISR() {
    flag_encoderButtonPressed = true;
}

void encoderRotISR() {
    if (digitalRead(PIN_ROTENC_ROT1) == digitalRead(PIN_ROTENC_ROT2)) {
        flag_encoderRotated++;
    } else {
        flag_encoderRotated--;
    }
}

void lcd_refresh_cursor() {
    lcd.setCursor ( 0, 0 );
    (cursor_position == 0) ? lcd.print(">") : lcd.print(" ");
    lcd.setCursor ( 0, 1 );
    (cursor_position == 1) ? lcd.print(">") : lcd.print(" ");
    lcd.setCursor ( 0, 2 );
    (cursor_position == 2) ? lcd.print(">") : lcd.print(" ");
    lcd.setCursor ( 0, 3 );
    (cursor_position == 3) ? lcd.print(">") : lcd.print(" ");
}

void pollMotors() {
    motor1.runSpeed();
    motor2.runSpeed();
    motor3.runSpeed();
}

void read_adcs() {
    opticaladc_1_vin = analogRead(PIN_OPTICALIN_1);
    opticaladc_2_vin = analogRead(PIN_OPTICALIN_2);
    opticaladc_3_vin = analogRead(PIN_OPTICALIN_3);
    opticaladc_4_vin = analogRead(PIN_OPTICALIN_4);
    opticaladc_5_vin = analogRead(PIN_OPTICALIN_5);
}

void log_to_SD() {
    SD_logfile = SD.open("test1.txt", FILE_WRITE);

    if (SD_logfile) {

```

```

        SD_logfile.print(currentTime());
        SD_logfile.println("");
        SD_logfile.close();
    } else {
        lcd.clear();
        lcd.print("SD file error");
        delay(1000);
        lcd.clear();
    }
}

String currentTime() {
    String currentTime;
    DateTime now = rtc.now();
    currentTime = now.unixtime();
    return currentTime;
}

```

Appendix E. Using the Parametric CMAS Form Factor

In rapid prototyping, there is often a need for custom enclosures to fit particular user interface elements, fluidics, electronics, and the like. It can be convenient to fabricate such enclosures in-house: a process that may answer a specialized need in a few hours, rather than the days that may be required to buy and receive a commercial order. A simplified, parametric version of the form factor used for the concentration measurement and adjustment system (CMAS) is therefore provided as a Fusion 360 design file (.f3d format; Figure E.1) to allow the rapid fabrication of enclosures with specified dimensions.

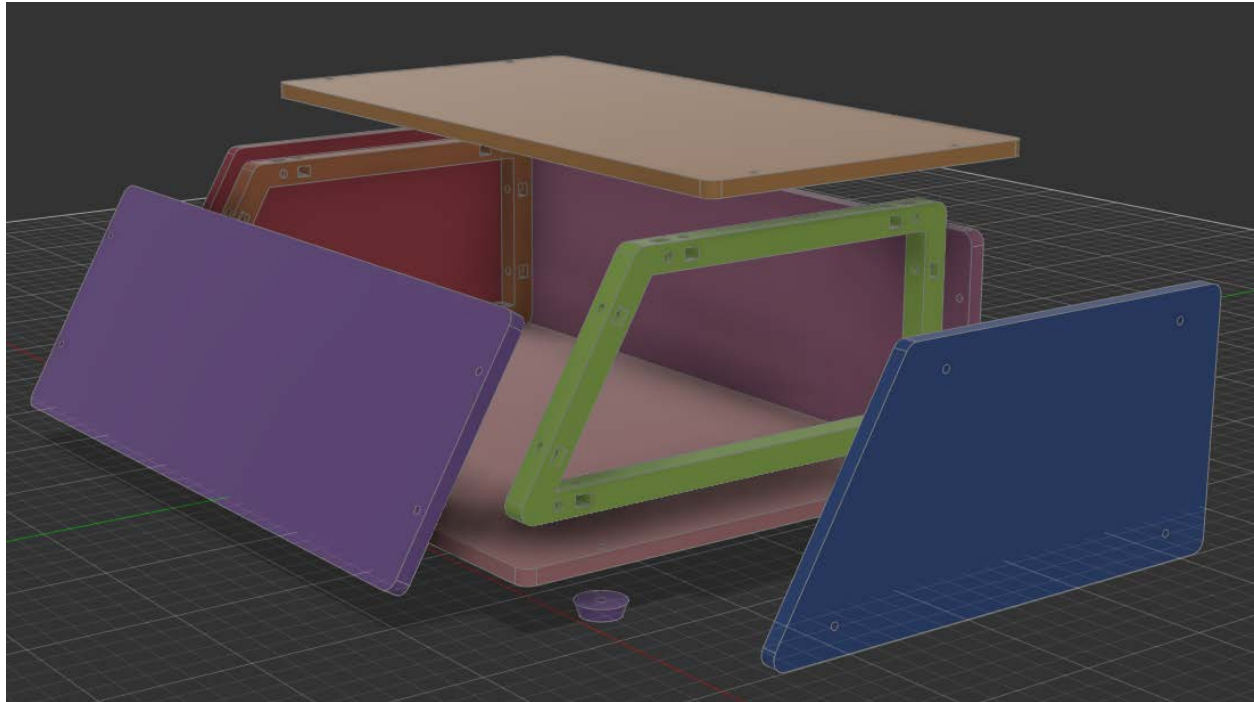


Figure E.1. An exploded view of the elements of the CMAS form factor within the CAD software Fusion 360. Visible are the six laser-cut acrylic panels making up the outside of the case, the two internal 3-D printed braces, and one of the four 3-D printed feet.

To fabricate an enclosure of the CMAS form factor, the maker must have access to a 3-D printer and a laser cutter capable of cutting 6 mm acrylic. The supplies and tools listed in table E.1 are also required.

Table E.1. Supplies and tools to fabricate the CMAS form factor.

| Item | Example link | Quantity |
|------------------------------------|---|-----------|
| 3-D printing filament, such as PLA | amazon.com/dp/B01EKEMDA6 | 1 kg roll |
| M3 14 mm machine screw | amazon.com/dp/B08H2HQ3VZ | 24 |
| M3 hex nut or nylock nut | amazon.com/dp/B082D6M295 | 24 |
| M3 hex screwdriver | amazon.com/dp/B000NZ5QE2 | 1 |
| Needle-nose pliers | amazon.com/dp/B093K71F9F | 1 |

Table E.2. Parameters that may be modified in Fusion 360 to generate a custom-dimensioned CMAS form factor.

| Parameter name | Default value | Comment |
|-----------------------|---------------|---|
| acrylic_bore_diameter | 3 mm | For the laser cutter on which this was tested, a bore diameter equal to the nominal machine screw diameter (3 mm for an M3 screw) produces a clearance hole that will take the screw smoothly. |
| acrylic_corner_radius | 5 mm | The radius of corners on the laser-cut acrylic panels. This value is mainly an esthetic choice. |
| acrylic_thickness | 6 mm | Acrylic sheets are available in 6 mm (or ¼”) standard thickness. |
| brace_corner_radius | 5 mm | The radius of corners on the 3-D printed braces. This value is mainly an esthetic choice. |
| case_angle | 120° | The angle, as measured from the horizontal top face, of the front face plate. |
| case_height | 100 mm | The overall height of the case, excluding the feet. |
| case_top_depth | 150 mm | The distance from front to back of the top panel only. Note that the overall distance from front to back of the whole case will be determined by this and the parameter case_angle. |
| case_width | 300 mm | The overall width of the case. |
| locknut_diameter | 6 mm | The width of the holes that will accommodate captive nuts in the 3-D printed braces. |
| locknut_height | 4.5 mm | The height of the holes that will accommodate captive nuts in the 3-D printed braces. |
| printed_bore_diameter | 3.8 mm | The diameter of the holes that will accommodate machine screws in the 3-D printed braces. These are intended to be clearance holes for the screws without the need to clear the holes with a drill bit after printing. This value may need modification depending on the particular 3-D printer and slicer used, or the thermoplastic expansion may be compensated for in the slicer by experience. |

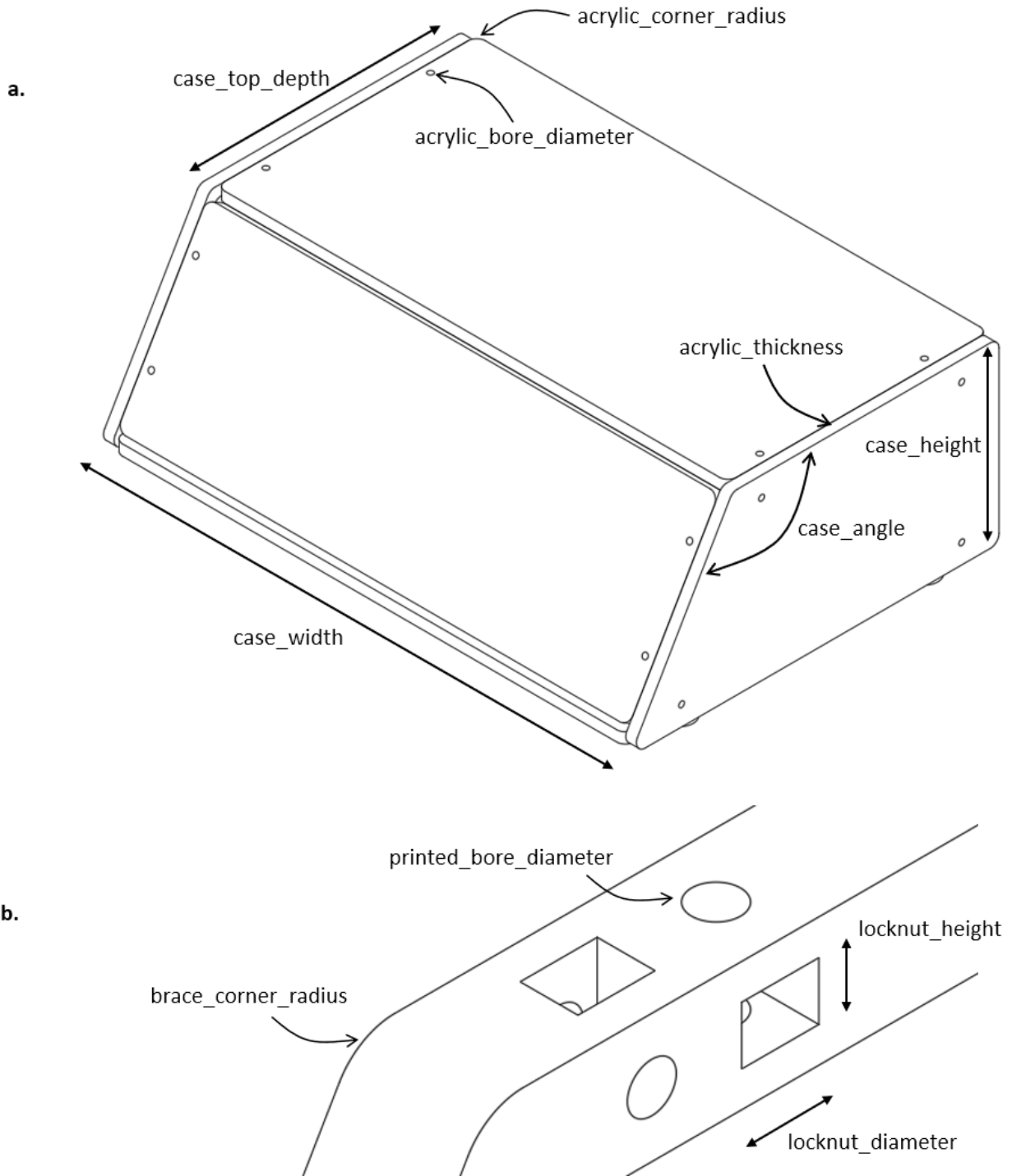
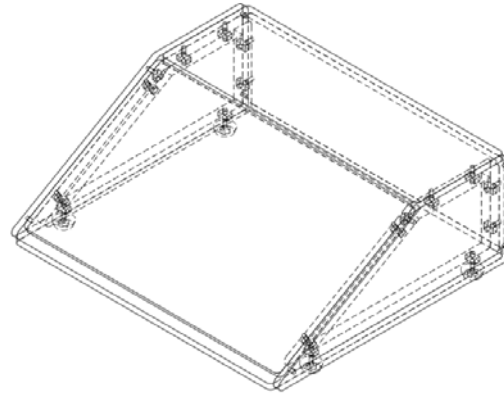
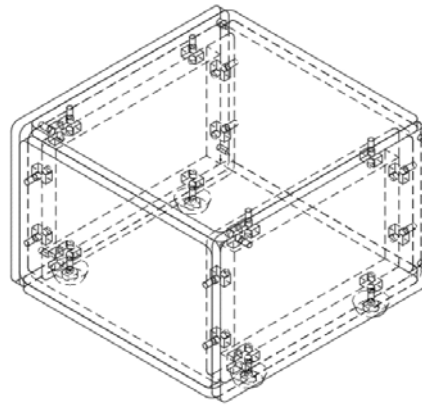


Figure E.2. Illustrations of the customizable parameters in the CMAS form factor. Panel a, an external view of the form factor. Panel b, a close view of part of a 3-D printed internal brace, showing small features that accommodate machine screws and nuts.

| Parameter name | Value |
|-----------------------|---------------|
| acrylic_bore_diameter | 3 mm |
| acrylic_corner_radius | 5 mm |
| acrylic_thickness | 6 mm |
| brace_corner_radius | 5 mm |
| case_angle | 150° |
| case_height | 100 mm |
| case_top_depth | 100 mm |
| case_width | 300 mm |
| locknut_diameter | 6 mm |
| locknut_height | 4.5 mm |
| printed_bore_diameter | 3.8 mm |



| | |
|-----------------------|---------------|
| acrylic_bore_diameter | 3 mm |
| acrylic_corner_radius | 5 mm |
| acrylic_thickness | 6 mm |
| brace_corner_radius | 5 mm |
| case_angle | 90° |
| case_height | 100 mm |
| case_top_depth | 150 mm |
| case_width | 150 mm |
| locknut_diameter | 6 mm |
| locknut_height | 4.5 mm |
| printed_bore_diameter | 3.8 mm |



| | |
|-----------------------|---------------|
| acrylic_bore_diameter | 3 mm |
| acrylic_corner_radius | 5 mm |
| acrylic_thickness | 6 mm |
| brace_corner_radius | 5 mm |
| case_angle | 100° |
| case_height | 200 mm |
| case_top_depth | 150 mm |
| case_width | 200 mm |
| locknut_diameter | 6 mm |
| locknut_height | 4.5 mm |
| printed_bore_diameter | 3.8 mm |

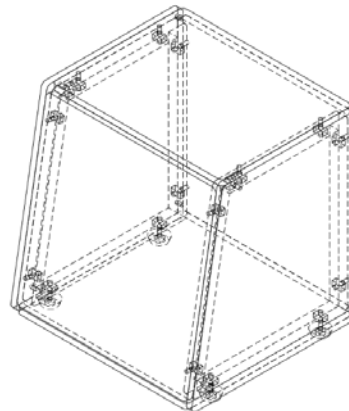


Figure E.3. Three variations of the CMAS form factor that are possible with custom parameters. Deviations from the default values are bolded.

Appendix F. Preparation of Hanks' Balanced Salt Solution (HBSS), 300 mOsmol/kg

To prepare 1 L of 300 mOsmol/kg HBSS, weigh the following compounds into a weighing boat, and transfer into a 1-L container:

Table G.1. Ingredients to produce Hanks' balanced salt solution.

| Compound | Mass (g) |
|---|----------|
| NaCl | 8.00 |
| KCl | 0.40 |
| CaCl ₂ ·2H ₂ O | 0.16 |
| MgSO ₄ ·7H ₂ O | 0.20 |
| Na ₂ HPO ₄ | 0.06 |
| KH ₂ PO ₄ | 0.06 |
| NaHCO ₃ | 0.35 |
| C ₆ H ₁₂ O ₆ | 1.00 |

Fill the container to the 1 L mark with deionized water and agitate to dissolve the solutes. Verify the osmolality with an osmometer (e.g., Precision Systems Osmette III freezing-point osmometer, or Wescor Vapro 5520 vapor pressure osmometer), following the manufacturer operating instructions.

References

1. Childress, W. M., Liu, Y. & Tiersch, T. R. Design, alpha testing, and beta testing of a 3-D printed open-hardware portable cryopreservation device for aquatic species. *J Appl Aquac* 1–24 (2021).
2. Commission on Genetic Resources for Food and Agriculture. *Cryoconservation of animal genetic resources*. (Food and Agriculture Organization of the United Nations, 2012).
3. Torres, L. & Tiersch, T. R. Addressing reproducibility in cryopreservation, and considerations necessary for commercialization and community development in support of genetic resources of aquatic species. *J World Aquacult Soc* **49**, 644–663 (2018).
4. Gao, D. & Critser, J. K. Mechanisms of cryoinjury in living cells. *ILAR Journal* **41**, 187–196 (2000).
5. Benson, J. D., Woods, E. J., Walters, E. M. & Critser, J. K. The cryobiology of spermatozoa. *Theriogenology* **78**, 1682–1699 (2012).
6. Benson, E. E., Betsou, F., Fuller, B. J., Harding, K. & Kofanova, O. Translating cryobiology principles into trans-disciplinary storage guidelines for biorepositories and biobanks: a concept paper. *CryoLetters* **34**, 277–312 (2013).
7. Comizzoli, P. Superficial and profound considerations about sperm quality. *J Assist Reprod Genet* **36**, 1361–1362 (2019).
8. Woods, E. J., Benson, J. D., Agca, Y. & Critser, J. K. Fundamental cryobiology of reproductive cells and tissues. *Cryobiology* **48**, 146–156 (2004).
9. Fogarty, N. M., Maxwell, W. M. C., Eppleston, J. & Evans, G. The viability of transferred sheep embryos after long-term cryopreservation. *Reprod Fert Develop* **12**, 31–37 (2000).
10. Fuller, B. *et al.* Applications and optimization of cryopreservation technologies to cellular therapeutics. *Cell Gene Ther Insights* **3**, 359–378 (2017).
11. Torres, L., Hu, E. & Tiersch, T. R. Cryopreservation in fish: current status and pathways to quality assurance and quality control in repository development. *Reprod Fertil Dev* **28**, 1105 (2016).
12. Gallego, V., Pérez, L., Asturiano, J. F. & Yoshida, M. Relationship between spermatozoa motility parameters, sperm/egg ratio, and fertilization and hatching rates in pufferfish (*Takifugu niphobles*). *Aquaculture* **416–417**, 238–243 (2013).
13. Dong, Q., Huang, C. & Tiersch, T. R. Control of sperm concentration is necessary for standardization of sperm cryopreservation in aquatic species: evidence from sperm agglutination in oysters. *Cryobiology* **54**, 87–98 (2007).

14. Judycka, S. *et al.* Optimal sperm concentration in straws and final glucose concentration in extender are crucial for improving the cryopreservation protocol of salmonid spermatozoa. *Aquaculture* **486**, 90–97 (2018).
15. Hu, E., Bosworth, B., Baxter, J. & Tiersch, T. R. On-site evaluation of commercial-scale hybrid catfish production using cryopreserved blue catfish sperm. *Aquaculture* **426–427**, 88–95 (2014).
16. Polge, C., Smith, A. U. & Parkes, A. S. Revival of spermatozoa after vitrification and dehydration at low temperatures. *Nature* **164**, 666 (1949).
17. Smith, A. Prevention of hæmolysis during freezing and thawing of red blood-cells. *Lancet* **256**, 910–911 (1950).
18. Kuleshova, L., Gianaroli, L., Magli, C., Ferraretti, A. & Trounson, A. Birth following vitrification of a small number of human oocytes. *Hum Reprod* **14**, 3077–3079 (1999).
19. Rall, W. F., Reid, D. S. & Polge, C. Analysis of slow-warming injury of mouse embryos by cryomicroscopical and physiochemical methods. *Cryobiology* **21**, 106–121 (1984).
20. Jin, B., Kleinhans, F. W. & Mazur, P. Survivals of mouse oocytes approach 100% after vitrification in 3-fold diluted media and ultra-rapid warming by an IR laser pulse. *Cryobiology* **68**, 419–430 (2014).
21. Brockbank, K. G. M., Chen, Z., Greene, E. D. & Campbell, L. H. Ice-free cryopreservation by vitrification. *MOJ Cell Sci Rep* **1**, (2014).
22. Mazur, P., Leibo, S. P. & Chu, E. H. Y. A two-factor hypothesis of freezing injury. *Exp Cell Res* **71**, 345–355 (1972).
23. Matthews, J., Murphy, J., Carmichael, C. & Varga, Z. ZIRC E400/RMMB sperm cryopreservation & IVF protocol. (2017).
24. van der Horst, G., Bennett, M. & Bishop, J. D. D. CASA in invertebrates. *Reprod Fertil Dev* **30**, 907–918 (2018).
25. Zuchowicz, N. *et al.* Assessing coral sperm motility. *Sci Rep* **11**, 61 (2021).
26. Holt, W. V., O'Brien, J. & Abaigar, T. Applications and interpretation of computer-assisted sperm analyses and sperm sorting methods in assisted breeding and comparative research. *Reprod Fertil Dev* **19**, 709 (2007).
27. Childress, W. M., Bosworth, B., Chesney, E., Walter, R. B. & Tiersch, T. R. On-site capabilities of a mobile laboratory for aquatic germplasm cryopreservation. *North Am J Aquaculture* **81**, 349–363 (2019).
28. Caetano Da Silva, C. *et al.* An easy method for cryopreservation of zebrafish (*Danio rerio*) sperm. *Zebrafish* **16**, (2019).

29. Childress, W. M., Caffey, R. H. & Tiersch, T. R. Design and cost analysis of a self-contained mobile laboratory for commercial-scale aquatic species cryopreservation. *J World Aquacult Soc* **49**, 805–826 (2018).
30. Crump, S. S. Apparatus and method for creating three-dimensional objects. US Patent 5121329 (1992).
31. Kristiawan, R. B., Imaduddin, F., Ariawan, D., Ubaidillah & Arifin, Z. A review on the fused deposition modeling (FDM) 3D printing: filament processing, materials, and printing parameters. *Open Eng* **11**, 639–649 (2021).
32. Kodama, H. 3D figure production device. Japan Patent S56-144478 (1981).
33. Waheed, S. *et al.* 3D printed microfluidic devices: enablers and barriers. *Lab Chip* **16**, 1993–2013 (2016).
34. Yazdi, A. A. *et al.* 3D printing: an emerging tool for novel microfluidics and lab-on-a-chip applications. *Microfluid Nanofluid* **20**, 50 (2016).
35. Liu, Y. *et al.* The emerging role of open technologies for community-based improvement of sperm cryopreservation throughput and quality management for repository development in aquatic species. *Submitted for review*.
36. von Krogh, G. & von Hippel, E. Special issue on open source software development. *Res Policy* **32**, 1149–1157 (2003).
37. Bonvoisin, J., Mies, R., Boujut, J.-F. & Stark, R. What is the “Source” of Open Source Hardware? *J Open Hardw* **1**, 5 (2017).
38. Wu, M.-H., Huang, S.-B. & Lee, G.-B. Microfluidic cell culture systems for drug research. *Lab Chip* **10**, 939 (2010).
39. Byun, C. K., Abi-Samra, K., Cho, Y.-K. & Takayama, S. Pumps for microfluidic cell culture: Microfluidics and Miniaturization. *Electrophoresis* **35**, 245–257 (2014).
40. Yobas, L., Tang, K.-C., Yong, S.-E. & Kye-Zheng Ong, E. A disposable planar peristaltic pump for lab-on-a-chip. *Lab Chip* **8**, 660 (2008).
41. Jönsson, A., Toppi, A. & Dufva, M. The FAST Pump, a low-cost, easy to fabricate, SLA-3D-printed peristaltic pump for multi-channel systems in any lab. *HardwareX* **8**, e00115 (2020).
42. Xiang, J., Cai, Z., Zhang, Y. & Wang, W. A micro-cam actuated linear peristaltic pump for microfluidic applications. *Sens Actuator A Phys* **251**, 20–25 (2016).
43. Tsuda, S. *et al.* Customizable 3D printed ‘plug and play’ millifluidic devices for programmable fluidics. *PLoS ONE* **10**, e0141640 (2015).

44. Glotz, G. & Kappe, C. O. Design and construction of an open source-based photometer and its applications in flow chemistry. *React Chem Eng* **3**, 478–486 (2018).
45. Beddows, P. A. & Mallon, E. K. Cave Pearl data logger: a flexible Arduino-based logging platform for long-term monitoring in harsh environments. *Sensors* **18**, 530 (2018).
46. Beirão, J. *et al.* Sperm handling in aquatic animals for artificial reproduction. *Theriogenology* **133**, 161–178 (2019).
47. Kouba, A. J., Vance, C. K. & Willis, E. L. Artificial fertilization for amphibian conservation: current knowledge and future considerations. *Theriogenology* **71**, 214–227 (2009).
48. Segur, J. B. & Oberstar, H. E. Viscosity of glycerol and its aqueous solutions. *Ind Eng Chem* **43**, 2117–2120 (1951).
49. Babiak, I. *et al.* Effects of extender, storage and sperm-to-egg ratio on cryopreservation success of Atlantic cod (*Gadus morhua* L.) sperm. *J Appl Ichthyol* **28**, 941–947 (2012).
50. Pšenička, M., Saito, T., Rodina, M. & Dzyuba, B. Cryopreservation of early stage Siberian sturgeon *Acipenser baerii* germ cells, comparison of whole tissue and dissociated cells. *Cryobiology* **72**, 119–122 (2016).
51. Hagedorn, M. & Carter, V. L. Cryobiology: principles, species conservation and benefits for coral reefs. *Reprod Fert Develop* **28**, 1049–1060 (2016).
52. Cosson, J. *et al.* Studying sperm motility in marine fish: an overview on the state of the art. *J Appl Ichthyol* **24**, 460–486 (2008).
53. Dong, Q., Eudeline, B., Huang, C. & Tiersch, T. R. Standardization of photometric measurement of sperm concentration from diploid and tetraploid Pacific oysters, *Crassostrea gigas* (Thunberg). *Aquac Research* **36**, 86–93 (2005).
54. Bosworth, B. & Waldbieser, G. Development of improved catfish germplasm at the Warmwater Aquaculture Research Unit, USDA-ARS. *Bull Jap Fish Res Edu Agen* **45**, (2017).
55. Bosworth, B., Chatakondi, N. & Avery, J. Producing hybrid catfish fry: workshop manual. (2011).
56. World Health Organization. *WHO laboratory manual for the examination and processing of human semen*. (World Health Organization, 2021).
57. Certified Semen Services. CSS minimum requirements for disease control of semen produced for artificial insemination. (2021).
58. Dong, Q., Huang, C., Eudeline, B. & Tiersch, T. R. Cryoprotectant optimization for sperm of diploid Pacific oysters by use of commercial dairy sperm freezing facilities. *Aquaculture* **271**, 537–545 (2007).

59. Martínez-Páramo, S. *et al.* Cryobanking of aquatic species. *Aquaculture* **472**, 156–177 (2017).
60. Wildt, D. E., Comizzoli, P., Pukazhenth, B. & Songsasen, N. Lessons from biodiversity—the value of nontraditional species to advance reproductive science, conservation, and human health. *Mol Reprod Dev* **77**, 397–409 (2010).
61. Hagedorn, M., Varga, Z., Walter, R. B. & Tiersch, T. R. Workshop report: cryopreservation of aquatic biomedical models. *Cryobiology* **86**, 120–129 (2019).
62. Babcock, R. C. *et al.* Synchronous spawnings of 105 scleractinian coral species on the Great Barrier Reef. *Mar Biol* **90**, 379–394 (1986).
63. Bouwmeester, J. *et al.* Multi-species spawning synchrony within scleractinian coral assemblages in the Red Sea. *Coral Reefs* **34**, 65–77 (2015).
64. Nynca, J., Judycka, S., Liszewska, E., Dobosz, S. & Ciereszko, A. Standardization of spermatozoa concentration for cryopreservation of rainbow trout semen using a glucose-methanol extender. *Aquaculture* **477**, 23–27 (2017).
65. Hu, E., Liao, T. W. & Tiersch, T. R. Simulation modelling of high-throughput cryopreservation of aquatic germplasm: a case study of blue catfish sperm processing. *Aquac Res* **46**, 432–445 (2015).
66. Blackwell, G. R. Surface mount technology. in *Electronic systems maintenance handbook* (CRC Press, 2002).
67. Yang, H. & Tiersch, T. R. Current status of sperm cryopreservation in biomedical research fish models: zebrafish, medaka, and *Xiphophorus*. *Comp Biochem Physiol Part C: Toxicol Pharmacol* **149**, 224–232 (2009).
68. Weibel, D. B., DiLuzio, W. R. & Whitesides, G. M. Microfabrication meets microbiology. *Nat Rev Microbiol* **5**, 209–218 (2007).
69. Au, A. K., Bhattacharjee, N., Horowitz, L. F., Chang, T. C. & Folch, A. 3D-printed microfluidic automation. *Lab Chip* **15**, 1934–1941 (2015).
70. Razavi Bazaz, S. *et al.* Rapid softlithography using 3D-printed molds. *Adv Mater Technol* **4**, 1900425 (2019).
71. Scherr, T. *et al.* A planar microfluidic mixer based on logarithmic spirals. *J Micromech Microeng* **22**, 055019 (2012).
72. Beckham, J. *et al.* A microfluidic device for motility and osmolality analysis of zebrafish sperm. *Biomed Microdevices* **20**, 67 (2018).

73. Park, D. S., Egnatchik, R. A., Bordelon, H., Tiersch, T. R. & Monroe, W. T. Microfluidic mixing for sperm activation and motility analysis of pearl *Danio* zebrafish. *Theriogenology* **78**, 334–344 (2012).
74. Zhou, Y. The recent development and applications of fluidic channels by 3D printing. *J Biomed Sci* **24**, 80 (2017).
75. McDonald, J. C. *et al.* Fabrication of microfluidic systems in poly(dimethylsiloxane). *Electrophoresis* **21**, 27–40 (2000).
76. Herrmann, J. W. *et al.* New directions in design for manufacturing. in *Volume 3d: 8th Design for Manufacturing Conference* 853–861 (ASMEDC, 2004). doi:10.1115/DETC2004-57770.

Vita

Nikolas earned his Bachelor of Arts in Biology and Religion from Carleton University in his hometown of Ottawa, Canada. He worked for several years in the Canadian Armed Forces army reserve, organizing training events, courses, and personnel allocation. He began his scientific career in the laboratory of Dr. Mary Hagedorn of the Smithsonian Conservation Biology Institute, where he learned the principles of cryobiology and cryopreservation. Working at the Hawai'i Institute of Marine Biology alongside postdoctoral fellow Dr. Jonathan Daly, he helped develop techniques and tools that resulted in the first cryopreservation and rapid laser warming of coral larvae.

He moved to Baton Rouge in 2019 to pursue his Master of Science degree at Louisiana State University with Dr. Terrence Tiersch. His principal research interest at the Aquatic Germplasm and Genetic Resources Center, an element of the LSU Agricultural Center, is rapid prototyping of open hardware in support of germplasm repository development.

Nikolas plans to move to Minneapolis to pursue a Ph.D. in mechanical engineering. He aims to become a leader in the development of technology and approaches for the conservation of imperiled species.